2022

Graphene based electrochemical biosensors for the detection of blood biomarkers of Alzheimer's disease

Sethi, Jagriti

Copyright

UNIVERSITY OF
PLYMOUTH

Graphene based electrochemical biosensors for the detection of blood biomarkers of Alzheimer's disease

by

Jagriti Sethi

A thesis submitted to the University of Plymouth
in partial fulfilment for the degree of

DOCTOR OF PHILOSOPHY

School of Engineering, Computing and Mathematics

March 2022

Acknowledgements

It is with utmost sincerity that I express my gratitude to all of those who have supported me throughout my Ph.D. research. This unique experience has greatly expanded my knowledge and skills for further research. First and foremost, I would like to thank my director of studies, Prof. Genhua Pan for his guidance, support, patience and understanding. He has always been and continues to be an endless source of inspiration. I would like to express appreciation to my second supervisor, Dr. Yinghui Wei, for her guidance, time and support. I would also like to thank Dr. David Jenkins for his time and guidance, Dr. Nick fry for providing time, advise and teaching me how to use various instruments and Dr. Glenn Harper for helping me with SEM and image analysis.

Furthermore, I would like to thank my colleagues and lab mates, especially Ms. Mina Safarzadeh, Dr. Ahmed Suhail and Mr. Jonathan Bloor, for their support and suggestions. Thanks to them, my stay in the UK has been lively and enjoyable. I also want to thank all the BBDiag ESRs, especially Hina, Michiel, Jessica, Chima and Arianna for being such good friends and colleagues. I want to thank my best friends Harleen and Aanchal for being my pillars of support and for constantly cheering me on to be the best version of myself.

Last but not the least, I am grateful to my parents, Sunita and Vinod, for their constant love, support and encouragement, especially when things were hard. I am grateful to my brother and sister in law, Sahil and Keerthi, for their love, guidance and support. A special thanks to my nephew, Trijal, for being a ray of sunshine and always bringing a smile on my face.

To each of the above, I want to extend my deepest appreciation and I couldn't have done it without them.

Author's declaration

At no time during the registration for the degree of Doctor of Philosophy has the author been registered for any other University award.

Work submitted for this research degree at University of Plymouth has not formed part of any other degree either at University of Plymouth or at another establishment.

This study was financed with the aid of H2020 MSCA-ITN-ETN BBDiag project under grant no. 721281.

Publications:

1. **Jagriti Sethi**, Michiel Van Bulck, Ahmed Suhail, Mina Safarzadeh, Ana Perez-Castillo and Genhua Pan, A label-free biosensor based on graphene and reduced graphene oxide dual-layer for electrochemical determination of beta-amyloid biomarkers. Microchim Acta 187, 288 (2020), **https://doi.org/10.1007/s00604-020-04267-x**

2. **Jagriti Sethi**, Ahmed Suhail, Mina Safarzadeh, Anas Sattar, Yinghui Wei and Genhua Pan, NH_2 linker for femtomolar label-free detection with reduced graphene oxide screen-printed electrodes, Carbon (2021), **https://doi.org/10.1016/j.carbon.2021.04.074**

3. Ahmed Suhail, Genhua Pan, **Jagriti Sethi** and Mina Safarzadeh, Label-free electrochemical biosensor for the detection of bodyfluid based biomarkers, patent application number: EP20217463.7

4. Kamrul Islam, Samar Damiati, **Jagriti Sethi**, Ahmed Suhail and Genhua Pan, Development of a Label-Free Immunosensor for Clusterin Detection as an Alzheimer's Biomarker, Sensors 2018, 18(1), 308, **https://doi.org/10.3390/s18010308**

5. Mina Safarzadeh, Ahmed Suhail, **Jagriti Sethi**, Anas Sattar and Genhua Pan, A label-free DNA-immunosensor based on functionalised rGO electrode for the quantification of DNA methylation, Nanomaterials 2021, 11(4), 985, **https://doi.org/10.3390/nano11040985**

6. Vikram Raghavan, Benjamin O Driscoll; J M Bloor; Bing Li; Prateek Katare; **Jagriti Sethi**; Sai Siva Gorthi; David Jenkins, Emerging graphene-based sensors for the detection of food adulterants and toxicants - A review, Food Chemistry 2021, Volume 355, 129547, **https://doi.org/10.1016/j.foodchem.2021.129547**

Presentations at conferences:

1. **11th International conference on genomics and pharmacogenomics**, Philadelphia (USA), September 2018

Title of the presentation: Graphene biosensors for label free detection of blood based biomarkers for Alzheimer's disease

2.**2nd world conference on analytical and bioanalytical chemistry**, Las Vegas (USA), July 2019

Title of the presentation: Graphene biosensors for label free detection of blood-based biomarkers for Alzheimer's disease

3. **PhD micro and nano sensors summerschool**, Copenhagen (Denmark), August 2019

Title of the poster: Electrochemical sensors for the label-free detection of Alzheimer's disease biomarkers

4. **2nd world summit on advances in science, engineering and technology**, Indianapolis (USA), October 2019

Title of the presentation: Label-free detection of beta amyloid from plasma using improved graphene screen-printed electrodes

5. **International virtual conference on advanced nanomaterials**, June 2020

Title of the presentation: Dual-layer graphene and reduced graphene oxide biosensor for label-free detection of beta-amyloid

6. **30th Alzheimer Europe Conference**, October 2020

Title of the presentation: Emerging technologies for AD: from novel detection protocols to business models

7. **Biosensors**, July 2021

Title of the poster: Highly sensitive and label-free detection of beta amyloid biomarkers with a novel linker based electrochemical biosensor

A list of the BBDiag network training events is provided below. The title of oral presentation in these events were: 'Graphene based biosensors for the detection of blood based biomarkers of Alzheimer's Disease'

1. **Multidisciplinary Foundation Courses for Alzheimer's Disease (AD) Diagnosis**, Swansea (Wales,UK), September 2017

2. **Blood Biomarker-based Diagnostic Tools for Early Stage Alzheimer's Disease**, Rome (Italy), March 2018

3. **China-Europe Alzheimer's Disease Symposium: Biomarkers and early diagnosis**, Beijing (China), May 2018

4. **Residential workshop on Innovation and entrepreneurship**, Madrid (Spain), October 2018.

5. **BBdiag summer school**, Rostock (Germany), June 2019

6. **Biomarkers for Alzheimer's disease early diagnosis, communication in science and ESR career development**, Milan (Italy), October 2019

Word count for the main body of this thesis: **27417**

Signed: Jagriti Sethi

Date: 18-03-2022

Abstract

Graphene based electrochemical biosensors for the detection of blood biomarkers of Alzheimer's disease
by **Jagriti Sethi**

Alzheimer's disease (AD) is a neurodegenerative disorder that affects millions of people around the world with no available treatments to cure, reverse or even slow down the disease progression. Detection of AD in the early stages, before the massive neuronal loss, is key to developing disease modifying treatments and preventive strategies. The current AD diagnosis is largely based on evaluation tests such as Mini-Mental State Examination (MMSE), imaging techniques such as Magnetic Resonance Imaging (MRI), Positron Emission Tomography (PET), and postmortem autopsies. It is expensive and only available at the later/severe stages when the brain of the patient is already damaged or after the death of the patient. Cerebrospinal fluid (CSF) tests have the ability to identify earlier stages with the help of certain biomarkers but large scale use is often limited by invasive CSF collection protocols.

This study is a part of Blood Biomarker-based diagnostic tools for Alzheimer's disease (BBDiag) network. It is aimed at developing graphene based electrochemical biosensors for the detection of blood biomarkers as blood sampling is far less complex, minimally invasive, and cheaper compared to CSF sampling. Electrochemical biosensors are extremely advantageous for biomarker detection. This is due to their rapid response (fast analysis with results available in a few minutes), portability (home testing of diseases), cost-effectiveness (inexpensive analysis which allows the possibility of large scale implementation, particularly to low-income communities with no access to sophisticated instrumentation such as MRI/PET scanners), easy handling (user friendly with easy to understand results) and disposability (single use sensors with no requirement for maintenance). Using graphene as a base material helps in improving the sensitivity of these biosensors as the absence or presence of very few analyte molecules can trigger a recognisable change in its electrical properties.

In this work, two label-free graphene based electrochemical biosensors have been developed and validated with well-known biomarkers, Aβ. The first biosensor is a graphene/ reduced graphene oxide (rGO) dual-layer biosensor for the detection of Aβ_{1-42}. The dual-layer is obtained by modifying graphene screen printed electrodes (SPEs) with electrochemically reduced rGO. The dual-layer is further modified with 1-pyrenebutyric acid N-hydroxysuccinimide ester (Pyr-NHS) linker, which attaches non-covalently via $\pi - \pi$ stacking on the surface of rGO and facilitate the immobilisation of antibodies. The surface characterisation is achieved using various techniques including Raman spectroscopy, X-ray photo electron spectroscopy (XPS), scanning electron microscopy and cyclic voltammetry. Differential pulse voltammetry is used to evaluate the analytical performance of the biosensor. The limit of detection (LOD) is found to be 2.4 pM over a linear range of 11 pM to 55 nM. The biosensor depicts high selectivity for Aβ_{1-42} in the presence of Aβ_{1-40} and ApoE ϵ4 species. This is an important requirement for reliable detection from biofluids as these interfering species can be present in excess. The graphene/rGO dual-layer biosensor shows this improvement over existing Aβ

biosensors that fail to distinguish between $A\beta_{1-40}$ and $A\beta_{1-42}$. It was employed for the detection of spiked human and mice plasma samples. The sensing results obtained from an age-based study of mice samples revealed a decrease in the plasma levels of $A\beta_{1-42}$ with a progression of AD from 9 months to 12 months. This is correlated to the increased $A\beta$ plaques in the brain of 12 months old mice as revealed by immunohistochemistry and magnetic resonance imaging data.

The second biosensor is based on an amine (NH_2) functionalised rGO SPE for the detection of both $A\beta_{1-40}$ and $A\beta_{1-42}$. NH_2 linkers are predominantly attached on the edge and defect sites of rGO SPE via chemisorption as revealed by XPS, FTIR, and Raman analysis. LOD of the biosensor is calculated to be of 9.51 fM over a linear range of 10 fM-10 pM for $A\beta_{1-40}$ and 8.65 fM over a linear range of 10 fM-50 pM for $A\beta_{1-42}$. This is the lowest reported LOD by a label-free graphene biosensor. This improvement in sensitivity is attributed to higher antibody binding sites on the surface provided by the NH_2 linker. In addition, the biosensor depicts excellent selectivity in the presence of interfering $A\beta$ and ApoE $\epsilon 4$ species. It is also successfully validated with spiked human plasma within its linear range. Therefore, both graphene/rGO and rGO/NH_2 biosensors show potential to be developed into point of care technologies to provide rapid, sensitive and selective detection of blood-based AD biomarkers. Due to the difference in the sensitivity of the two biosensors, they can be applied for the detection of different biomarkers (depending on their concentration in plasma) or one biomarker in different stages of disease progression. However, further validation with clinical samples is needed before they can be developed into commercial devices for minimally invasive and time-efficient routine screening of AD.

List of Abbreviations

ACh Acetylcholine.

AChE Acetylcholinesterase.

aCSF Artificial CSF.

AD Alzheimer's disease.

AgNPs Silver nanoparticles.

ALP Alkaline phosphatase.

ap aminophenol.

APMES 3-Aminopropyl triethoxysilane solution.

ApoE Apolipoprotein E.

APP Amyloid precursor protein.

Au Gold.

AuNPs Gold nanoparticles.

AuNWs Gold nanowires.

BBB Blood brain barrier.

BSA Bovine serum albumin.

Cab Capture antibody.

CE Counter electrode.

ChO Choline oxidase.

CNTs Carbon nanotubes.

CRP C- reactive protein.

CSF Cerebrospinal fluid.

Cu-MOF Copper metal organic framework.

CV Cyclic voltammetry.

Dab Detection antibody.

DI Deionised.

DPV Differential pulse voltammetry.

EDC 1-ethyl-3-(3-dimethylaminopropyl)carbodiimide hydrochloride.

EIS Electrochemical impedance spectroscopy.

ELISA Enzyme-linked immunosorbent assay.

FTIR Fourier Transform Infrared Spectroscopy.

GC Glassy carbon.

GLA Glutaric dialdehyde.

GO Graphene oxide.

GQDs Graphene quantum dots.

GSHs Graphene@mesoporous silica hybrids.

HRP Horseradish peroxidase.

IHC Immunohistochemistry.

IHC Immunohistochemistry.

ITO Indium tin oxide.

LOD Limit of detection.

LSV Linear sweep voltammetry.

MB Methylene blue.

MBs Magnetic beads.

MHA Mercaptohexanoic acid.

MIPs Molecular imprinted polymers.

MMSE Mini-mental state examination.

MOFs Metal organic frameworks.

MPA Mercaptopropionic acid.

MRI Magnetic resonance imaging.

MS Mass Spectrometry.

MV Methylviologen.

$NaBH_4$ Sodium borohydride.

NFL Neurofilament light.

NFTs Neurofibrillary tangles.

NHS N-hydroxysuccinimide.

PBS Phosphate buffered saline.

PbS Lead(II) sulfide.

PCR Polymerase chain reaction.

PEDOT Poly(3,4-ethylenedioxythiophene.

PEG Polyethylene glycol.

PET Positron emission tomography.

PGE Pencil graphite electrode.

POC Point of care.

pPG Trimethylolpropane tris[poly(propyleneglycol)].

Pt Platinum.

PTSA 1,3,6,8-pyrenetetrasulfonic acid.

PVP-CHO Polyvinyl pyrrolidone-aldehyde solution.

Pyr-NHS 1-pyrenebutyric acid n-hydroxysuccinimide ester.

QDs Quantum dots.

RE Reference electrode.

rGO Reduced graphene oxide.

RT room temperature.

SAMs Self-assembled monolayers.

SCAP Signal cancellation and amplification processing system.

SEM Scanning electron microscope.

SEM Scanning electron microscopy.

SERS Surface Enhanced Raman Spectroscopy.

SIMOA Single molecule array.

SPE Screen printed electrode.

SPEs Screen printed electrodes.

SPR Surface Plasmon Resonance.

SWV Square wave voltammetry.

TERS Tip-Enhanced Raman Spectroscopy.

Tg Transgenic.

WE Working electrode.

WOR Water oxidation reaction.

WT Wildtype.

XPS X-ray photoelectron spectroscopy.

XPS X-Ray photo electron spectroscopy.

ZIF Zinc zeolite imidazole framework.

Zn Zinc.

Contents

List of Figures

List of Tables

Chapter 1

Introduction

Dementia is an age-related clinical syndrome, which is characterized by progressive decline in cognitive functions including memory, thinking, language, orientation, learning capacity and judgement (Duthey (2013)). Dementia can reduce a person's ability to perform everyday activities leading to an increased dependency on informal and professional care (Chertkow et al. (2013)). Alzheimer's disease (AD) is one of the most common causes of dementia in older adults contributing to 60-70% of all cases (Liang et al. (2010)). It affects more than 30 million people around the world, out of which 60% patients are from low or middle income countries (Duthey (2013); Zhou & Ashford (2019)). With the average course of disease being 8-12 years and final years demanding around the clock care, the total cost of dementia was estimated to be US $1 trillion in 2018 and is expected to double by 2030 (Zhou & Ashford (2019)). It is not only burdensome to the patients, but also their families and caregivers (Mokdad et al. (2018)). Despite the huge socioeconomic burden, AD is the only major disease with no effective treatments to cure, reverse or even slow down disease progression (Zhou & Ashford (2019)). The major reason being that the current AD diagnosis is available in later/severe stages when brain of the patient is already damaged (Zhao et al. (2015)). For instance, the most commonly used cognitive test, mini mental state examination (MMSE), is based on clinical symptoms that appear after the irreversible neuronal damage has occurred in patients (Arevalo-Rodriguez et al. (2015)). Another commonly used definitive test is a postmortem autopsy to confirm the presence of senile plaques along with neurofibrillary tangles (NFTs), which are hallmarks of AD (Zhao et al. (2015); Zhou & Ashford (2019)). These autopsies are very common as an estimated 50% of patients are not diagnosed during their lifetime in developed countries (Connolly et al. (2011)). This number is even higher

in developing countries (Zhou & Ashford (2019)).

In the past decade, significant efforts have been made by researchers around the world, to understand AD pathogenesis for developing reliable disease diagnoses. Studies reveal that disease pathology starts years to decades before the initial symptoms surface i.e. there is a long preclinical phase followed by an early clinical phase with mild dementia before preceding to a fully manifested dementia stage (Albert et al. (2011); Sperling et al. (2011); Jack Jr et al. (2018)). The detection of pathological changes in early stages (preclinical and/or early clinical phase) is the key for developing disease modifying treatments or even cure (Zhou & Ashford (2019)). For this purpose, several techniques based on cerebrospinal fluid (CSF) and imaging biomarkers have been identified. However, the use of expensive instruments for imaging such as positron emission tomography (PET) scanners and invasive CSF collecting protocols, often create barriers in clinical implementation (de Almeida et al. (2011); Henriksen et al. (2014)). AD is a global health concern with more than half of the cases from low or middle income countries, which may not have access to sophisticated CSF sampling or imaging techniques (Blennow (2010)). In this regards, techniques based on blood biomarkers appear to be the best choice for early diagnosis of AD (Henriksen et al. (2014); Zhao et al. (2015)). Firstly, because blood sampling is minimally invasive, far less complex, and cheaper to obtain than CSF sampling. Secondly, CSF/imaging based methods perform well in controlled clinical settings but their application to communities is still questionable and thus, a standard blood-based test can be very useful (Henriksen et al. (2014)). As a result, blood-based platforms which are rapid, sensitive, reliable, and cost-effective are required to develop routine screening tools.

1.1 Need for biosensors

Biosensors are emerging technologies and provide simple yet effective way of detecting disease biomarkers. In particular, electrochemical biosensors are dominant in AD research (Wang et al. (2017); Hassan & Kerman (2019)). This is attributed to their rapid response (Li et al. (2016)), portability (Liu et al. (2018)), inexpensiveness (Li et al. (2016)), easy handling and disposability (Lien et al. (2015)). However, existing biosensors (Lien et al. (2015); Yoo et al. (2017a); Le et al. (2019a)) display drawbacks such as insufficient sensitivity, non-specific bindings, labor intensiveness and/or need for complicated instrumentation

for real-time detection (Hassan & Kerman (2019); You et al. (2020)) which creates barrier in developing routine screening tools that can identify preclinical stages of AD. Therefore, it is necessary to develop biosensors that provide equal or higher sensitivity to the existing tools but with simpler instrumentation and/or easy handling. In case of blood biomarkers, detection is even more challenging owing to the presence of blood brain barrier (BBB) (Henriksen et al. (2014)). The BBB restricts the exit of molecules such as proteins from the brain and only small size fragments can pass the barrier, which results in very low concentrations (fM-nM) in the blood (Patel et al. (2011); Hanon et al. (2018); Chen et al. (2019)). For this reason, there is an urgent need to improve the sensitivity, reliability and cost-effectiveness of the AD biosensors for wide clinical implementation.

Recent advances in nanotechnology has added a new dimension to the field of electrochemical biosensors (Yogeswaran & Chen (2008)). Several nanomaterials such as metal nanoparticles, graphene, carbon nanotubes (CNTs) etc. can improve the sensitivity of biosensors (Kuila et al. (2011); Sun et al. (2018)). Since the discovery of graphene in 2004, it has been attracting enormous attention due to remarkable properties such as high electrical conductivity (Islam et al. (2017)) that leads to high signal response of biosensors, (Kuila et al. (2011)) and large surface to volume ratio that leads to higher active sites for improved immobilisation/interaction of molecules (Li et al. (2015); Shahdeo et al. (2020)). Graphene biosensors are capable of detecting a tremendously low concentration of biomarkers. This is due to the fact that absence or presence of very few analyte molecules can trigger a recognisable change in electrical properties of graphene (Balasubramanian & Kern (2014)). One of the derivatives of graphene, reduced graphene oxide (rGO), is also preferred as a sensing material. It is structurally similar to graphene with additional electroactive sites and few oxygen functionalities (Gómez-Navarro et al. (2007); Li et al. (2015)). These structural defects in rGO provide ease of surface functionalisation along with a high electron transfer rate (Li et al. (2015)). Both graphene and rGO show remarkable electrochemical performance in comparison to other materials such as glassy carbon, graphite, and CNTs (Yang et al. (2010a)). In addition, graphene provides consistent signal amplification which is not the case with metal nanoparticles (Kuila et al. (2011)). Hence, graphene based electrochemical biosensors can provide highly sensitive and rapid detection of blood-based AD biomarkers. Also, these can be easily integrated into point of care (POC) technology (Kampeera et al. (2019)) for routine screening of AD patients.

1.2 Aim and outline of thesis

This study is a part of **BBDiag** network, which stands for **B**lood **B**iomarker-based **diag**nostics tools for early stage Alzheimer's disease. The network is focused on developing minimally invasive, highly sensitive and inexpensive clinically applicable diagnostic tools for detection of early stage blood-based biomarkers of AD. As a part of the network, this research aims to develop biosensors based on graphene and its derivatives for highly sensitive and selective detection of blood biomarkers. To achieve that, a detailed review is carried out on the state-of-the-art electrochemical biosensors. It supports the development of novel biosensors to overcome the existing issues in the reported platforms. To fabricate biosensors with improved sensing performance, two novel structures are developed and validated with a candidate AD biomarker called beta amyloid. The thesis is divided into two distinct parts. The first part is background section in Chapter 2 that presents literature review on the state-of-the art AD diagnosis, electrochemical biosensors and graphene technology. The second part is the experimental section in Chapter 3 and 4 with details of the experiment, fabrication process and results obtained for the developed biosensors.

The outline of the thesis is as follows:

Chapter 2 reviews state-of-the-art AD diagnosis, presenting information about the well-known biomarkers, available technologies for their detection and importance of blood-based diagnosis. Then, it highlights the importance of bio-sensing technology as an alternate tool for the detection of various AD biomarkers. Electrochemical biosensors are explained in detail with their structure, sensing mechanism, parameters and advantages with a comprehensive review on current state-of-the-art. Subsequently, it reviews the graphene in all aspects including its structural, physical/ chemical properties, types of functionalisation and application in biosensors.

Chapter 3 presents the experimental and characterisation techniques used for the developed biosensors. It includes the details of the fabrication process, optimisation experiments and blood sampling. It also discusses the experimental set up and working mechanism of various characterization techniques such as Electrochemical technique, Raman spectroscopy, X-ray Photo electron Spectroscopy (XPS), Scanning Electron Microscopy (SEM), Immunohistochemistry (IHC), Fourier transform infrared

spectroscopy (FTIR) and Magnetic resonance imaging (MRI).

Chapter 4 presents result for the assembly and characterization of the two biosensors: a graphene/rGO dual layer and an aminated rGO electrode. It discusses their surface chemistry in detail. It presents the optimisation results of experimental conditions to attain the best sensing performance. Subsequently, it discusses the results for analytical performance of the biosensors and quantitative parameters, such as dynamic range, limit of detection (LOD) and specificity. Lastly, it presents the validation results obtained using spiked human and mice plasma.

Chapter 5 summarises major progress as well as results of this work highlighting the contribution to knowledge and proposes future work that is needed to further improve the biosensing technology for detection of other blood biomarkers.

Appendix A presents the list of journal publications; appendix B presents a list of all the conferences and network events attended as a part of this project along with titles of the presentations and lastly appendix C contains a list of all the materials used in this work.

Chapter 2

Background

2.1 State-of-the-art AD diagnosis

2.1.1 Biomarkers of AD

The recent trends in medical science explores the molecular principles of diseases instead of following a symptomatic approach (Balasubramanian & Kern (2014)). A similar trend is observed in AD, where a significant research is underway to develop effective screening tools for identifying high risk individuals or patients in asymptomatic or early stages. This is the best approach to combat AD, before the occurrence of massive irreversible neuronal loss (Crous-Bou et al. (2017)). As a result, extensive biomarker studies have been conducted because these are crucial for understanding the early phases of the disease (Hampel et al. (2018); Zhou & Ashford (2019)). In definition, biomarkers are quantifiable indicators of a pathological condition or a biological state and are useful in confirming diagnosis, predictive testing and monitoring disease progression (Ronald et al. (1998)). Abnormal amounts of specific biomarkers in body fluids can be linked to AD progression, some of which are stated below:

1. **Amyloid beta (Aβ)**: It is responsible for the senile plaques, which are present in the brain of AD patients (Growdon (1999)). Senile plaques are extracellular deposits, resulting from the accumulation and aggregation of Aβ fragments (Shoji et al. (1992); Growdon (1999); Hardy & Selkoe (2002)). These plaques obstruct the normal functioning of neurons leading to cell death, cognitive dysfunction and behavioral abnormalities. In addition, they also initiate inflammation and tau aggregation as NFTs (Murphy & LeVine (2010);

Prabhulkar et al. (2012)). The Aβ peptides are generated via proteolytic pathway using amyloid precursor protein (APP) and are usually present in small amounts in a normal functioning brain (Shoji et al. (1992); Santin et al. (2016); Hwang et al. (2019)). However, some toxic species such as $A\beta_{1-40}$ and $A\beta_{1-42}$ rapidly aggregate into neurotoxic oligomers, which accumulate to form fibrils, leading to the formation of amyloid plaques in the brain, causing AD (Tanzi et al. (1996); Prabhulkar et al. (2012); Eisele (2013)). Nonetheless, these toxic forms of Aβ could be detected before the formation of plaques and provide important biochemical information related to the different stages of disease progression (Yoo et al. (2017b)). Currently, there is a growing potential of plasma Aβ ratios as an AD biomarker in diagnostics, prognostics and therapeutic research (Blennow (2004); Hampel et al. (2010); Nakamura et al. (2018)). The biochemical levels of Aβ in bio-fluids is low (fM-nM), depending on their monomeric and oligomeric forms (Hölttä et al. (2013)). It results from the retention of these proteins in plaque-laden tissues in brain and makes the detection process difficult (Hölttä et al. (2013)). Therefore, ultra sensitive tools operating in fM ranges are required to accurately identify AD patients (Park & Kim (2021)).

2. **Tau**: It promotes the stabilization of microtubules, regulation of transport of vesicles or organelles, supports out-growth of axons and lastly, acts as an anchor for the enzymes (Mandelkow (1999)). When tau becomes abnormally hyper-phosphorylated, its affinity for microtubules is weakened. As a result, it detaches and aggregates forming abnormal filaments leading to formation of NFTs that causes neurodegeneration (Vestergaard et al. (2008); Petry et al. (2014)). The concentration of tau is found to be slightly higher in AD patients than normal cohorts. It is found amongst the fM ranges of healthy individuals' peripheral blood (Kim et al. (2016)) whereas it is slightly increased in AD individuals, ranging from 0.11 to 0.25 pM (Zetterberg et al. (2013)). Tau levels are slightly higher in CSF and a clinical cut- off value of 4.3 pM in is capable of differentiating AD individuals from healthy controls (Sunderland et al. (2003)). A recent study conducted by Janelidze et al. (2021) used the plasma cut- off levels of 0.032 pM for phospho-tau 217 to identify the early stages of AD. Plasma phospho tau 217 has also been shown to distinguish AD from other neurodegenerative disorders with high diagnostic accuracy. It has been correlated to the buildup of amyloid plaques in the brain as measured by PET scan, highlighting its potential as an important biomarker of AD (Palmqvist et al. (2020)). However, possible bias and heterogeneity exists for plasma tau between various studies with some reporting a decrease (Sparks et al. (2012); Krishnan & Rani (2014)) and no change in AD patients (Wang

et al. (2014)), attributed to the sensitivity of the analytical method used for measurement (Shanthi et al. (2015)).

3. **Apolipoprotein E (ApoE)**: It is a glycoprotein associated with lipid metabolism (Mahley (1988). Being polymorphic in nature, gene coding of ApoE generates three major isoforms in humans, namely E2, E3 and E4 from alleles $\epsilon 2$, $\epsilon 3$, and $\epsilon 4$ respectively, combined in six different genotypes. These isoforms differ from each other based on the amino acid residues at sites 112 and 158. E3 is a commonly occurring isoform of ApoE with site 112 occupied by cysteine and 158 occupied by arginine whereas E2 and E4 isoforms have cysteine and arginine occupying the two positions respectively (Utermann et al. (1980). E4 isoform is a substantial genetic risk factor for AD, high cholesterol as well as coronary heart diseases (Mayeux et al. (1998); Lahoz et al. (2001); Calero et al. (2018)). Also, research shows that individuals with ApoE $\epsilon 4$ carriers have higher Aβ levels in the brain and low bio-fluidic levels of $A\beta_{1-42}$, both of which are associated with AD (Sunderland et al. (2004); Morris et al. (2010); Berkowitz et al. (2018)). Furthermore, it is also found to modulate tau pathology in mice from an early age ultimately leading to tau induced neurotoxicity (Shi et al. (2017)).

4. **Other biomarkers**: Some other biomarkers and their role in AD pathogenesis are described below in table 2.1 and table 2.2:

Biomarkers	Role in AD pathogenesis	References
Clusterin (Apolipoprotein J)	It binds to hydrophobic residues on the misfolded and aggregated Aβ proteins and toxic oligomers preventing their further aggregation. It reduces the toxicity by stabilising the structures into less toxic aggregates and hence, is often elevated in AD patients.	Oda et al. (1995); Poon et al. (2002); Islam et al. (2018); Oh et al. (2019)
miRNA	MicroRNA (miRNA) is a 22 nucleotide long non-coding RNA molecule which regulates 60% of all known genes. Its dysregulation in peripheral blood is an indicative of AD pathology and other brain related disorders. The blood of AD patients depict down-regulation of miR-9, miR-29a/b, miR-137 and miR-181c compared to their healthy counterparts.	Schipper et al. (2007); Geekiyanage et al. (2012); Leidinger et al. (2013); Ha & Kim (2014); Sharma & Singh (2016);

Table 2.1: AD biomarkers and their role in disease pathogenesis (1/2)

Biomarkers	Role in AD pathogenesis	References
C- reactive protein (CRP)	It is usually synthesized by liver in case of infections, acute injury or other inflammatory stimuli. It is associated with the formation of both senile plaques and NFTs. Recent research shows an age dependent association of CRP (adverse for 60-70.5 years and inverse for $\geqslant$70.6 years) with development of AD. Additionally, CRP levels of AD patients are lower than normal cohorts.	Iwamoto et al. (1994); Duong et al. (1997); O'Bryant et al. (2010); O'Bryant et al. (2013); Gabin et al. (2018)
Neurofilament light (NFL)	It is a 68 kDa protein chain which is a major component of axonal cytoskeleton. In case of AD, there's axonal damage leading to the release of the NFL molecules into the body fluids. Therefore, an elevated levels of NFL are observed in the AD patients compared to normal cohorts.	Sjögren et al. (2000); Van Geel et al. (2005); Kuhle et al. (2016); Steinacker et al. (2017); Lewczuk et al. (2018)
Unfolded p53	It is a multi-functional protein that maintains genomic integrity and prevents tumour growth in case of a genotoxic stimuli by generating antioxidant behavior to eliminate oxidative stress. Several studies have shown the potential of unfolded p53 as a potential AD biomarker as it is found in a much higher amount in the fibroblasts of AD patients compared to their healthy counterparts	Stanga et al. (2010); Buizza et al. (2013); Amor-Gutiérrez et al. (2020)
Acetylcholine (ACh)/ Acetylcholinesterase (AChE)	ACh is an organic chemical and a neurotransmitter, which is secreted by the nerve cells to send the electrical impulses to different cell types. Both ACh and its metabolite choline play a significant role in brain functions including learning, memory and attention. ACh is also a neuromodulator in central and peripheral nervous system. AChE is a crucial enzyme, which catalyzes the hydrolysis of ACh and its abnormal functioning can promote Aβ aggregation in the brain. Therefore, both AChE and ACh are associated with neuronal disorder that leads to AD.	Chauhan & Pundir (2014); Chauhan et al. (2017); Panraksa et al. (2018)

Table 2.2: AD biomarkers and their role in disease pathogenesis (2/2)

It is also worth mentioning that various factors can have an impact on the biomarker levels leading to variability between different studies. Some of these factors include selection criteria for subjects, time of day for collection of samples, storage and shipping methods, assay kit handling and storage, assay optimisation methods, handling of lab equipment

etc (Blennow et al. (2015)). Due to this, there is high variability between the cut-off values of biomarkers in different studies and most laboratories use internally qualified cut-off values based on their measurement and study design (Mattsson et al. (2013)).

2.1.2 Conventional analytical techniques

Numerous techniques have been identified in the past decade to detect various AD biomarkers. Among them, enzyme-linked immunosorbent assay (ELISA) is commonly used for clinical detection (Mobed & Hasanzadeh (2020)). It is conducted in 96-well plates (reaction chambers) and allows measurement of multiple samples at the same time. The target biomolecule in the sample is detected with the help of specific capture antibody attached on the plate. Then, a secondary antibody labelled with an enzyme is added, which binds to the already bound target followed by addition of an enzyme substrate. The substrate is converted into a coloured product whose intensity corresponds to the concentration of target biomolecule. The technique provides high selectivity and is easy to perform with a simple protocol (Mayeux et al. (1999); Sakamoto et al. (2018)). However, it offers insufficient detection sensitivity (pM range), as several AD biomarkers are present in extremely low concentrations (fM range) in bio-fluids (Rissin et al. (2010); Hölttä et al. (2013)). In addition, it is time consuming, requiring up to two days for a standard test and utilises large volume of reagents (Hölttä et al. (2013)). Digital ELISA is a promising methodology that provides a thousand fold better detection sensitivity than a conventional ELISA (Rissin et al. (2010); Toppi et al. (2021)). A digital assay is achieved by microcompartmentalisation with the use of micrometer-sized reactor arrays in the form of wells or droplets, which leads to concentration of reaction products in small volumes and isolation of single molecules in each partition. In digital ELISA, beads are used as solid support for the immune reactions and are loaded into microwells for detection of binding event or a chip is used as solid support for formation of immunocomplexes as in the case of microdroplet arrays (Toppi et al. (2021)). Measurement is independent of the intensity of color (unlike conventional ELISA) and simply relies on the presence or absence of it (i.e. a signal/no signal readout) based on the presence or absence of target molecule. Single molecule array (SIMOA) technology by Quanterix is an example of bead based digital ELISA, which has now been developed for several AD biomarkers with excellent sensitivity (aM range) (Zhou et al. (2017); Hwang et al. (2019); Wu et al. (2020)). Target proteins are captured using specific antibodies conjugated with paramangnetic

beads followed by reaction of resulting complex with detection antibodies conjugated with enzymes. Beads are then confined in an array of fM sized microwells with either zero or one bead per well. After that, the wells are sealed in the presence of a fluorogenic substrate, which serves as label and only gets activated when the enzyme is present. The presence or absence of target protein is measured with a signal or no signal readout respectively (O'Connell et al. (2020)). The fM sized reaction chambers allows rapid build up of fluorescent product when the labeled protein is captured, which leads to a bright signal that can be readily observed (Hwang et al. (2019); Macchia et al. (2020)). Concentration of biomarker in a sample is estimated by counting the number of the active (signal-emitting) spots (Kim et al. (2012); Macchia et al. (2020)). Nonetheless, it is labour intensive and requires expensive instrumentation/set-up. Recently, Surface Enhanced Raman Spectroscopy (SERS) and Tip-Enhanced Raman Spectroscopy (TERS) have also been employed for the analysis of AD biomarkers. Bonhommeau et al. (2017) used TERS to distinguish between $A\beta_{1-42}$ fibrils and its highly toxic oligomeric form based on the amide bonds present in the two molecules at a nano meter scale. This can be useful for the detection of pathological species in neurons. However, their is a high risk of damaging the biological sample in high laser Gao et al. (2018). Demeritte et al. (2015) developed a nano platform based on core-plasmonic shell nanoparticles and graphene oxide to achieve SERS identification of $A\beta_{1-42}$ at even 11.07 fM. Despite the high sensitivity, SERS can also lead to sample degradation and rely on expensive Raman spectrometers.

Mass spectrometry (MS) is another method for the quantification of biomarkers, which measures the mass to charge ratio of ions in a complex media (Gross (2006)). Various methodologies have been developed over the last decades to enhance the sensitivity of MS (Hale (2013)). MALDI-TOF MS is a commonly used technique where a matrix assisted laser desorption/ionization (MALDI) is used as an ionisation source and a time of flight (TOF) analyser is used for mass analysis. In this technique, a laser pulse is directed onto a spot on the target where the analyte is embedded inside a matrix. The matrix molecules get ablated from the surface by absorbing laser energy and carry the embedded analyte (ionises during ablation) in the gas phase towards a detector. The mass of the ions determine the time of their flight across a path of known length, with the lighter ones arriving earlier at the detector than the heavier ones (Boesl (2017)). Despite the high throughput applications, MALDI-TOF requires complicated instrumentation, extensive sample preparation and sample cleanup prior to analysis. Immunoprecipitation coupled

MS (IP-MS) is also commonly used for biomarker analysis. It was recently employed by Nakamura et al. (2018) for the detection of Aβ biomarkers. In this technique, an antibody-antigen interaction is used to isolate the proteins from biological samples. The antibody-protein complex is then captured by antibody biding proteins attached to agarose or magnetic beads after which the target protein is eluted for further analysis (Hale (2013)). However, IP-MS requires extensive sample preparation, higher amount of reagents and may not be able to detect the low affinity protein interactions (Hale (2013)). This creates barrier in applying MS to global communities as a routine screening tool because of limited or no access to the sophisticated instrumentation and/or expert personnel. Portable hand-held MS tools such as one developed by Yang et al. (2008) may be able to overcome some of these limitations.

A brief summary of conventional analytical techniques for detection of AD biomarkers is provided in table 2.3 and 2.4, along with their advantages and disadvantages:

Techniques	Advantages	Disadvantages	LOD	References
Traditional ELISA	Simple operation, High selectivity	Time consuming, Large volume of reagents, Insufficient sensitivity, False positives, Requires expensive labels	46.52 pM*	Mayeux et al. (1999); Verwey et al. (2009); Lee et al. (2010); Nimse et al. (2016); Wang et al. (2017); Shui et al. (2018); Sakamoto et al. (2018)
SIMOA	High sensitivity and selectivity	Labour intensive, Requires expensive instrumentation and labels	9 fM*	Randall et al. (2013); Zhou et al. (2017); Hwang et al. (2019)
PET	Allows early detection of AD	Expensive, Poor spatial resolution, False positives, Invasive	-	Coleman (2007); Laurent et al. (2010); Shui et al. (2018)

* values have been converted from g.mL^{-1} to M

Table 2.3: Conventional techniques for the detection of AD biomarkers (1/2)

Techniques	Advantages	Disadvantages	LOD	References
Immunohistochemistry (IHC)	High sensitivity	Interpretation of data is often subjective, Variable antibody reactivity	-	Ramos-Vara (2005); Keene et al. (2018); Shui et al. (2018)
Magnetic resonance imaging (MRI)	High spatial resolution, Lack of ionizing radiation, Excellent soft tissue contrast	Expensive, Low scanning velocity	-	Laurent et al. (2010); Shui et al. (2018)
MS/ IP-MS/ MALDI-TOF	Acceptable sensitivity, Faster analysis	Requires advanced and expensive instrumentation, Extensive sample preparation	670 fM*	Hale (2013); Shui et al. (2018); Mobed & Hasanzadeh (2020); West et al. (2021)
Polymerase chain reaction (PCR)	Acceptable sensitivity	Requires advanced and expensive instrumentation, Labour intensive	100 copies.mL^{-1}**	Chen et al. (2005); Mobed & Hasanzadeh (2020); Arnaout et al. (2020)
Surface enhanced Raman spectroscopy (SERS)	High resolution, Speed of analysis	Requires Raman Spectrometers, Substrates degradation with time, Reproduciblity of signals	11.07 fM*	Chou et al. (2008); Demeritte et al. (2015); Mosier-Boss (2017)
Tip-Enhanced Raman Spectroscopy (TERS)	High resolution	Requires Raman Spectrometers, Sample degradation with time, time consuming	-	Bonhommeau et al. (2017); Gao et al. (2018); Lipiec et al. (2018) Ma et al. (2020)
Surface Plasmon Resonance (SPR)	High Sensitivity, Reusable sensor chips	Non-specific binding	860 fM	Helmerhorst et al. (2012); Kim et al. (2019); Špringer et al. (2020)

* values have been converted from g.mL^{-1} to M **for a biomarker with 9 copies.mL^{-1} to 2.5 billion copies.mL^{-1} in patient's sample

Table 2.4: Conventional techniques for the detection of AD biomarkers (2/2)

Some of the major drawbacks that create barriers for routine screening of biomarkers are: (1) high cost; (2) low sensitivity; (3) false positive results in case of ELISA and PET; (4) need for professional and skilled people; and (5) time consuming. Owing to these

limitations, conventional techniques can not be developed into routine methods for early stage AD diagnosis (Mobed & Hasanzadeh (2020)).

2.1.3 Importance of blood-based diagnosis

As mentioned above, abnormal levels of certain biomarkers are prevalent in the body fluids such as CSF and blood in asymptomatic/ early dementia phases of AD. Recently, CSF biomarkers have been made a part of AD detection parameters in clinical settings in many parts of the world due to their high accuracy (Zetterberg (2019)). This is attributed to the fact that CSF is in immediate connection with brain (interstitial fluid) through an unrestricted flow of proteins and can therefore, predict brain pathology accurately (Niemantsverdriet et al. (2017)). A combination of core CSF biomarkers such as $A\beta_{1-40}$, $A\beta_{1-42}$ and tau provides 85-95% sensitivity and selectivity for identifying AD in early dementia phases (Zetterberg (2017a); Zetterberg (2019)). These biomarkers are inexpensive, less challenging regards to infrastructure and are capable of showing early pathological alterations as opposed to neuroimaging biomarkers (Lewczuk & Kornhuber (2016)). However, the relative invasiveness of this method remains disputable and prevents long scale clinical implementation (Lewczuk et al. (2018)). Lumbar puncture (CSF sampling) process provides inconvenience for the subjects and can be quite challenging for repetitive monitoring, both of which are necessary aspects for developing routine screening tools (O'Bryant et al. (2017)). In this regard, blood-based biomarkers are extremely useful to develop inexpensive, targeted and relatively non-invasive screening tools for routine monitoring (Lewczuk et al. (2018)). This can revolutionize the way AD diagnostics is currently performed.

Detection of blood biomarkers is often challenging due to a plethora of reasons. The major reason is the extremely low concentration of the proteins in blood owing to the BBB, which restricts the exit of proteins from the brain (Henriksen et al. (2014)). Secondly, biomarkers such as $A\beta$ are also expressed in blood platelets as well as several tissues of the body. Therefore, it is difficult to determine if an altered concentration is due to the condition of the brain or secondary changes in the body. Additionally, blood contains high amounts of several proteins such as immunoglobulins and albumin, which can interfere with the detection process (Apweiler et al. (2009)). Lastly, the target biomarker may undergo degradation due to various enzymes present in blood, for instance tau protein has a very

short half-life (~ 10 hrs) in blood (Zetterberg (2017b)). These are the general considerations that need to be addressed when designing tests/assays for identification of blood-based biomarkers of AD.

Aβ proteins are one of the most important blood biomarkers of AD. Several independent studies have linked the plasma $A\beta_{1-42}$, $A\beta_{1-40}$ and their ratios with brain Aβ pathology (Zetterberg (2019)). Therefore, various analytical techniques such as conventional ELISA, SIMOA, MS etc. have been developed for their detection. As mentioned before, Nakamura et al. (2018) developed IP-MS technique to detect plasma Aβ ratio for predicting the amyloid PET positivity in cognitively normal, mild dementia and AD population with 90% accuracy. Similarly, Zetterberg et al. (2011) developed a digital ELISA for the detection of plasma $A\beta_{1-42}$ with high sensitivity. The matrix effect in plasma were reduced by diluting the sample to provide highly accurate results. Other AD biomarkers such as tau and NFL have also been properly validated and are found to be altered in AD patient (Zetterberg (2019)). SIMOA technology has emerged as gold standard for the ultra-sensitive detection of these biomarkers from blood (Randall et al. (2013); Gisslén et al. (2016)). Despite the effectiveness and sensitivity, the disadvantages of SIMOA and other conventional technologies prevent their clinical implementation as routine screening tools (Mobed & Hasanzadeh (2020)). Therefore, there is an immediate requirement for highly sensitive, rapid and inexpensive tools that allows AD diagnosis in the asymptomatic/early dementia stages.

2.2 Biosensors

2.2.1 Background

Biosensors are analytical devices for identifying the presence and levels of specific biomarkers and convert it into an output signal (Scheller & Schubert (1991)). These are rapidly emerging technologies in medical diagnostics to facilitate faster and efficient disease diagnosis, owing to their high performance, ability to measure in real-time and potential to be developed into a POC device (Baryeh et al. (2017); Mobed & Hasanzadeh (2020)). In recent years, biosensors have been able to achieve high sensitivity for the quantification of disease biomarkers (Malima et al. (2012)). They can detect extremely low amounts of target molecules, which is useful for early stage detection of diseases (Mobed

& Hasanzadeh (2020)). These advantages combined with simple operation, cost-effectiveness and reliability makes them a promising tool for the blood-based AD diagnosis.

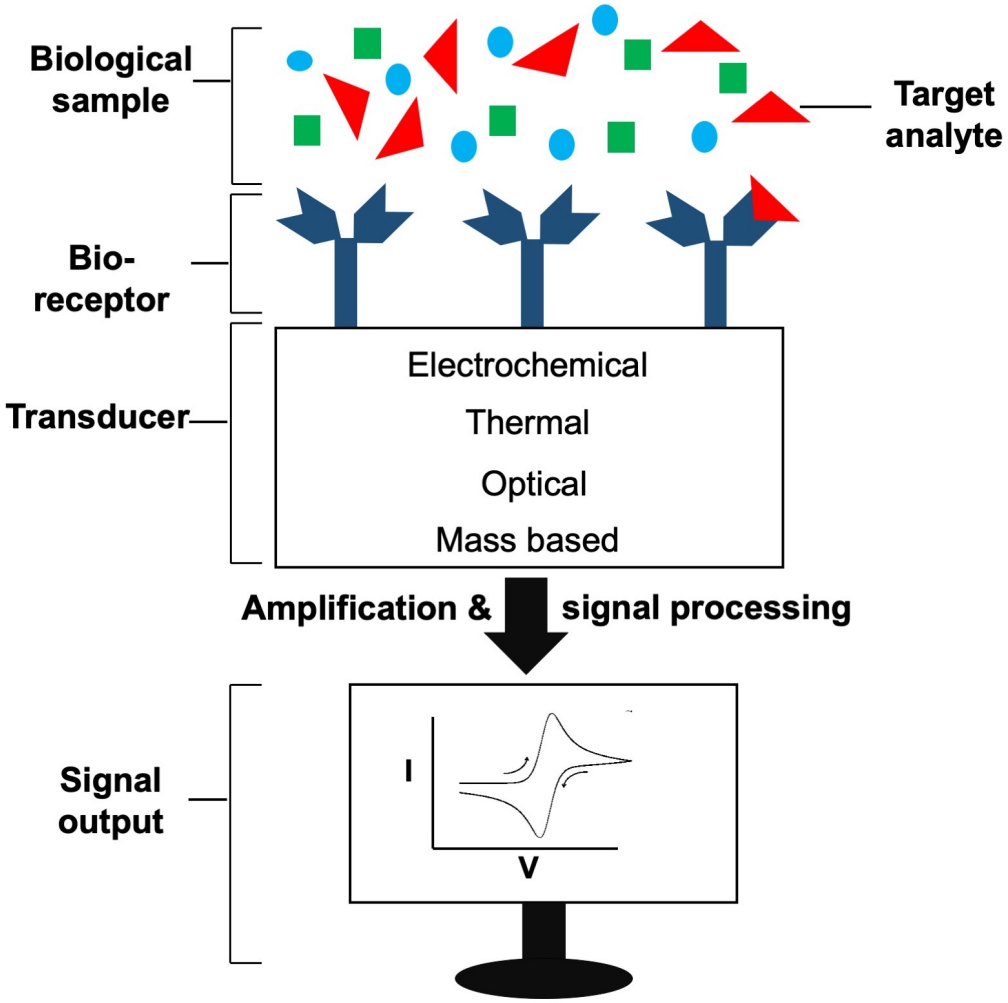

Figure 2.1: Schematic depicting working of a biosensor

A biosensor comprises of three elements as shown in figure 2.1: a bio-receptor (antibody, enzymes etc.) to recognize the target in biological samples, a transducer to convert this interaction into an electrical signal and a processing unit to process the transduced signal and display it in a user friendly manner (Scheller & Schubert (1991); Thévenot et al. (2001)). The presence of the bio-receptor element provides high degree of selectivity for the identification of target analyte, depending on their binding affinity (Thévenot et al. (2001)). Binding affinity is the strength of interaction between a biomolecule and its target, which can effect the performance of the biosensors. Equilibrium dissociation constant, K_D gives information about how much concentration of binder is required for a specific experiment and therefore is inversely related to its affinity for the target. It can be used to further calculate the 'on' and 'off' rate of a reaction, which is how

quickly the binder associates or dissociates from its target (Fei et al. (2011)). In the present study, antibodies are used as binders, which interact with their target using various interactions such as electrostatic interactions, hydrogen bonds, van der Waals forces etc. Among these, electrostatic interactions have shown to be controlled by the manipulation of charged amino acid residues on the sensing surface (Lippow et al. (2007); Lawrence et al. (2007). This approach can be used to improve the binding affinity by generating charge attractions on the sensing surface (Yoshida et al. (2019)). Alternatively, selecting an existing binder, which has affinity above the detection threshold is also an adequate approach for biosensors (De Picciotto et al. (2014)).

Depending on the transduction mechanism, biosensors can be categorised into optical, electrical, resonant, thermal, electrochemical, mass based and ion-sensitive (Chaubey & Malhotra (2002a)). Among these, electrochemical biosensor are most commonly used for the detection of AD biomarkers (Toyos-Rodríguez et al. (2020)). Further categorisation is based on bio-receptors and includes: bio-catalytic and bio-affinity sensors (Ziegler & Göpel (1998)). In bio-catalytic sensors, the receptor elements are usually enzymes that recognizes the target and increases the reaction rate significantly, as opposed to the uncatalyzed reaction. This leads to the production of a detectable electroactive species. As an example, glucose sensor is a commonly used biosensor, in which glucose oxidase enzyme is immobilized on the sensor strip for monitoring of diabetes (Wang (2000)). Bio-affinity sensors are based on specific binding of the target analyte to the receptor such as antibody or oligonucleotides, which produces an electric signal corresponding to the concentration of analyte (Byrne et al. (2009)). The biosensors fabricated in this work fall under the category of electrochemical bio-affinity biosensors, where antibodies are attached onto the sensing surface for the detection of target species.

2.2.2 Characteristics of a biosensor

The performance of a biosensor is evaluated based on the following attributes:

1. **Selectivity**: It is one of the most important attributes of a biosensor. It is the ability of a sensor to detect only the target analyte from a mixed solution or media (containing contaminants and other biological species) with minimum interference. The selectivity of a biosensor is largely dependent on the bio receptors such as antibodies, enzymes, aptamers etc. Therefore, these receptors should have high affinity for the target biomarker

and only interact with them even if exposed to a mixed solution (Peveler et al. (2016); Nikhil et al. (2016)). It can be further improved by blocking the surface with proteins such as BSA to prevent non-specific adsorption and/or using selective membranes that can interact with and block the interfering species present in complex fluidic samples (Njagi & Kagwanja (2011). Selectivity is attained by independently measuring a target biomarker against an interfering biomarker under similar experimental conditions but with 1000 or 10,000 excess concentration of interfering species.

2. **Reproducibility**: It is defined as the ability of a biosensor to produce identical responses for the same experiment. It is based on the precision (ability to provide same results every time the same sample is measured) and accuracy (ability to provide mean value closer to the true value every time the same sample is measured) of the transducer and electronics. Therefore, it is highly affected by the electrode material and subsequent surface chemistry involved in the fabrication of a biosensor (Chen et al. (2020). Reproducibility is a measure of reliability and robustness of a biosensor (Nikhil et al. (2016)). Response from 3 consecutive experiments (n=3) were collected in this work to show the reproducibility of the data. In addition, normalisation of the current response was conducted to eliminate the effect of electrode to electrode variability on the performance.

3. **Linearity**: It is the ability of a biosensor to generate a signal which is proportional to the amount of the target present in the sample. It is a straight line represented by y= mx+c, where y is output signal, m is slope of calibration plot, x is concentration of target and c is the y-intercept point. More commonly, linear range is the term used for biosensors, which is the range of target concentration over which biosensor's response changes linearly with concentration (Nikhil et al. (2016)). R- squared or R^2 value explains the proportion of variance of the dependant variable (y) that can be explained using the independent variable (x). It is calculated by the following formula

$$[R^2 = 1 - S_R/S_T] \tag{2.1}$$

where S_R is the sum of the squares of residuals. Residuals are the deviation of the predicted values from the actual values. S_T is the total sum of squares and is defined as sum over all squared differences between the observations and the overall mean (Joe (2004). Better the fit of linear regression, closer is the value of R^2 to 1.

4. **Limit of detection (LOD)/ detection limit**: It is the lowest concentration or the minimum amount of target analyte, which produces a reliable signal change compared to a blank sample (absence of target analyte) (Armbruster & Pry (2008)). Most commonly used method of LOD estimation is by calculating 3σ (standard deviation of the lowest detected concentration) divided by the slope of the calibration plot (Armbruster & Pry (2008)). Value 3 is the signal/noise ratio and is usually considered when calculating the LOD of the biosensors. Lowest detected concentration is measured 10 times and the standard deviation is calculated. For example, if the value of standard deviation for 10 replicates of blank sample (normalised current value) is 0.0375 and the value of slope of the calibration plot is 0.013 then the value of LOD is 8.65. A good resolution is necessary to detect low concentrations of target over a wide dynamic range.

5. **Sensitivity**: It refers to the changes in output signals corresponding to the changes in target concentration. It is obtained by dividing slope of calibration plot (m) with area of the electrode. Sensitivity is different from limit of detection or LOD, which takes into account the blank/noise signal (Thévenot et al. (2001)).

In context of clinical studies, term sensitivity and specificity are used slightly differently (as defined below), however, for the present study only the above definitions (1-5) are relevant.

Sensitivity is defined as the probability of a test to identify true positives (only people who have the disease testing positive). Specificity is defined as the probability of a test to identify true negatives (people who do not have the disease testing negative). Other commonly used terms are positive and negative predictive values which are used to clinically tell how likely it is for a patient to have a specific disease. Positive predictive value (PPV) is probability that a positive test result means an individual truly has a specific disease whereas a negative predictive value (NPV) indicates that a negative test result means an individual truly does not have the disease. Therefore, sensitivity and specificity are a measure of accuracy of a test relative to a reference standard while PPV and NPV are a measure of effectiveness of a test for assessing people for having or not having the disease (Trevethan (2017).

2.2.3 Electrochemical biosensors

Electrochemical biosensors detect a target analyte in real time using a specific bio receptor coupled with an electrochemical transducer, which produces an electrochemical signal (Chaubey & Malhotra (2002b); Gill et al. (2019)). Many biosensors use electrochemical transducers due to portability, ease of use and simplicity of construction (Ronkainen et al. (2010)). They are widely accepted in clinical research with some of them having reached the commercial stage and are used for routine monitoring of biomarkers such as glucose (Huang et al. (2017)). This is attributed to their rapid response (Li et al. (2016)), cost effectiveness (Islam et al. (2018)), better sensitivity (Li et al. (2015)) and disposability (Lien et al. (2015); Kampeera et al. (2019)). The detection mechanism is based on electrochemistry, which associates the flow of electrons with the chemical changes (Elgrishi et al. (2018)). Electrochemical biosensors do not require large sample volumes and provide low detection limits by using as low as a single drop of sample (10-15 µL) due to their small surface area. Not only that, they also require minimum sample preparation (including removal of interfering species such as electroactive compounds like uric acid, ascorbic acid from serum/plasma, removing surface fouling compounds such as plasma proteins and lipids, dilution of sample etc) for real-time analysis (Ronkainen et al. (2010)). Moreover, these steps can be easily incorporated into the sensor system using microfluidics and membrane separation systems as seen with glucose sensors, which are successfully used for a whole blood samples (Tothill (2009)). Further, electrochemical biosensors can be designed to prevent non-specific adsorption of interfering species and promote high selectivity for target biomarker. In addition, there is a possibility of improving the sensitivity with the use of nanomaterials such as graphene, metal nanoparticles etc., which can amplify the output signals of the immunological reactions (Justino et al. (2017); Qin et al. (2019b)). Nanomaterials provide high surface area, which leads to improvement in loading capacity of the electrode and mass transport of the reactants generating an improved sensing performance. Instrumentation used with electrochemical biosensors can be miniaturised into pocket-sized entities, which makes them useful for both doctor's surgery and home use applications (Tothill (2009)). Lastly, these biosensors are extremely fast and can provide results within minutes, which facilitates fast personalised health care delivery (Wang (2006)). Therefore, they can be easily developed into POC tools that can be used by the GPs and even at- home by people for regular monitoring of specific AD biomarkers,

which can help to detect the disease in early stages and make informed decisions about the future (requirement of more complex tests such as PET/MRI, changes in lifestyles etc.). Owing to these advantages, electrochemical biosensors are an attractive tools for for the rapid detection of blood-based AD biomarkers.

A typical electrochemical set-up consists of three elements: electrodes, electrolyte solution and a potentiostat. The sensing performance is largely dependent on the electrode material, its surface functionalisation and dimensions as the reactions occur in a close vicinity to the electrode surface (Grieshaber et al. (2008)). There are three electrodes in an electrochemical cell: working electrode (WE) made from carbon/gold/platinum, which operates as a transducer element in a biochemical reaction; a counter or auxiliary electrode (CE) made from platinum/carbon, which constitutes the electric circuit with WE; and a reference electrode (RE) made from silver, which provides a constant potential during the measurements (Grieshaber et al. (2008)).

The three electrodes need to be conductive and chemically stable for an electrochemical reaction to occur (Chaubey & Malhotra (2002b)). The electrolyte carries the current, balances the charges and completes the circuit. A good electrolyte shows high electroactivity, high solubility in the chosen solvent and displays electrochemical inertness during the experiment. Most commonly used electrolyte substances are $[Ru(NH_3)_6]^{2+/3+}$ and $[Fe(CN)_6]^{3-/4-}$ (Scott (2016); Elgrishi et al. (2018)). A supporting substance such as salt or acid is also extremely important part of the electrolyte solution and is often present in higher concentration to keep the system at equilibrium for fast transfer kinetics (Dryhurst (2012)). Finally, a potentiostat maintains a constant potential at WE as a function of RE's potential by adjusting the current of CE (Elgrishi et al. (2018)).

There are two different types of set-up used for electrochemical sensing as shown in figure 2.2. The first one (figure 2.2(a)) is a conventional electrochemical cell consisting of three solid electrodes (WE, RE and CE), which are immersed in the electrolyte solution (usually in few ml) and are connected to a potentiostat. Second one, shown in figure 2.2(b), is based on screen printed electrodes (SPEs) in which all three electrodes are printed on the same substrate and just enough electrolyte is drop-casted to cover the three electrodes (usually requires few μL). The molecules reach the biosensor surface from the bulk solution through diffusion and then either directly exchange an electron or interact with the electrode surface to facilitate the electron transfer process, which leads to changes in the analytical signal

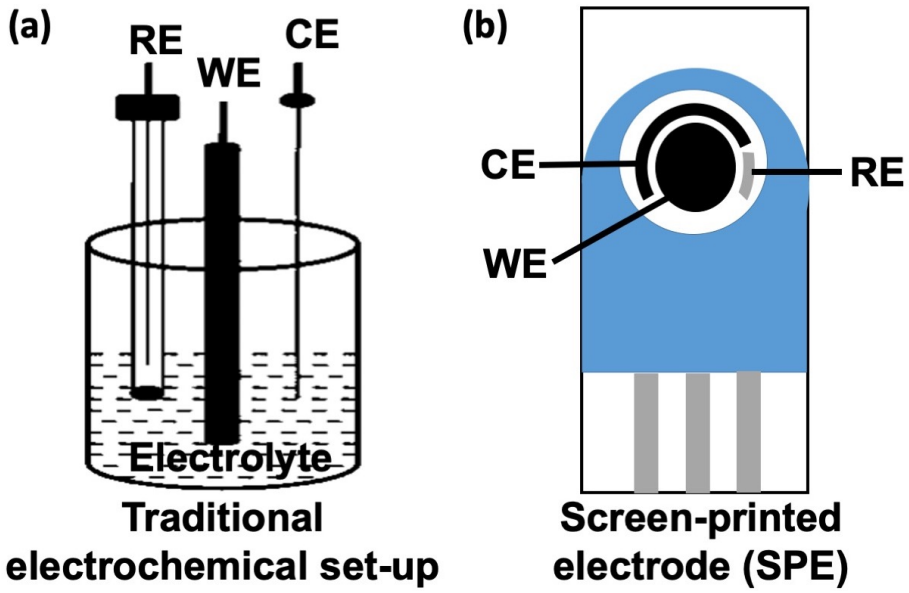

Figure 2.2: Illustration of two types of electrochemical set-up: (a) traditional set-up with three solid electrodes (working, counter and reference) and (b) screen printed electrode with all three electrodes printed on the same substrate

(Islam & Channon (2020)). Placing the bio-receptors close to the surface of the electrode or conducting nanomaterials generates a shorter diffusion path and enhanced signal generation (Purohit et al. (2020)). The electrochemical system can be connected to portable instrumentation to provide on-site testing of target (Taleat et al. (2014)). SPEs are preferred because of their cost effectiveness along with the ease and speed of mass production. In addition, they require low volume of reagents/samples, which helps in miniaturization of the diagnostic system (Elgrishi et al. (2018)). Medina-Sánchez et al. (2014) developed a lab-on-a-chip testing device with integrated SPE modified with cadmium-selenide/ zinc-sulfide quantum dots (QDs) as labels and microfluidics for the detection of ApoE from human plasma. The biosensor displayed high accuracy for blood sampling with a 370 pM LOD over a dynamic range of 290 pM to 5.88 nM (original values were in ng.mL^{-1}) using square wave anodic stripping voltammetry (SWASV). Microfluidic system makes this platform quite attractive, as these micrometer sized channels allow precise liquid handling, which leads to cost effective detection (Ortseifen et al. (2020)). Therefore, modified SPEs are an attractive tool for the detection of blood-based AD biomarkers. Additionally, they don't suffer from the common problems faced by solid electrodes such as tedious cleaning processes and memory effects (Taleat et al. (2014)).

For the fabrication of the biosensor, step by step modification of WE is done with conductive layer such as graphene, CNTs etc. followed by immobilisation of bio receptor

(specific to the target analyte) via linker molecule and blocking of surface functionalities. Then, a sample containing target is put on the electrode's surface and the receptor-target interaction is converted into an output signal. The fundamental principle is that when the electroactive species present in the electrolyte solution undergoes reduction/ oxidation at different electronic potentials due to donation or acceptance of electrons from the WE (redox peaks). Thus, when the target binds to the receptor on the surface of WE, electroactivity of WE is either reduced or increased, which obstructs or promotes the electron transport leading to the changes in redox peaks. This generates an output signal, which is proportional to the concentration of the target in the sample. It is based on measurable changes in potential/ charge accumulation (potentiometric), current (amperometric/voltammetric), conductivity of the medium between electrodes (conductometric) or impedance (impedimetric) (carried out using 'Electrochemical impedance spectroscopy (EIS)') (Grieshaber et al. (2008)). Among these, voltammetric is the most commonly used technique for biosensing. Our group has employed voltammetry techniques for the evaluation of a modified carbon based SPE for clusterin. The biosensor displayed high sensitivity with a LOD of 17 fM (value were converted from pg.mL^{-1}), much lower than the average concentration found in AD patients (Islam et al. (2018)). Some transistors such as organic electrochemical transistors (OECTs) also utilise the electrochemical mechanism to measure current output in response to the potential applied at gate electrode. Wustoni et al. (2019) developed an OECT for the detection of AβO with a LOD of 2.21 pM. In general, OECTs have an organic semi-conductor film, that is in contact with the electrolyte in which the gate electrode is immersed. The semiconductor film acts as a channel between source and drain electrode for carrying the charge carriers (holes/electrons). The charged ions are injected by the electrolyte onto the organic film by controlling the gate voltage and changes its doping level and conductivity. The drain produces a current proportional to the holes/ electrons in the channel and hence the doping state of the channel. The bio receptors are immobilised inside the channel or the gate electrode to achieve the detection as binding with the target blocks the ionic current flow leading to a decrease in the electrochemical signal (Rivnay et al. (2018)).

2.3 Electrochemical nanobiosensors

A nanomaterial is a type of material that has any external dimension, internal structure or surface structure between 1-100 nm range (Nanotechnologies (2015)). Their extraordinary properties such as high conductivity, high surface-to-volume ratio, better optical/mechanical properties, tunable size and structure etc. makes them useful for applications in the field of electronics, biology, chemistry and engineering (Vikesland & Wigginton (2010); Xu et al. (2017a); Zhong et al. (2018); Gill et al. (2019)). Recent advancements in the area of nanotechnology has led to the establishment of a new domain of diagnostic biosensors referred to as nano-biosensors. The transducer element of these biosensors are modified with nanomaterials, which not only improves the conductivity and catalytic activity of the transduction mechanism, but also favours the immobilisation of large amount of bio-receptors (Pumera et al. (2007); Walcarius et al. (2013); Syedmoradi et al. (2017)). This leads to the improvement in the sensitivity and selectivity of biosensors that in turn improves the overall performance (Walcarius et al. (2013); Chen & Chatterjee (2013); Syedmoradi et al. (2017); Carneiro et al. (2017)). In addition, nanomaterials also enhance the signal output (amplification) and biocompatibility of the biosensors (Colvin (2003); Gill et al. (2019)). Several nanomaterial based electrochemical biosensors have been successfully employed for the identification of AD biomarkers, particularly from bodily fluids including CSF, serum or plasma, despite their low concentrations (Zhao et al. (2015); Li et al. (2016); Yoo et al. (2017b); Le et al. (2019a); Carneiro et al. (2019)). Figure 2.3 depicts a schematic representation of the elements of an electrochemical detection process, including most frequently used nanomaterials.

Nanomaterials such as metal nanoparticles, CNTs and graphene and its derivatives are commonly used in biosensing (Noh (2018); Carneiro et al. (2019)). For instance, Xia et al. (2017) developed a competitive electrochemical biosensor for Aβ oligomer (AβO) detection. Modification with a polycrystalline gold substrate was achieved using a thiolated peptide (PrP_{95-110}), core region of cellular prion protein to achieve an antibody free detection of the target. Cellular prion proteins are glycoproteins, related with neurodegenerative disorders, which can be used as a bio receptor for AβO. Here, gold nanoparticles (AuNPs) were added in the last step along with $PrP_{95\text{-}110}$ (for making a sandwich structure) after the target attachment as the AuNPs may absorb other

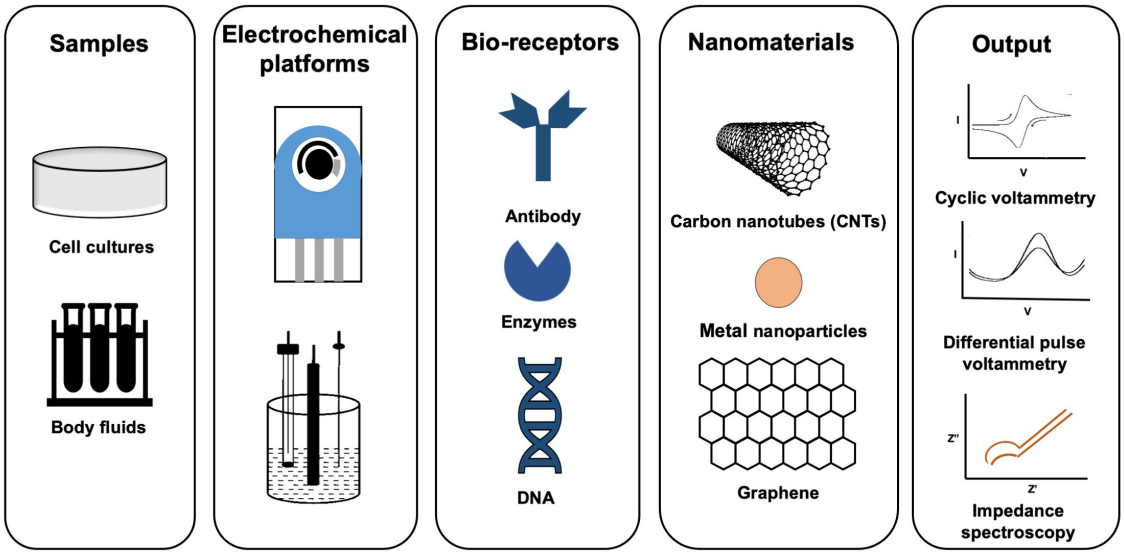

Figure 2.3: Elements of an electrochemical nanobiosensor

components during the real sample analysis. The surface peptides can capture the AuNPs and peptides forming a network of peptide-AuNPs-peptides-AuNPs leading to a decrease in the charge transfer resistance. However, peptides already bound with AβO lose their ability to trigger the formation of the AuNPs network, displaying an increased charge transfer. This mechanism led to a highly sensitive detection with LOD of 45 pM (Xia et al. (2017)). Before this, the same group employed this strategy using silver nanoparticles (AgNPs) and admantine labels achieving a LOD of 8 pM for the detection of AβO using linear sweep voltammetry (LSV) (Xia et al. (2016)). Therefore, the surface chemistry with AgNPs led to lower LOD than the one with AuNPs, which may be attributed to their higher electrochemical activity as shown by another group (Beck et al. (2022)). Cheng et al. (2014) utilised an indium tin oxide (ITO) electrode modified with AuNPs for identification of the Apo E gene and provided an LOD of 286 nM. The nanoparticles were electrodeposited on the surface in a single step by using cyclic voltammetry (CV). Despite the various advantages, use of metal nanoparticles can lead to inconsistent signal amplification (Pumera (2009)). Similarly, a sandwich electrochemical affinity biosensor was employed by Yu et al. (2015) for Aβ ratios identification. The biosensor was developed using a GC electrode modified via CNTs, AuNPs and gelsolin, which was used to bind to Aβ ligands instead of expensive antibodies. Following the binding of the target, a bio conjugate of AuNPs modified with gelsolin and horseradish peroxidase were used to attain a sandwich assay. The LOD was attained to be 28 pM for $A\beta_{1-42}/A\beta_{1-40}$ in the concentration ratio of 6:1 (Yu et al. (2015)). Nonetheless, CNTs contain metal impurities

(such as transition metals like Fe, Co, Mo, Y, Ni and Cr), which can interfere with their electrochemistry and can create toxicological hazards when reacting with biomolecules (Pumera (2009); Kuila et al. (2011); Ge et al. (2012)). Use of graphene has shown to overcome the aforementioned problems with metal nanoparticles and CNTs (Kuila et al. (2011); Justino et al. (2017)). These nanomaterials are also prone to fouling, which can be overcome by developing composites/new materials or developing single use sensors (adapted in the current study) (Yuan et al. (2018); Zhao et al. (2020); Zupančič et al. (2021))

2.3.1 Graphene

Graphene was discovered in the year 2004 using the method of mechanical exfoliation on a graphite crystal by Nobel prize winning Professors Andre Geim and Konstantin Novoselov (Novoselov et al. (2004b)). Since then, it has been a disruptive technology in the development of next generation healthcare diagnostics devices (Tehrani et al. (2014)). This is attributed to its remarkable properties that allows identification and tracking of very small concentrations of target biomolecules (Kuila et al. (2011)). Its low cost, transparency and low environmental impact makes it an ideal material for biosensors based on various transduction modes (Pumera (2011)). In particular, low cost and low environmental impact combined with high conductivity makes them a great choice for electrochemical biosensors. Recently, Mars et al. (2018a) developed a sensing platform using graphene quantum dots (GQDs) to achieve Apo E4 DNA detection. The GQDs were coated in a layer by layer approach over the ITO electrode followed by electropolymerization of curcumin, which possess both electrochemical and fluorometric properties. The GQDs have a wrinkled surface with active carboxylic sites that forms hydrogen bonds with curcumin molecules and enhances its electroactivity. Immobilisation of amino functionalised DNA probe on the biosensor was achieved via 1-ethyl-3-(3-dimethylaminopropyl)carbodiimide hydrochloride (EDC) and N-hydroxysuccinimide (NHS) chemistry. EDC is a cross linker, which is reactive towards the carboxyl/ amine groups and NHS is a reagent that stabilizes the intermediates formed during the two-step conjugation (Panchaud et al. (2008)). The hybridisation of DNA caused blocking of the electron transfer process, which in turn led to the quenching of curcumin signals. Sensing platform depicted 2.18 pg.mL^{-1} LOD. It demonstrated good selectivity, reproducibility and applicability in spiked plasma (Mars et al. (2018a)). Chauhan et al. (2017) employed an enzymatic biosensor developed using nanocomposite

of an electrochemically reduced rGO, ferric oxide (Fe_2O_3) nanoparticles and poly(3,4-ethylenedioxythiophene) (PEDOT) for the detection of ACh. Enzymes AChE and choline oxidase (ChO) were immobilized on the sensing surface and the following enzymatic reactions were involved in the detection of ACh.

$$ACh + H_2O \xrightarrow{AChE} Choline + Acetate \tag{2.2}$$

$$Choline + O_2 \xrightarrow{ChO} Betaine - aldehyde + H_2O_2 \tag{2.3}$$

According to the above reaction, choline is generated due to the reaction of ACh with water (H_2O) in the presence of AChE. The electrochemical sensing is based on the fact that the oxidation of hydrogen peroxide (H_2O_2) generates a current that is proportional to choline which in turn will be proportional to the amount of ACh used in the specific reaction. The biosensor demonstrated 4 nM LOD with excellent stability and selectivity. The evaluation of clinical serum samples displayed a slightly lower concentration of ACh in AD patients compared to their healthy counterparts. This biosensor displayed a much higher sensitivity compared to the ACh biosensor based on the nanocomposite of chitosan and gold coated iron oxide (Fe_3O_4) nanoparticles, which showed a LOD of 5 nM (Chauhan & Pundir (2014)). The enhanced sensitivity can be attributed to a combination of rGO and poly(3,4-ethylenedioxythiophene) that leads to higher conductivity and large surface to volume ratio (Chauhan & Pundir (2014)). The same group synthesized another biosensor based on a nanocomposite of rGO, manganese oxide (MnO_2) nanoparticles and CNTs (Chauhan et al. (2020)). The biosensor displayed a LOD of 100 nM, which could be due to the fact that CNTs contain metal impurities that can interfere with the electrochemistry (Pumera (2009); Kuila et al. (2011); Chauhan et al. (2020)). On the other hand, Panraksa et al. (2018) developed a paper-based graphene modified SPE for the detection of AChE. The biosensor displayed 0.1 $U.mL^{-1}$ LOD with 1 min incubation time and was successfully employed for the detection of blood samples.

Apart from the aforementioned properties, graphene materials display other exciting properties discussed below.

2.3.2 Structure and properties of graphene

Graphene represents a mono layer of sp^2 hybridized carbon atoms packed in a two dimensional (2D) hexagonal lattice, which is a basic building block of carbon allotropes such as 0 dimensional (0D) fullerenes, 1 dimensional (1D) CNTs and 3 dimensional (3D) graphite (Yang et al. (2013)). The electronic configuration of carbon is $1s^2 2s^2 2p^2$ with inner shell consisting of 2 electrons and the outer (valence shell) consisting of 4 electrons. The valence shell electrons are readily accessible for bonding with other atoms (Peres (2009)). Every carbon atom is linked to the neighbouring atoms via three sigma (σ) bonds with a 0.14 nm bond length and one π bond, which is developed between non-bonded electrons in p_z orbitals (figure 2.4) (Ishigami et al. (2007); Zhu et al. (2010)). The π electrons are perpendicular to the graphene plane and are readily available for electrical conduction (Peres (2009)). Graphene depicts semiconductor behaviour with zero band gap due to the meeting of conduction and valence band at the Dirac points (Balaji & Zhang (2017)), which are six positions in momentum space at the brilluion zone edge (Cooper et al. (2012)). Delocalized π electron system across the entire structure and zero band gap leads to extremely high electron mobility (Geim & Novoselov (2010)). Graphene has a reported value of 15000 cm^2/Vs for electron mobility at room temperature and can go as high as ≈ 100,000 cm^2/Vs (Novoselov et al. (2004a); Balaji & Zhang (2017)). Some other remarkable properties include excellent electrical conductivity (1738 siemens/m) (Weiss et al. (2012)), high thermal stability and conductivity (Balandin et al. (2008)), large surface area ($2630 m^2/g$) (Zhu et al. (2010)), large surface to volume ratio (Geim & Novoselov (2010)), mechanical strength of around 1100 GPa (Yang et al. (2013)), tensile strength of 125 GPa (Lee et al. (2008)), easily controllable doping levels (Wang et al. (2009a)) and ease of surface functionalisation (Georgakilas et al. (2012)). High sensitivity of graphene comes from its large surface to volume ratio and atomic thickness, which makes it extremely responsive towards any changes in the local environment (Justino et al. (2017)). However, during the practical applications, some of these properties get effected by toxicity, susceptibility to oxidative environment and unwanted defects introduced during the fabrication (especially during the graphene transfer process) (Reina et al. (2017)). Nevertheless, these problems can be addressed by improving the fabrication process as shown by Suhail et al. (2018).

The structure of graphene and its derivative namely, graphene oxide (GO) and rGO is

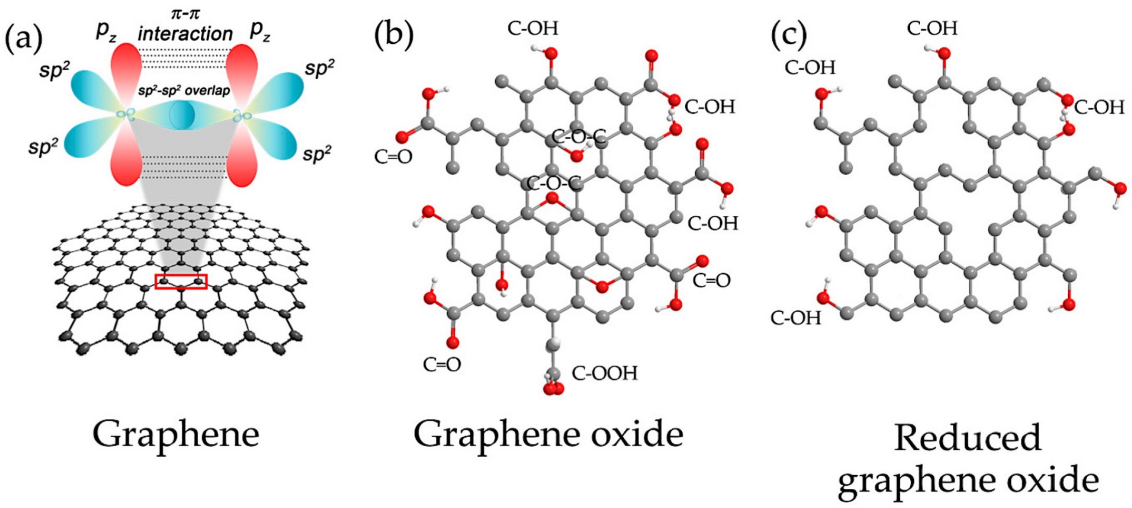

Figure 2.4: Structure of graphene (a), graphene oxide (b) and reduced graphene oxide (c) (Suvarnaphaet & Pechprasarn (2017))

shown in figure 2.4. GO is an oxygenated and layered graphene sheet containing oxygen functionalities such as hydroxyls, carboxyls, epoxides and alcohols. These functional group are present on the surface and edge of the sheet with the ratio of carbon to oxygen being 3:1 (Chang et al. (2014)). The heterogeneous electron transfer in electrochemistry of sp^2 hybridized carbon occurs on the defects and the edges, and not on the basal plane (Pumera (2011)). Therefore, presence of these groups may improve the heterogeneous rate transfer, in turn improving the water solubility and biocompatibility (Justino et al. (2017)). GO can be reduced to rGO via thermal, chemical and/ or other procedures (Tadyszak et al. (2018)). The reduction process effects the composition and intrinsic properties by reducing the oxygen content and creating defects in rGO, which in turn provides structural similarities to graphene (Justino et al. (2017); Carneiro et al. (2019)). The disorders and defects act as active sites providing ease in electron transfer process and immobilisation of biomolecules (Pumera (2011). Graphene based electrodes depict excellent electron transfer behavior with well-defined redox peaks in redox active solutions such as $[Ru(NH_3)_6]^{2+/3+}$ and $[Fe(CN)_6]^{3-/4-}$ (Shao et al. (2010)). In addition, graphene, GO and rGO shows improved electrochemical performance compared to other materials including glassy carbon (GC), CNTs and graphite (Yang et al. (2010b)). Moreover, thermal conductivity of rGO is comparable to those of doped conducting polymers, is around 36 times better than silicon and about 100 times better than Gallium arsenide (Bao & Loh (2012)). Thermal conductivity of pristine graphene is even higher than rGO (Mu et al. (2014)). The graphene materials can also be easily tuned into insulators, semiconductors, or semi-metals (Morales-Narváez et al. (2017)).

These unique properties of graphene materials make them a preferred choice to improve the analytical performance of biosensors either individually or in combination with other nanomaterials (Justino et al. (2017)). Recently, a GO and AuNPs hydrogel-based sensing platform was employed for AβO detection. The specific detection of the target was done using a 'cellular prion protein' peptide probe with impedance technique. The sensor was successfully applied for the analysis of spiked CSF and plasma over a dynamic range of 100 fM- 10 nM with a 100 fM LOD (Sun et al. (2018)). Prior to this, the same group developed a GO/DNA hydrogel electrode with a detection limit of 0.01 aM for the identification of DNA samples of ovarian cancer patients. The high performance was attributed to the tunable conductivity and bionic structure of the hydrogel electrode (Sun et al. (2014)). Similarly, Li et al. (2016) developed a biosensor using graphene electrodes for simple and rapid $A\beta_{1-42}$ detection. The sensor was fabricated by depositing superparamagnetic magnetite (Fe_3O_4) nanoparticles over n-doped graphene on gold (Au) electrode to form magnetic-n-doped graphene (MNG) followed by immobilisation of $A\beta_{1-28}$ antibody. The analytical performance of the sensor was obtained using differential pulse voltammetry (DPV) and depicted 1.11 pM LOD over a range of 1.11-177.22 pM (original values were in $pg.mL^{-1}$) with target incubation time of only 30 minutes. Also, this sensor was shown to be highly selective towards the target species. Wu et al. (2016) also reported a mesoporous silica hybrid nanomaterials and graphene based biosensor referred to as graphene@mesoporous silica hybrids (GSHs) for the detection of Apo E gene. The GSHs were prepared by homogeneously coating mesoporous silica onto graphene sheet and serve as nano-reservoirs for loading methylene blue (MB), an electroactive substance. Then, covalent conjugation of ferrocenecarboxylic acid (Fc) was obtained on the surface as a reference molecule to provide information about amount of GSHs. When the duplex DNA molecules are attached on the sensing surface, leakage of MB molecules are prevented and vice versa. This led to generation of an 'on-off' current based on the presence/absence of MB. Calculation of signal ratios of MB and Fc molecules provided the detection results. The biosensor demonstrated a reliable and reproducible detection with an attractive LOD of 10 fM (Wu et al. (2016)). However, the fabrication process is complex, expensive and time consuming which can limit its use for large scale clinical implementation.

2.3.3 Chemical functionalisation of graphene

Chemical functionalisation of graphene is crucial for the electronic and biosensing applications as it helps to overcome its low solubility, zero band gap and chemically inert nature (Kuila et al. (2012)). It also prevents layered graphene's agglomeration in solvent phase and helps in maintaining its properties. This leads to better solubility and provides active functionalities for tailoring the physical/ chemical properties for application in various fields (Kuila et al. (2012)). As a result, graphene's chemistry, particularly its functionalisation, needs to be clearly understood for developing graphene based biosensors and for overcoming its poor solubility in most organic solvents and aqueous solutions (Lonkar et al. (2015)).

The most commonly used materials for the functionalisation of graphene materials are a) nanoparticles, to improve the conductivity and thermal stability; b) polymers, to obtain materials with high strength and conductivity; c) linker, to attach biomolecules on to the sensing surface and d) biomolecules such as proteins, DNA, peptides (Justino et al. (2017)). All of these can be attached on the graphene surface by two distinct routes: covalent and non-covalent functionalisation (Georgakilas et al. (2012)). In covalent functionalisation, all the aforementioned materials are covalently linked to the graphene surface whereas in non-covalent functionalisation, modification is achieved through secondary interactions such as vander wall forces, adsorption or π- π interactions (Lonkar et al. (2015)) as shown in figure 2.5. This section will discuss the chemical functionalisation of graphene surfaces for biosensor applications in detail.

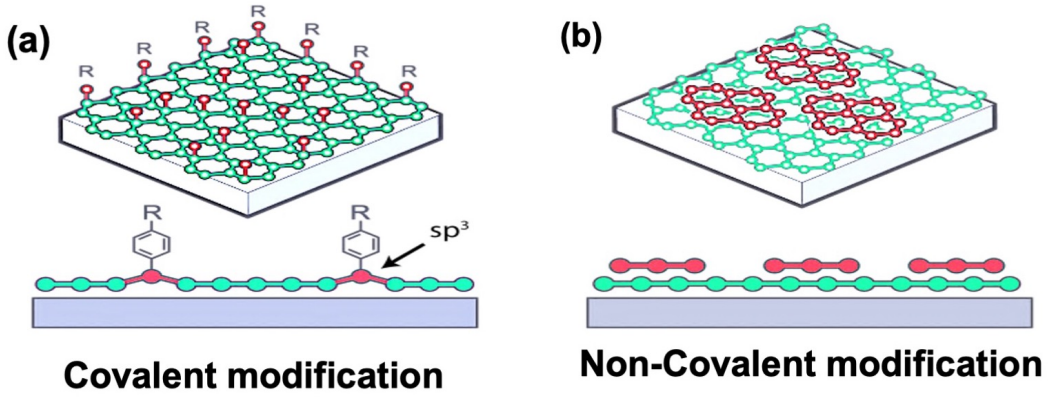

Figure 2.5: Two methods for chemical functionalisation of graphene materials: covalent (a) and non-covalent (b) modification; R denotes the functional group

Covalent functionalisation

The existence of sp^2 carbon atoms in graphene's lattice makes it possible for graphene to make covalent bonds with other atoms (Mao et al. (2013)). One s orbital and two p orbitals hybridise to form an energetically equivalent sp^2 orbital. Covalent functionalisation is associated with the re-hybridisation of one or more sp^2 hybridized carbon atoms into sp^3 configuration and leads to the formation of free radicals (Kuila et al. (2012)). This in turn leads to the introduction of chemically active functionalities into the lattice or at the edges of graphene, which can interact with different molecules. Therefore, functional groups are attached through the oxygen functionalities (such as carboxyl, epoxyl and hydorxyl) present at the edges of GO and rGO or through the structural π- π network (Lonkar et al. (2015)).

Covalent modification of graphene is achieved using two routes: a) Reaction of C-C bonds in pristine graphene with free radicals or dienophiles and b) Reaction of oxygen functionalities in GO with organic functional groups (Lonkar et al. (2015)). However, this type of functionalisation creates undesirable disturbances to the graphene's electronic structure and may diminish its excellent electronic properties (Georgakilas et al. (2012)).

1. **Functionalisation of pristine graphene**

Free radical addition is a common method for graphene modification (Lonkar et al. (2015)). Tour and coworkers reported functionalisation of graphene with nitrophenyl groups by reaction it with diazonium salt at an elevated temperature (Sinitskii et al. (2010)). The general molecular structure of diazonium salt is R-$N_2^+X^-$, where R denotes the organic component such as an aryl and X denotes the anion component. Functionalisation process involves electron transfer from graphene to aryl diazonium ions, which leads to the formation of free radicals. These radicals are highly reactive and attack the graphene lattice to form covalent bonds with sp^2 carbon atoms (Lonkar et al. (2015)). This in turn leads to a sharp drop in the conductivity of graphene sheet because of the production of sp^3 hybridized structure from a sp^2 hybridized structure. However, it can be manipulated by changing the reaction times as longer times leads to lower conductivity (Lonkar et al. (2015)). Niyogi et al. (2010) displayed that nitrophenyl modification of graphene introduces a controllable band gap, which provides a huge possibility for graphene as a semiconductor. Tehrani et al. (2014) employed the diazonium addition reaction for developing a graphene sensing platform for the identification of a cancer risk biomarker

(8-hydroxydeoxyguanosine) with a LOD of 0.35 nM. The extent of functionalisation can be determined using Raman Spectroscopy by calculating ratio of D to G band, which indicates an increase in density of sp^3 carbon atoms (Lonkar et al. (2015)).

Fenton's method involves the use of hydrogen peroxide (H_2O_2) and ferrous iron salt (Fe^{2+} as a catalyst) for degradation of organic solvents and has been successfully employed to introduce oxygen functionalities to graphene (Fenton (1894); Teixeira et al. (2014)). This is due to the fact that the catalytic decomposition of H_2O_2 at room temperature generates one of the most powerful oxidants, hyrdroxyl radical ($HO^{\cdot}$) (Buxton et al. (1988)). These radicals attack the graphene sheet using the mechanism explained above, attaching large amounts of hydroxyl and few carboxyl (COOH) and quinone functional groups (C=O) (Teixeira et al. (2014)). The modified Hummer's method works on the same mechanism but adds more number of COOH and C=O functional groups as opposed to Fenton's method (Gilje et al. (2007)). It is the most commonly used method for large scale production of GO (Liu et al. (2010); Bo et al. (2011)). Although, it is a highly efficient method of oxidation, however, the strong oxidizing agents limit its use for functionalisation of electronic devices as they can easily damage graphene thin films on the substrate (Pottathara et al. (2019)).

Apart from free radicals, sp^2 carbon atoms in graphene can also react with dienophiles to achieve the covalent modification (Georgakilas et al. (2012)). The most commonly used dienophile is Azomethine ylide which reacts with graphene using a 1,3 dipolar cycloaddition (Lonkar et al. (2015)). This was employed by Georgakilas et al. (2010) to decorate graphene sheets with pyrrolidine rings. The reaction improved the solubility of graphene in organic solvents like N,N-dimethylformamide (DMF) as well as ethanol. A remarkable increase in the intensity ratio of D to G band (I_D/I_G) and peak broadening was observed, which confirmed that the functionalisation was successfully completed (Georgakilas et al. (2012); Lonkar et al. (2015)).

EDC-NHS chemistry is also commonly used for the chemical modification of graphene surfaces. Zhou et al. (2016) developed a sandwich biosensor using carboxylated graphene as an electrode modifier for rapid electron transfer process and anchoring antibodies over the surface. Initially, GC based sensor was functionalised with carboxyl graphene along with EDC/NHS followed by capture antibodies (Cab). After the incubation with the target, the sensor was incubated with aptamer/AuNPs functionalised with thionine label to form a sandwich assay. The electrochemical reduction of thionine in phosphate

buffered saline (PBS), with 0.1 M concentration, was used for the quantitative analysis of AβO and a LOD of 100 pM was obtained. The schematic representation of the sensing process is shown in figure 2.6. The biosensor was applied for the analysis of artificial CSF (aCSF). Similarly, a graphene immunosensor was developed by Lee et al. (2017) for norepinephrine detection, a biomarker for neurodegenerative diseases. A gold electrode was modified with graphene sheets after which AuNPs were electrodeposited over it. The sensor had a LOD of 200 nM.

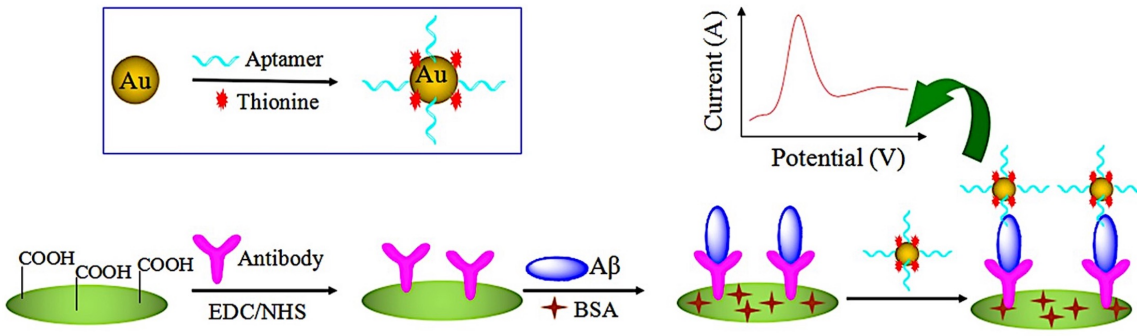

Figure 2.6: Sandwich biosensor based on capture antibodies and detection aptamers developed by Zhou et al. (2016)

2. **Functionalisation of GO**

GO is a monolayer of carbon atoms, which are either sp^2 hybridized in the form of aromatic regions or sp^3 hybridized in the form of oxygenated aliphatic regions containing carboxyl, carbonyl, epoxy and hydroxyl functional groups. The carboxyl and carbonyl groups are present on the defect or edge sites of the layers whereas epoxy and hydroxyl are present above and below the basal plane. As a result, several functional groups can be anchored on to the GO by reacting with graphene lattice and/or the oxygen functionalities. GO is also a commonly used starting entity for producing graphene derivatives, rGO (Georgakilas et al. (2012); Kuila et al. (2012); Lonkar et al. (2015)).

Congur et al. (2015) developed a label-free and disposable biosensor for miRNA-34a detection. The sensor was fabricated by modifying a disposable pencil graphite electrode (PGE) with GO by passive adsorption. This was followed by covalent immobilisation of amino linked hybridized miRNA-34a on the surface of GO. A detection limit of 261.7 nM was obtained. Also, the sensor displayed good selectivity for the target against fetal bovine serum (FBS) and non-complementary RNAs namely, miRNA-15a, miRNA-155 and miRNA-660. However, despite the simple fabrication protocol and brilliant selectivity, sensitivity of the biosensor was questionable due to high detection limit. Similarly, Derkus

et al. (2017) developed an electrochemical biosensor based on SPEs modified with GO for the simultaneous detection of two proteins tau and myelin basic protein (MBP). GO was covalently functionalised with EDC-NHS to attach amine functionalised first generation trimethylolpropane tris[poly(propyleneglycol)] (pPG) dendrimers. Cab were immobilized via glutaraldehyde for the quantification of tau protein. A sandwich complex was obtained by using detection Tau antibodies (Dab) in conjugation with pPG/ Lead(II) sulfide (PbS) as an electrochemical probe. The probe was reacted with nitric acid to produce Pb^{2+} ions thereby allowing the detection of protein signals. LOD for the tau protein was obtained to be 150 pM with high selectivity and reproducibility. The detection of MBP is achieved with a similar detection mechanism using a pPG/ cadmium sulfide as an electrochemical probe, which generates Cd^{2+} on reaction with nitric acid. This allows the simultaneous detection of two proteins. Simultaneous detection of biomarkers is necessary for the early and reliable detection of AD to yield high sensitivity and specificity. Various panels of plasma biomarker are now being studied and tested that can identify at-risk/ AD patients from their healthy counterparts in early stages (Gupta et al. (2013)). GO can also be combined with a range of nanomaterials to form nanocomposites with enhanced sensitivity for biosensing applications (Krishnan et al. (2019)). Devi et al. (2020) developed a biosensor based on a nanocomposite of GO-nickel ferrite-chitosan-AuNPs for the detection of $A\beta_{1-42}$ peptides. The biosensor depicted an improvement in the conductivity and active surface area with a LOD of 660 fM.

3. **Functionalisation of rGO**

As mentioned above, GO can be reduced to generate rGO, however a complete reduction is difficult to achieve with residual epoxy and hydroxyl groups always present on basal plane (Gilje et al. (2010); Lonkar et al. (2015)). It was confirmed through Density functional theory (DFT) studies that complete reduction using chemical, thermal or combination reaction is not possible (Boukhvalov & Katsnelson (2008); Ghaderi & Peressi (2010)).

Several rGO biosensors have been employed for AD biomarkers detection. One of them was developed by Ye et al. (2020) for tau 441 detection. The single layer rGO was modified using 1,3,6,8-pyrenetetrasulfonic acid tetra sodium salt ((PTSA) via $\pi - \pi$ interactions followed by the modification with Cu^{2+} to form a conductive interface. The attachment of PTSA generates a negative charge on rGO due to the presence of sulfonic group, which attracts the Cu^{2+} ions. Then, the surface was covalently modified with EDC-NHS for the

immobilisation of antibodies. EDC-NHS was used to activate the carboxylic group on rGO so that they react with the amine of antibodies. LOD of the biosensor was obtained to be 75 fM with high selectivity and good accuracy. It was then employed for the analysis of spiked and clinical serum samples (Ye et al. (2020)). Similarly, Li et al. (2020) developed a rGO nanocomposite with multi- walled CNTs and chitosan for the detection of tau-441. The nano composite was mixed with glutaric dialdehyde (GLA) prior to attachment on an Au electrode. This was followed by drying in infrared radiation, which causes the electrostatic adsorption of the nanocomposite onto the electrode. GLA has two aldehyde groups that binds to the chitosan and antibody on each side. Then, a bio-conjugate of AuNPs-cystamine-tau 441 protein was formed for the further signal enhancement. The cysteamine has sulfhydryl group on one side that bonds to the Au and amino group on the other side that bonds to the protein. When the antibody-protein complex is formed, the electron transfer process is hindered, which in turn leads to a decrease in the signals and vice versa. The LOD of the biosensor was obtained as 460 aM and it was evaluated with human serum samples of normal, MCI and dementia patients.

Non-covalent functionalisation

The non-covalent functionalisation is achieved through $\pi - \pi$ interactions or van der Waals' forces of attraction amidst graphene and other organic molecules (Chen et al. (2013)). Graphite (also refereed as bulk graphene) embodies a good instance of $\pi - \pi$ interactions with multiple graphene layers stacked up on each other through the interaction of their separate π-electron clouds (Georgakilas et al. (2012)). This functionalisation is particularly interesting because the graphene is modified without diminishing its electronic and structural properties related to the sp^2 network. Therefore, non-covalent mode of functionalisation is widely applied to graphene for achieving surface modification with specific molecules for the biosensor applications (Lonkar et al. (2015)). Often the molecules have a poly-aromatic hydrocarbon as a base, which includes benzene, pyrene or naphthalene that exhibits an acute affinity for graphene by creating $\pi - \pi$ stacks (Lonkar et al. (2015)). An example of such a linker is 1-pyrenebutyric acid N-hydroxysuccinimide ester (Pyr-NHS), which is used for the non-covalent modification of graphene. Pyrene end strongly attaches to graphene while NHS binds to the amine groups of different biomolecules including nucleic acid, enzymes, antibodies and bacterial probes (Ping et al. (2016); Islam et al. (2017)). Singal et al. (2015) developed a biosensor by

modifying an electrode based on graphene and CNT hybrid with Pyr-NHS for anchoring the antibodies. The immunosensor was employed for troponin-I detection and depicted a 0.94 pg. mL^{-1} detection limit. The similar linker chemistry has been utilised by (Saltzgaber et al. (2013); Ping et al. (2016); Xu et al. (2017b); Islam et al. (2017)). Additionally, Chen et al. (2013) demonstrated the effect of some electrons donating and withdrawing groups on the electronic properties of graphene. The results depicted that functionalisation using an electron donor such as tetrathiafulvalene (TTF) can lead to p-doping of graphene, whereas using an electron acceptor such as hexaazatriphenylene-hexacarbonitrile (HATCN) can lead to n-doping of graphene. Nevertheless, both molecules did not have any adverse effect on the properties of graphene.

Azimzadeh et al. (2017) reported a labelled sensing platform developed using electrochemically-reduced graphene oxide (ErGO) along with gold nanowires (AuNWs) for miR-137 detection. The sensor was developed by modification of SPE with GO and then the self-assembly of AuNWs was obtained on the surface of GO. Then, GO was electrochemically reduced to obtain ErGO and thiolated probes were immobilised on the surface in an extremely humid environment for obtaining the AuNWs self-assembly and then a layer for 6-mercaptohexanol was added to block unspecific binding. The complementary miRNA was tagged with an intercalating and electroactive label, doxorubicin, before hybridisation with the probe. LOD was estimated to be 1.7 fM over a linear range of 5 fM to 750 fM. Moreover, the sensor displayed excellent recovery in human serum for miR-137 (Azimzadeh et al. (2017)). Despite the excellent sensitivity, adding labels increase the overall fabrication cost making the sensing technology more expensive. Similarly, Tao et al. (2019) developed a carboxyl graphene based biosensor for tau 381 detection from human serum. The GC was modified with carboxyl graphene followed by thionine through $\pi - \pi$ stacking. Thionine was used a redox probe due to its electrochemical reversibility properties. Then, electrodeposition of AuNPs stabilised with cysteamine was done as a probe for signal enhancement. Cysteamine is an aminothiol that is used in the synthesis of nanoparticles due to its amino terminal, which provides an external positive charge to facilitate the interaction with negatively charged oligonucleotides and prevents the aggregation of nanoparticles (Toyos-Rodríguez et al. (2020)). Aptamers, single-stranded oligonucleotides that can bind to proteins, were immobilised on the surface. The LOD of the biosensor was found to be 420 fM and was

successfully verified with the serum of AD patients. Similarly, Gao et al. (2019) developed an immunosensor based on rGO by depositing a conjugate of AuNPs- thionine-rGO onto the GC electrode prior to immobilisation of Cab. Subsequently, a conjugate of Dab with gold-copper (I) oxide-copper(II) oxide embedded mesoporous cerium oxide nanoparticle was attached to create a sandwich immunoassay. The biosensor depicted a LOD of 7.97 fM.

2.3.4 State-of-the-art electrochemical nanobiosensors for AD biomarker detection

Apart from the graphene based electrochemical biosensors, several others have been developed for AD biomarkers detection in the past decade. This section will review the biosensors that have not been discussed in the previous sections.

1. Aptamers/ molecular imprinted polymers (MIPs)

Biomarkers can be identified using several biorecognition elements such as aptamers, polymers, specific proteins or antibodies. These materials are either obtained directly from nature through an animal source or can be created artificially to mimic these molecules. Antibodies are the commonly used recognition elements due to their exceptionally high affinity (binding strength) and selectivity towards the target biomarker (Sharma et al. (2016)). Alternatively, aptamers can also be used as they show high affinity and selectivity for their targets (including small ions or small molecules) and widen the field of biosensors. They are easy to modify chemically, provide cost effective recognition and are stable at elevated temperatures compared to antibodies (Han et al. (2010)). However, they tend to degrade faster (as quickly as in few minutes) in biological media particularly blood, which maybe too short for most clinical applications (Lakhin et al. (2013)). Zhou et al. (2018) developed an aptasensor for the detection of AβO. The GC electrode was modified with gold nanoflowers for the strong immobilisation of aptamers. After that, a sandwich assay was formed by attaching a bio conjugate of aptamers-AuNPs and copper metal organic framework (Cu-MOF) on the sensor surface. The gold nanoflowers provide high conductivity whereas Cu-MOF generate large amounts of Cu^{2+} that produces distinct electrochemical signals and can be used for the quantification of AβO. This led to a LOD of 450 pM without the use of expensive antibodies. To check the applicability in bio-fluids, the biosensor was evaluated with aCSF samples where it displayed good recovery

percentage (97-103 %).

Plastic antibodies based on MIPs are also an excellent alternative to the normal antibodies. MIPs are synthetic polymers that are generated using the polymerisation reaction in the presence of specific template (target protein). These materials display high sensitivity, selectivity, resistance to pH and varying temperatures. However, most of the research is still at a proof of concept stage and transferring the complexity of imprinting process to an industrial scale production is still a significant challenge (Ashley et al. (2017); Gui et al. (2018)). Moreira et al. (2018) developed a carbon SPE based biosensor using the poly aniline plastic antibodies. The carbon SPE was initially modified with a mixture of CNTs and copper nanoparticles followed by the direct electro polymerisation of aniline using $A\beta_{1-42}$ as a template. After the polymerisation, peptide templates were removed using a solution oxalic acid. An LOD of 88.6 fM was obtained showing the potential for detecting extremely low concentration of biomarkers from bio-fluids. This was a significant improvement from an AβO biosensor developed by the same group, which displayed an LOD of 44 pM. It had an additional α-cyclodextrin film assembled onto a nano structured poly aniline for capturing the target antigens. α-cyclodextrin demonstrate amphiphilic properties, with hydrophilic external surface and hydrophobic inner cavity. These inner cavities interact with the target peptides/proteins (Moreira & Sales (2017)). Özcan et al. (2020) developed MIPs of pyrrole for the detection of $A\beta_{1-42}$ on a delaminated titanium carbamide MXene/ multi-walled CNTs platform. MXene are 2 dimensional materials that are formed using early transition metal carbides and/or carbonitrides. CNTs were used to prevent the aggregation of MXene. The LOD of the biosensor was found to be the lowest with a value of 44 aM. However, the platform was not evaluated using fluid samples, which raises the questions about its applicability in real-time analysis.

2. Self-Assembled mono layers (SAMs)

Several biosensors have been developed using SAMs for $A\beta_{1-42}$ detection. SAMs are usually formed by the chemisorption of an organic molecule over a substrate to obtain ultra-thin films at room temperature (Chaki & Vijayamohanan (2002)). These create multi-functional interfaces for the immobilisation of bio-receptors, provides bio compatibility and resist non-specific adsorption, which makes them highly desirable for biosensing applications (Wang et al. (2018b)). Recently, a gold electrode biosensor based on mercaptopropionic acid (MPA) SAMs and AuNPs was developed for the analysis of

$A\beta_{1-42}$. The biosensor displayed high sensitivity with a LOD of 1.15 pM, however, it failed to show selectivity against other abundant proteins present in the bio-fluids of patients (Carneiro et al. (2017)). Similarly, Dai et al. (2017) used 3-MPA SAMs to develop a thin gold film based biosensor within a linear range of 15 nM-111 nM. An interdigitated gold electrode was modified with 6-mercaptohexanoic acid (6-MHA) followed by EDC-NHS for preparation of a highly sensitive biosensor by Le et al. (2019b). LOD was found to be around 22.15 pM in human serum. Alternatively, Lien et al. (2015) used 16-mercaptohexadecanoic acid (MHDA) along with protein G and AuNPs to obtain 570 pM LOD. Use of protein G led to an optimised orientation of antibodies on the surface and thus improved their capture efficiency, which improved the detection sensitivity by lowering the LOD from 2.65 nM to 570 pM. Liu et al. (2014) developed a biosensor for the detection of $A\beta_{1-42}$ and total $A\beta$. For the immobilisation of antibody, MPA SAMs were formed over a gold electrode and EDC-NHS was used as a linker. A streptavidin-conjugated alkaline phosphatase (ALP) was attached with the targets, which convert the p-aminophenyl phosphate (app) substrate (added in the next step) to an electrochemically active p-aminophenol (ap). LOD of the biosensor was found to be 5 pM and it was also evaluated with aCSF samples. A slightly modified version of this biosensor was developed by Diba et al. (2017) where instead of gold electrode, AuNPs modified SPE was used. Here too, MPA SAMs were used for the immobilisation of antibodies, however, additional mono layers of thiol modified polyethylene glycol (PEG) was added to lower the non-specific adsorption. A sandwich assay strategy was developed for the detection of $A\beta_{1-42}$, where Dab was tagged with ALP generating an antibody/peptide/antibody-ALP complex. Similar to the aforementioned strategy, when 4-app reacts with ALP, 4-ap is generated which is further oxidised by applied current. Since, ALP depends on the amount of target, the reaction is correlated with the quantitative analysis of the target as well. The biosensor depicted a LOD of 100 fM and was successfully tested with both plasma and serum samples.

3. Signal amplifiers (systems, nanoparticles and labels)

Amplification of electrochemical signals is a common way of improving the detection sensitivity of biosensors. Recently, a signal cancellation and amplification processing system (SCAP) have been developed by Yoo et al. (2017a) to be used alongside an interdigitated micro electrode system for the detection of $A\beta_{1-42}$. The SCAP improved the detection sensitivity of the system by 100 folds. The silicon dioxide (SiO_2) electrode

was modified with 3-aminopropyl triethoxysilane solution (APMES), sodium borohydride ($NaBH_4$), polyvinyl pyrrolidone-aldehyde solution (PVP-CHO) along with glutaraldehyde for the immobilisation of antibodies on the surface. The biosensor depicted a linear range in $fg.mL^{-1}$ and was successfully employed for the detection of mice plasma samples. The SCAP system was also tested alongside a sandwich biosensor by the same group. The surface functionalisation strategy was similar to the aforementioned biosensor except the use of a Dab to prepare a sandwich assay. AuNPs were bound to the Dab to enhance the sensitivity of the platform even further. The lowest detected concentration was obtained as 0.022pM. The platform also displayed selectivity against $A\beta_{1-40}$ biomarker by using specific Dab, which is necessary for bio-fluid analysis as both $A\beta_{1-40}$ and $A\beta_{1-42}$ forms are usually present in AD patients (Yoo et al. (2020)). Wu et al. (2014) used AuNPs for the preparation of a platform based on a gold modified anodic aluminum oxide layer having a honeycomb-like surface. In this, AuNPs were electrodeposited on a gold substrate followed by 11-mercaptoundecanoic acid as well as EDC-NHS for antibody immobilisation. The use of AuNPs leads to an increase in the surface area of sensing platform for the increased capture of target. Increasing the concentration of target led to an aggregation of the nanoparticles. The biosensor was employed for the detection of $A\beta_{1-42}$ with a LOD of 22.2 fM. Similarly, Amor-Gutiérrez et al. (2020) developed an AuNPs modified SPE based immunosensor for unfolded p53 detection from plasma of MCI and AD patients. Sensing was achieved via competitive assay between non-biotinylated (unfolded) and biotinylated p53 peptides trying to attach to the antibodies on the surface. The antibodies already bound to unfolded p53 will not bind to the biotinylated p53. Following this, streptavidin labelled ALP is added to specifically bind to the biotinylated peptide. Streptavidin and biotin display strong non-covalent interaction with each other. Then, 3-indoxyl phosphate and silver nitrate solution were added, which leads to the enzymatic reduction of silver by ALP into metallic silver, which can be detected by doing an anodic stripping scan. Higher the amount of unfolded p53 in the sample, lower is the amount of biotinylated p53 that reacts and therefore, lower is the electrochemical signal. The scheme of the sensing platform is shown in the figure 2.7. It demonstrated a detection limit of 50 pM.

A similar detection strategy was followed by another platform developed by Rama et al. (2014) for the detection of $A\beta_{1-42}$. The only difference was that the streptavidin is first attached onto the AuNPs followed by the addition of biotinylated peptides. In the next

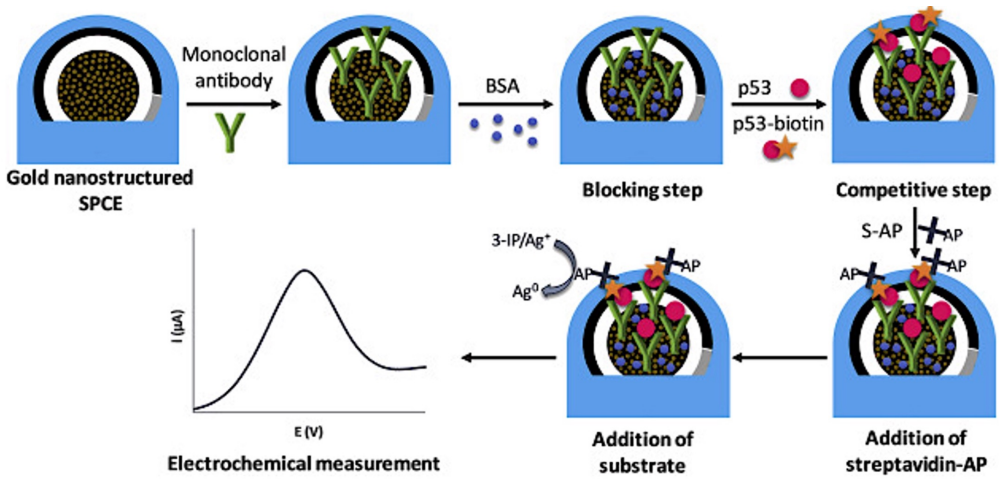

Figure 2.7: Competitive assay developed by Amor-Gutiérrez et al. (2020) for the detection of unfolded p53

step, $A\beta_{1-42}$ peptides and the specific antibodies are added. This leads to a competitive reaction between binding of antibodies to the the previously immobilised biotinylated peptides or the ones freshly added. In the last step, Dab labelled with ALP is added, which leads to generation of metallic silver by reaction with 3-indoxyl phosphate and silver nitrate solution. LOD of 22.2 pM was achieved using this platform. Qin et al. (2019b) developed a biosensor based on cellular prion protein modified gold electrode for the detection of AβO. The AuNPs were embedded onto a poly-(3,4-ethylene dioxythiophene) layer over which a layer of poly(thiophene-3-acetic acid) was electro-deposited followed by EDC-NHS for the anchoring of prion proteins. The biosensor was employed for the real-time detection in animal samples and depicted an impressive LOD of 10 aM. This is the lowest reported LOD for the Aβ by an electrochemical biosensor till date. It was attributed to the unique surface functionalisation including the use of cellular prion protein, which increased the overall selectivity and sensitivity of the platform. More recently, Ding et al. (2020) developed a platform using polyethyleneimine covered AuNPs as electrochemical labels for the detection of Aβ peptide. Here, hemin was used as a bio-receptor due to its high affinity towards Aβ. The platform was based on a gold micro electrode over which the cystemine and EDC-NHS were attached for the proper immobilisation of hemin. A label nanoprobe based on Cu^{2+} -polyethyleneimine-AuNPs- hemin was used. The hemin present on the surface could capture both the analyte as well as the nanoprobes based on the hemin-Aβ-Cu^{2+} coordination. The nanoprobe (due to the presence of hemin) can also capture more Aβ monomers leading to formation of nanoprobe aggregates. In the last step, deposition of silver nanoparticles is promoted on the surface by the aggregates of

AuNPs (from the nanoprobe), which led to an enhancement of the detection sensitivity of the platform and 200 fM LOD was obtained.

Various nanomaterials with new morphologies are being developed to improve the surface to volume ratio, which in turn increases the amount of binding sites. Higher number of binding sites increases the chances of attaching higher number of antibodies on the surface (Dong et al. (2010); Li et al. (2013a); Kwak et al. (2014)). This approach has been followed by Liu et al. (2015) using a fractal gold nanostructure in a sandwich biosensor. Initially, the nanostructure was electrodeposited on the surface of an ITO electrode and due to its ramified conformation increased the number of monoclonal antibodies against the target ApoE4 biomarker. The Horseradish peroxidase (HRP) enzyme was used as a label on Dab for the catalysis of the hydroquinone oxidation reaction to form quinine in the presence of H_2O_2 that leads to a change in current. The biosensor depicted 8.78 pM LOD. The same group developed another biosensor based on Pt nanoparticles coated gold nanobipyramids on a GC/Au electrode to improve the electroactive area and conductivity. Instead of HRP, a polydopamine nanotubes based nanoenzyme doped with gold and palladium were employed as labels. The biosensor depicted a detection limit of 450 fM, which was lower compared to their prior work and was attributed to the structure of the nanomaterial (Liu et al. (2020)). The HRP labelling strategy was also employed in an immunosensor developed by Razzino et al. (2020). Here, carbon SPEs were modified with p-aminobenzoic acid and 3 dimensional AuNPs-polyamidoamine dendrimer nanocomposite for anchoring the antibodies via glutaraldehyde. It was applied for the evaluation of tau from brain tissues and human plasma of healthy and AD cohorts. The detection limit was recorded as 31 fM. Negahdary & Heli (2019b) developed an aptasensor for the detection of $A\beta_{1-42}$ by electrodepositing gold nanostructure that looks like fern leaves like on an Au electrode in the PEG 6000's presence. The nanostructures provided high surface area for the aptamer immobilisation whereas the PEG 6000 controlled the shape and size of it. A ferro/ferricyanide redox marker was used to enhance the detection signals, which gets depleted with increment in the concentration of target. An excellent LOD of 88.6 fM was obtained. The same group developed another sensor using a synthetic Aβ peptide as the bio receptor, immobilised onto micro porous gold nanostructures. This lowered the LOD of the biosensor further down to 44 fM attributed to the nanostructure and the redox markers (Negahdary & Heli (2019a)).

Magnetic particles are another extremely useful class of materials for the immobilisation of bio receptors. The magnetic behaviour is useful for minimising the matrix effect as it allows analyte preconcentration from complex biological samples (Toyos-Rodríguez et al. (2020)). Matrix effect refers to the impact of an analyte's matrix or environment such as plasma or serum on the sensitivity of a biosensor (Kim et al. (2020); Masson (2020)). Iglesias-Mayor et al. (2020) developed a competitive immunoassay based on magnetic beads (MBs) with Au-platinum (Pt))/AuNPs as labels for the quantitative analysis of unfolded p53 biomarker. The label was synthesized by deposition of Pt on AuNPs surface followed by a galvanic replacement reaction where some Pt atoms get substituted with Au atoms. These substituted atoms were utilised to attach the antibodies forming Au-Pt/AuNPs/anti-p53 conjugate. In parallel, biotinylated p53 were immobilized on the streptavidin modified MBs forming MBs/p53 conjugate. Then, the Au-Pt/AuNPs/anti-p53 conjugate was incubated with sample containing analyte followed by the incubation of resultant complex with MBs/p53 conjugate. In the absence of analyte, a coupling reaction occurs between the conjugates generating a high catalytic current by the water oxidation reaction (WOR), which is electrocatalyzed by the Au-Pt/AuNPs and vice versa is true if the analyte (unfolded p53) is present in the sample. The LOD of the biosensor was obtained to be 66 nM with the detection performed in the same medium as the immunoreaction, which reduces the steps and amount of reagents. This detection mechanism based on the catalysis of WOR has been previously explored by Rivas et al. (2014) for ApoE. The biosensor was fabricated using carboxylated MBs as anchoring platforms for the antibodies and iridium oxide nanoparticles as electrochemical labels. The detection was based on the catalytic effect of the nanoparticles towards the WOR. The biosensor depicted a LOD of 1.99 nM with high reproducibility and was evaluated with human plasma samples.

Electrochemical reporters can also be added during the fabrication process to enhance the signals, which further enhances overall performance of the biosensor (Li et al. (2013b)). Li et al. (2013b) group developed a platform using methylviologen (MV) as an electrochemical reporter. The biosensor was based on a gold electrode modified with protein binding peptides specific for AβO. After the binding of the target, some of the peptides become protein bound, however, some remain unbound and are coupled with MV via non-covalent interaction leading to the formation of supermolecules. This mechanism could be used for the development of different protein assays as the MV couples with peptides through a single aromatic amino acid, which are present in all protein binding peptides. LOD

of the biosensor was estimated to be 48 pM using Square wave voltammetry (SWV). Similarly, Lu et al. (2018) employed ferrocene capped AuNPs for the signal amplification and reported a low LOD of 100 fM for ApoE gene. The gene was specifically trapped using a biotinylated oligonucleotide to generate a DNA double helix structure with a GCGC sequence. This particular sequence is the cleavage site for the HhaI enzyme and is used to increase the specificity of the biosensor. When the ApoE gene is attached with the the probe, GCGC sequence is generated in the middle and gets cleaved by the enzyme generating biotinylated fragments of the double helix structure. On the other hand, in case an interfering species is attached to the probe the GCGC sequence will not be generated and no fragments will be released. The presence of biotinylated fragments helps the attachment of streptavidin conjugated ferrocene capped AuNPs that enhances the electrochemical signals whereas the absence of it leads to the low signal.

4. Metal organic frameworks (MOFs)

MOFs are a combination of organic and inorganic ingredients, which depict various advantages such as porous structure, chemical stability and facile synthesis (Wang et al. (2018c); Jiang et al. (2019)). Zinc zeolite imidazole framework (ZIF) is a MOF made from zinc (Zn) ions and imidazole linker and has shown potential as an electrode modifier owing to the affinity of Zn^{2+} towards proteins such as BSA (Ohyoshi et al. (1999)), Aβ (Gaggelli et al. (2008)) and IgG (Yamanaka et al. (2016)). Qin et al. (2019a) prepared nanoparticles of ZIF-8 and ferrocene for the detection of AβO. The principal of the biosensor is that when the AβO target comes in contact with ferrocene-ZIF-8, zinc ions coordinate with AβO, it causes a dissociation of ZIF-8 molecule releasing ferrocene. The concentration of the ferrocene found to be linearly proportional to AβO concentration. LOD of biosensor was estimated to be 10 pM and recovery studies were performed using aCSF. Similarly, MOFs can also be employed as labels as indicated by Han et al. (2017). They developed a sandwich biosensor using a ferrocene bonded flower like Zn MOF as an electrochemical label for the detection of Aβ. Initially, GC electrode was modified with graphene attached to amino- terminated polyamidoamine, followed by AuNPs to attach the primary antibodies on the surface. After the binding of the target, a bio-conjugate of Dab, AuNPs and ferrocene-Zn-MOF was attached to it. The biosensor demonstrated an excellent LOD of 6.6 fM.

2.3.5 Barriers in clinical application

As mentioned above, electrochemical biosensors have been extensively explored for AD biomarkers detection, many of which have demonstrated promising results. However, many challenges need to be overcome for the adoption of these sensors in clinical applications. Some of which are mentioned in detail below:

1. Low sensitivity: Concentration of AD biomarkers can be as low as <10 pM to fM ranges in plasma or CSF depending on the stage of the disease (Wang et al. (2013); Zetterberg et al. (2013); Kim et al. (2016); Hanon et al. (2018); Chen et al. (2019)). Therefore, in order to ensure proper monitoring of the disease progression, highly sensitive biosensors are required. However, most of the biosensors depict LOD in the range of 10s of pM-μM, which is insufficient for the biofluidic analysis and creates barriers in clinical application.

2. Use of labels, nanoparticles and/or amplification systems: As described above, labelled biosensors have the analyte sandwiched between a Cab and Dab, with specific agents such as nanoparticles, enzymes etc. attached to Dab for signal enhancement (Sin et al. (2014)). Various biosensors use labels and/ or additional amplification systems to lower the LOD and improve the sensitivity. However, this enhancement requires extra chemicals, equipment and processing time, which increases the complexity and cost of the overall platform. Also, use of nanoparticles can lead to inconsistent signal amplification that can raise question regarding the reliability and reproducibility of the platform (Pumera (2009); Sin et al. (2014)). On the other hand, CNTs may contain metal impurities that can interfere with their electrochemistry and can create toxicological hazards when reacting with biomolecules (Pumera (2009); Kuila et al. (2011)). Therefore, the challenge is to develop a highly sensitive platform without the additional complexities so that it can be easily adapted into a POC tool.

3. Selectivity tests: Several proteins are present in the bio-fluids of humans and most of them have a higher concentration than the biomarker of interest (Henriksen et al. (2014)). For instance, blood consists of proteins including albumins (>50%), globulins, fibrinogen, specific proteins such as transferrin, lipoproteins, C-reactive proteins, alpha fetoprotein, alpha-1- acid glycoprotein among others (Smith et al. (2013); Leeman et al. (2018); Wiencek et al. (2020))). Hence, a selectivity test is important to show the ability of biosensor to detect specific targets in complex media and avoid false positive results. For instance, a biosensor for $A\beta_{1-42}$ needs to be selective against other proteins such as

ApoE ϵ4 and $A\beta_{1-40}$ biomarkers as they are also found in the fluid of MCI/AD patients. In fact, ApoE ϵ4 can exist in excess in human plasma (up to 10,000-fold) (Martínez-Morillo et al. (2014)). Similarly, $A\beta_{1-40}$ often interferes with the detection of $A\beta_{1-42}$ due to the similarity in their structure. Several instances show that the antibodies used by the biosensors can identify both $A\beta_{1-40}$ and $A\beta_{1-42}$ (Yoo et al. (2017a); Carneiro et al. (2017); Hassan & Kerman (2019)). However, with $A\beta_{1-42}/A\beta_{1-40}$ ratios gaining attention as a potential AD biomarker (Graff-Radford et al. (2007); Lambert et al. (2009); Nakamura et al. (2018)), reliable detection of individual biomarker is more important than ever. In addition, deposition of $A\beta_{1-42}$ starts earlier compared with $A\beta_{1-40}$, which underlines the importance in indicating AD progression (Mehta et al. (2000)). Therefore, specific determination of biomarkers is an important prerequisite for bio-fluid analysis and understanding AD progression. However, most of the biosensors either failed to carry out the selectivity tests altogether or did not do it with important interfering proteins. This is particularly true for most of the Aβ biosensors reviewed in the above section except the ones developed by Zhou et al. (2016); Xia et al. (2016); Xia et al. (2017); Zhou et al. (2018); Devi et al. (2020), which demonstrated other barriers discussed here.

4. Lack of bio-fluidic analysis: Detection of biomarkers from bio-fluids is necessary for the rapid, early and timely detection of AD. It is also necessary for the large scale implementation of diagnostic platforms for communities (Henriksen et al. (2014)). However, some of the biosensors were not evaluated with any biofluids, putting their reliability in question.

Therefore, there is an immediate requirement for cost-effective, rapid, simple and sensitive platforms for the detection of AD biomarkers. In this work, we have developed two distinct label-free graphene biosensors using SPEs for detection of Aβ biomarkers. Label-free biosensors detect the analyte directly through the biochemical reaction that occur on the transducer's surface (Hunt & Armani (2010); Rapp et al. (2010)). The developed biosensors display high sensitivity and selectivity for the target against the interfering species. They have also been successfully validated with plasma samples. Due to the simplicity of fabrication process, they can be adopted for the detection for other AD biomarkers.

Analyte	Materials	Techniques	LOD	Labels	Matrices	References
AβO	Gold/ AuNPs/ poly-(3,4-ethylene dioxythiophene)/ poly(thiophene-3-acetic acid)/ EDC-NHS	EIS	10 aM	No	Mice tissue	Qin et al. (2019b)
	GO-AuNPs hydrogel/cellular prion protein peptide	EIS	0.1 pM	No	CSF, plasma	Sun et al. (2018)
	Gold/ β-cyclodextrin/ TCEP/ 6-mercapto-1-hexanol/ admantine PrP_{95-110}/ AgNPs	LSV	8 pM	Yes	Serum	Xia et al. (2016)
	Gold/ ZIF-8/ ferrocene	CV	10 pM	Yes	aCSF	Qin et al. (2019a)
	Gold/ polyaniline/ α-cyclodextrin/ oxalic acid	SWV, EIS	44 pM	No	fetal bovine serum	Moreira & Sales (2017)
	Gold/ PrP_{95-110}/ 6-mercapto-1-hexanol + AuNPs/ PrP_{95-110}(sandwich assay)	EIS	45 pM	No	PBS	Xia et al. (2017)
	Gold/protein binding peptide + cucurbituril-MV	SWV	48 pM	Yes	PBS	Li et al. (2013b)
	GC/ carboxyl-graphene/ EDC-NHS + aptamers/ AuNPs/ thionine (sandwich assay)	DPV	100 pM	Yes	aCSF	Zhou et al. (2016)
	GC/ gold nanoflowers+ AuNPs/ Cu-MOF (sandwich assay)	DPV	450 pM	No	aCSF	Zhou et al. (2018)

Table 2.5: Electrochemical biosensors for detection of AD biomarkers (1/6)

Analyte	Materials	Techniques	LOD	Labels	Matrices	References
$A\beta_{1-42}$	GC/ delaminated titanium carbamide MXene/ CNTs/ pyrrole MIPs	DPV	44 aM	No	PBS	Özcan et al. (2020)
	Gold/ AuNPs/ 11-mercaptoundecanoic acid/ EDC-NHS	EIS	22.2 fM	No	Serum	Wu et al. (2014)
	Gold/ micro porous gold nanostructure/ Mercapto-1-hexanol/ ferro-ferricyanide redox marker	DPV	44 fM	Yes	aCSF, plasma	Negahdary & Heli (2019a)
	Carbon/ CNTs/ Cu nanoparticles/ polyaniline/ oxalic acid	SWV	88.6 fM	No	Cormay serum (human)	Moreira et al. (2018)
	Gold/ fern leaves like gold nanostructure/ PEG 6000/ Mercapto-1-hexanol/ ferro-ferricyanide redox marker	DPV	88.6 fM	Yes	aCSF, plasma	Negahdary & Heli (2019b)
	Carbon/ AuNPs/ MPA/ PEG/ EDC-NHS + ALP/ 4-app (sandwich assay)	DPV	100 fM	Yes	Serum, Plasma	Diba et al. (2017)
	GC/ GO/ nickel ferrite/ chitosan/ AuNPs EDC-NHS	DPV	660 fM	No	CSF	Devi et al. (2020)
	Gold/ Fe_3O_4 nanoparticles/ N-doped graphene	DPV	1.11 pM	No	PBS	Li et al. (2016)
	Gold/ MPA SAMs/ AuNPs	SWV	1.15 pM	No	PBS	Carneiro et al. (2017)
	Gold/ 6-MHA SAMs/ EDC-NHS	EIS	22.15 pM	No	Serum	Le et al. (2019b)

Table 2.6: Electrochemical biosensors for detection of AD biomarkers (2/6)

Analyte	Materials	Techniques	LOD	Labels	Matrices	References
$A\beta_{1-42}$	Carbon/ AuNPs/ streptavidin/ biotin + ALP/ 3-indoxyl phosphate/ silver nitrate (sandwich assay)	CV	22.2 pM	Yes	PBS	Rama et al. (2014)
	Carbon/ 16-MHDA SAMs/ EDC-NHS/ protein G	EIS	570 pM	No	PBS	Lien et al. (2015)
	SiO_2/ APMES/ PVP-CHO/ $NaBH_4$/ glutaraldehyde + SCAP	impedance	–	No	Mice plasma	Yoo et al. (2017a)
	Gold film/ 3-MPA SAMs/ EDC-NHS	DPV	–	No	Serum	Dai et al. (2017)
	SiO_2/ APMES/ PVP-CHO/ $NaBH_4$/ glutaraldehyde/ Cab + Dab/ AuNPs (sandwich assay)	impedance	—	No	Mice plasma	Yoo et al. (2020)
Aβ	GC/ graphene/ amino-terminated polyamidoamine/ AuNPs+ Dab, AuNPs and ferrocene-Zn-MOF (sandwich assay)	SWV	6.6 fM	Yes	Serum	Han et al. (2017)
	GC/ rGO/ thionine/ AuNPs/ Cab + Dab/ AuCuxO/ mesoporous cerium oxide nanoparticle (sandwich assay)	LSV	7.97 fM	Yes	aCSF	Gao et al. (2019)
	Gold/ cystemine/ EDC-NHS/ Hemin+ Cu^{2+}/ polyethyleneimine covered AuNPs/ hemin/ Silver (sandwich assay)	LSV	200 fM	Yes	CSF	Ding et al. (2020)

Table 2.7: Electrochemical biosensors for detection of AD biomarkers (3/6)

Analyte	Materials	Techniques	LOD	Labels	Matrices	References
Aβ aggregate	poly(ethylenedioxythiophene): poly(styrenesulfonate)/ poly(styrene-b-4-vinylpyridine)/ 4-chlorobutan-1-ol/ APTES/ glutaraldehyde/ Congo red	transfer characteristics	2.21 pM	No	Serum	Wustoni et al. (2019)
$A\beta_{1-42}$/ $A\beta_{1-40}$	GC/ CNTs/ AuNPs/ EDC-NHS/ Gelsolin + Gelsolin/ AuNPs/ horseradish peroxidase	DPV	28 pM	No	Rat brain (in vivo)	Yu et al. (2015)
$A\beta_{1-42}$ and Aβ	Gold/ MPA SAMs/ EDC-NHS/ streptavidin-conjugated ALP + p-app/ TCEP	amperometry	5 pM	No	aCSF	Liu et al. (2014)
Tau-381	GC/ carboxyl graphene/ thionine/ AuNPs/ Cysteamine	DPV	420 fM	Yes	Serum	Tao et al. (2019)
Tau-441	Gold/ Chitosan-CNTs-rGO/ GLA + AuNPs-cystamine tag	DPV	460 aM	Yes	Serum	Li et al. (2020)
	GC/ PTSA/ Cu^{2+}/ EDC-NHS	SWV	75 fM	No	Serum	Ye et al. (2020)
Tau	Carbon/ p-aminobenzoic acid/ EDC-NHS/ AuNPs-polyamidoamine dendrimer/ glutaraldehyde + HRP (sandwich assay)	amperometry	31 fM	Yes	Plasma/ Brain tissues	Razzino et al. (2020)
	Carbon/ GO/ EDC-NHS/ pPG / glutaraldehyde/ anti-Tau + pPG/ PbS/ anti-Tau (sandwich assay)	DPV	150 pM	No	Serum/ CSF	Derkus et al. (2017)

Table 2.8: Electrochemical biosensors for detection of AD biomarkers (4/6)

Analyte	Materials	Techniques	LOD	Labels	Matrices	References
ApoE	GSHs/ MB/ Fc	DPV	10 fM	No	PBS	Wu et al. (2016)
	Gold/ biotin-probe/ 6-mercaptohexanol + AuNPs/ferrocene/ streptavidin (sandwich assay)	CV	100 fM	yes	Serum	Lu et al. (2018)
	GC/ Au/ gold nanobipyramids+ polydopamine nanotubes doped with gold and palladium (sandwich assay)	amperometry	450 fM	yes	PBS	Liu et al. (2020)
	ITO/ fractal gold nanostructure + HRP (sandwich assay)	amperometry	8.78 pM	yes	PBS	Liu et al. (2015)
	Graphite/ MBs-Cab + biotinylated-Dab/ streptavidin/ QDs (sandwich assay)	SWASV	370 pM	Yes	Plasma	Medina-Sánchez et al. (2014)
	Carbon/ MBs/ EDC-NHS/ Cab + Dab/ iridium oxide nanoparticles (sandwich assay)	Chrono amperometry	1.99 nM	Yes	Plasma	Rivas et al. (2014)
	ITO/ AuNPs	EIS	286 nM	No	PBS	Cheng et al. (2014)
miRNA-34a	PGE/ GO/ amino linked hybridized miRNA-34a	EIS	261.7 nM	No	PBS	Congur et al. (2015)
miR-137	Carbon/ ErGO-AuNWs/ thiolated probe/ 6-mercaptohexanol/ doxorubicin	EIS	1.7 fM	Yes	Serum	Azimzadeh et al. (2017)
Clusterin	Carbon/ Pyr-NHS	DPV	17 fM	No	Plasma	Islam et al. (2018)

Table 2.9: Electrochemical biosensors for detection of AD biomarkers (5/6)

Analyte	Materials	Techniques	LOD	Labels	Matrices	References
unfolded p-53	Carbon/ AuNPs + biotin/ streptavidin labelled ALP/ 3-indoxyl phosphate/ silver nitrate (sandwich assay)	LSV	50 pM	Yes	Plasma	Amor-Gutiérrez et al. (2020)
	Au-Pt/AuNPs + streptavidin-MB (sandwich assay)	Chrono amperometry	66 nM	Yes	Plasma	Iglesias-Mayor et al. (2020)
ACh	Fluorine doped tin oxide/rGO-PEDOT/ Fe_2O_3 nanoparticles/ glutaraldehyde/ AChE)/ ChO	CV	4 nM	No	Serum	Chauhan et al. (2017)
	Gold/ gold coated Fe_3O_4 nanoparticles/ chitosan/ glutaraldehyde/ AChE)/ ChO	SWV	5 nM	No	Plasma	Chauhan & Pundir (2014)
	Gold/rGO/ CNTs- MnO_2 nanoparticles/ PEDOT/ chitosan/ glutaraldehyde/ AChE)/ ChO	CV	100 nM	No	Serum	Chauhan et al. (2020)

Table 2.10: Electrochemical biosensors for detection of AD biomarkers (6/6)

Chapter 3

Experimental techniques

3.1 Introduction

This section focuses on the fabrication and characterisation techniques used for development of biosensors. The steps involved in the fabrication process are explained in a chronological order followed by details of the optimisation experiments that were carried out to obtain the best sensing performance. Principle of each characterisation technique and its relevance in the present study is explained.

3.2 Fabrication process

In the present work, two electrochemical biosensors were developed for the detection of two most important AD biomarkers, namely $A\beta_{1-40}$ and $A\beta_{1-42}$. Carbon SPEs coated with graphene and rGO were used as substrates and were modified in a step by step fashion to fabricate the sensors. The materials involved in this process are described in detail below:

1. **Linkers**: Immobilisation of specific bio-receptors is a crucial step and directly influences the sensing performance (Su et al. (2019)). Graphene surfaces can be chemically functionalised with linker molecules for anchoring the bio-receptors (Wu et al. (2011)). In this work, two linkers namely, Pyr-NHS and primary amines (NH_2) were used to attach antibodies on the surface of biosensor.

2. **Bio-receptors**: Specific $A\beta_{1-40}$ and H31L21 $A\beta_{1-42}$ antibodies were used for the detection of target biomarkers to provide high selectivity. These specific antibodies were

preferred over commonly used $A\beta_{1-16}$ antibody (6E10) that can recognize both $A\beta_{1-40}$ and $A\beta_{1-42}$ targets (Yoo et al. (2017b); Hassan & Kerman (2019)).

3. **Blocking agents**: Non-specific bindings of the target generates background noise, which in turn produces unreliable results and increase the LOD. These occur due to the binding of target protein to the sensor using surface functionalities, even in the absence of antibodies (Shen et al. (2012)). Bovine serum albumin (BSA) is widely employed as a blocking agent in various biosensors to avoid non-specific interactions (Islam et al. (2017); Islam et al. (2018); Wang et al. (2018a); Amor-Gutiérrez et al. (2020)). This is attributed to its low cost, stability, and lack of effect/ interference in biochemical reactions (Shen et al. (2012). It has been shown to promote the selective bindings as compared to other blocking agents such as casein and fat free milk (Shen et al. (2012)).

A schematic showing step by step modification of SPEs for the fabrication of electrochemical biosensor is shown in figure 3.1 below.

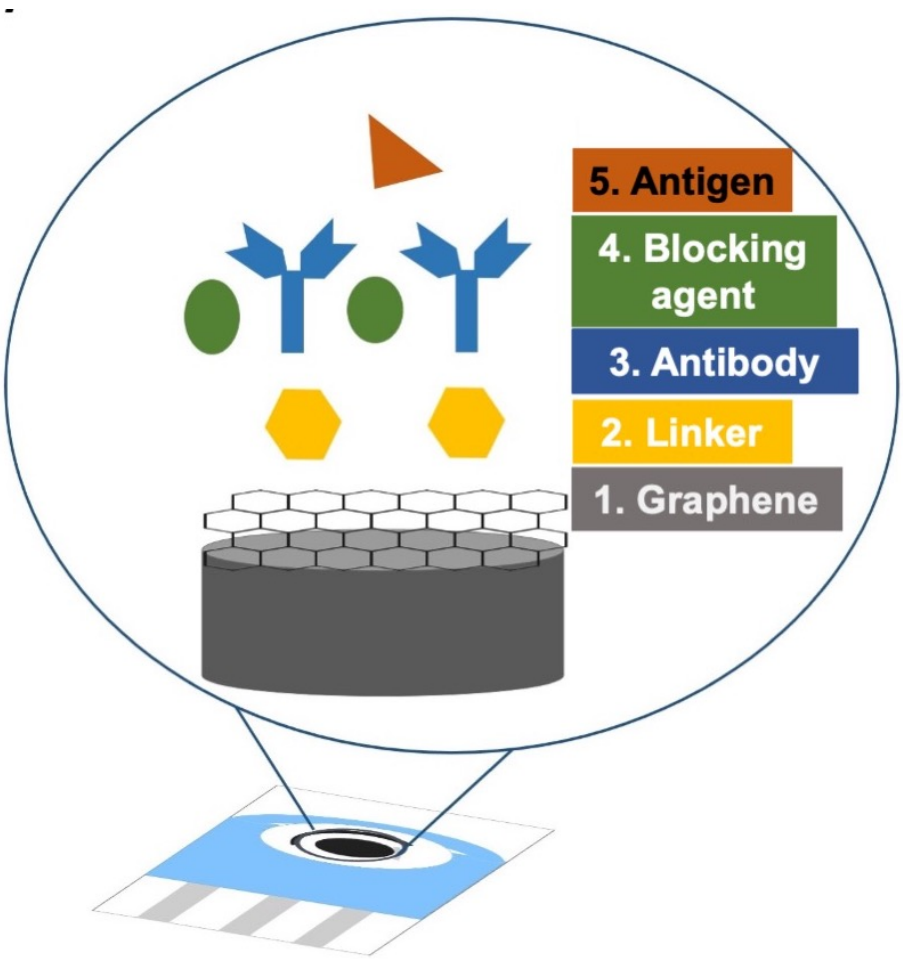

Figure 3.1: Step by step modification of graphene or rGO based SPEs for the fabrication of electrochemical biosensor

3.3 Optimisation experiments

The performance of the biosensors is highly dependent on the experimental parameters and/or conditions during their fabrication. To have control over the conditions such as temperature, moisture etc. such that they do not interfere with the fabrication and optimisation process, all the biosensors were fabricated inside a clean room. Also, clean room ensures quality, safety, and success of the biosensor by minimising contamination during the fabrication process. Important experimental parameters associated with linker, antibody and antigen were optimised. Linkers are crucial for the effective immobilisation of antibodies on the sensing surface and directly affects the sensitivity of biosensors (Balasubramanian & Kern (2014)). Therefore, concentration or time for linker attachment was optimised with extensive experiments. Incubation times for antibodies and antigen were also optimised. Effect of each parameter on target detection was studied by plotting the normalised current responses (for target detection) with respect to the optimising parameter. The times/concentration corresponding to highest current were chosen as the optimised responses.

3.4 Characterisation techniques

3.4.1 Voltammetry

The performances of the biosensors were evaluated using voltammetric analysis. In this technique, a variable potential is applied to WE (with respect to RE) over set potential range and then, the corresponding current (proportional to the concentration of target) is measured (Ronkainen et al. (2010)). Current is generated in response to the oxidation/reduction at WE. Therefore, it is limited by the rate of transport of molecules to the WE. Depending on the way potential is varied, voltammetric techniques are of various types such as LSV, CV, SWV, DPV, hydrodynamic voltammetry, stripping voltammetry and ac voltammetry (Kissinger & Heineman (2018)). These techniques can be used for quantification of low levels of target due to their wide dynamic range (Ronkainen et al. (2010)). The two voltammetry techniques employed for the present work are described below:

1. **Cyclic voltammetry** (CV): It is a simple, versatile and widely used electroanalytical

technique for acquiring information on the electroactive behavior of molecular species (Elgrishi et al. (2018)). In this technique, the applied potential at WE is swept at a steady scan rate in both forward and reverse directions. The current is evaluated as the potential's output function. The subsequent current *versus* scanned potential plot is called a voltammogram (Trnkova et al. (1980)). An example of a typical CV curve is presented in figure 3.2(a).

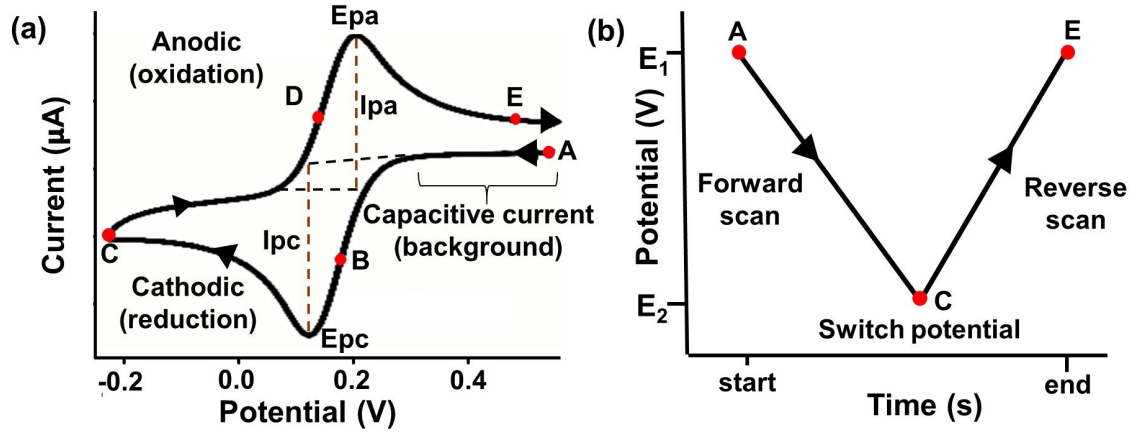

Figure 3.2: CV measurement: (a) a standard voltammogram depicting reduction (E_{pc}) and oxidation potential ((E_{pa})) peaks along with their corresponding currents i_{pc} and i_{pa} and (b) applied potential as a function of time for a CV measurement; initial, switching and end potentials are depicted with points A, C and E respectively.

The arrow indicates direction of the scanned potential for recording the data. It shows the beginning as well as the sweep direction of the forward and reverse scans. These scans are taken at a particular 'scan rate (ν)', the speed at which the potential is scanned linearly with time (Trnkova et al. (1980)). The variation in applied potential with respect to time for one cycle is shown in figure 3.2(b). In the forward scan, potential is scanned in the negative direction from points A to C. From figure 3.2(a), it is seen that the current scanned from point A, first depicts a capacitive (resting) state and then starts to decrease until the potential is sufficiently negative (B) after which, the cathodic (reductive) potential peak (E_{pc}) is reached and then, it starts increasing. When the applied potential surpasses the point C (switching potential), scan direction is reversed. In the reverse scan, potential is scanned in positive direction from point C to E. When the potential is sufficiently positive (D), current increases until the anodic (oxidative) potential peak (E_{pa}) is reached after which it starts to decrease. The corresponding current at peak E_{pc} and E_{pa} are denoted with i_{pc} and i_{pa} respectively. As the reaction proceeds (towards point E), the reductive and oxidative curves become closer and closer together, which indicates that the reaction is nearing completion (Baca & Dennis (1978); Mabbott (1983)). These changes in current

are due to the reduction/ oxidation of the molecular species (or electroactive species) provided by the electrolyte. The reaction for the potassium ferricyanide $K_3[Fe(CN)_6]$ electrolyte is:

$$[Fe(CN)_6]^{3-} + e^- \rightleftharpoons [Fe(CN)_6]^{4-} \tag{3.1}$$

In a negative scan, the forward reaction occurs from B to C until the concentration of $[Fe(CN)_6]^{3-}$ species in the electrolyte is reduced near the electrode surface. In positive scan, reverse reaction occurs from E to F until $[Fe(CN)_6]^{4-}$ species start to diminish. The CV characteristics can be used for calculating the diffusion coefficients and effective area of modified electrodes using Randles-Sevcik equation (Jennings et al. (1970)):

$$I_p = (2.69X10^5)n^{3/2}AD^{1/2}C\nu^{1/2} \tag{3.2}$$

where I_p is peak current of electrode (in Amperes), A is surface area of electrode (0.126 cm^2, for present work), D indicates the diffusion coefficient (in $cm^2\ s^{-1}$), n stands for the number of transferred electrons (for $K_3[Fe(CN)_6]$, n=1), ν is the scan rate ($V.s^{-1}$) and C is concentration of the redox species (10 mM, for present work).

The rate at which electron transfer between WE and electrolyte occurs is referred to as electrochemical reversibility. If the transfer is quick without any thermodynamic barriers, the reaction is said to be reversible and if it's not fast due to some complications, the reaction is considered irreversible. If the reaction has an intermediate rate of electron transfer, it's referred to as a quasi-reversible reaction (Nicholson (1965); Evans (1972)). This can be determined by calculating the heterogeneous rate constant (K_s) using Lavrion model (Laviron (1979); Wang et al. (2009b)):

$$K_s = \frac{mnF\nu}{RT} \tag{3.3}$$

where m denotes peak to peak separation between E_{pc} and E_{pa} (in V), n is number of transferred electrons (for $K_3[Fe(CN)_6]$, n=1), F is Faraday's constant (96485.34 $C.mol^{-1}$), ν stands for scan rate ($V.s^{-1}$), R is universal gas constant (8.314 $J.mol^{-1}.K^{-1}$) and T is absolute temperature (298 K). K_s<0.35 indicates fast electron transfer at biosensor's surface. Additionally, for a reversible process, value of m is about 0.059 V, i_{pc}/i_{pa}=1 and

peak current is proportional to the $\nu^{1/2}$. For a quasi-reversible process, only one of the characteristics is usually present that is the linear dependence of peak current on $\nu^{1/2}$. Similarly, in an irreversible process, none of the characteristics are present (Aristov & Habekost (2015)).

Surface density of the molecules present on the surface were calculated based on the following equation:

$$\Gamma = \frac{QN}{nFA} \tag{3.4}$$

where, Γ is the surface density, Q is charge calculated from the integration of the reduction peak of the CV peak (C), N is the Avogadro's number (6.022 X 10^2 mol^{-1}), n is number of transferred electrons (for $K_3[Fe(CN)_6]$, n=1), F is Faraday's constant (96485.34 C.mol $^{-1}$) and A is surface area of electrode (0.126 cm^2, for present work) (Puiu et al. (2014); Tehrani et al. (2021)).

2. **Differential pulse voltammetry** (DPV): It is an extensively utilised electrochemical method in which the potential is varied and the resulting current is determined (figure 3.3 (inlet)). It is similar to CV (Kounaves (1997)) except that in DPV, difference between two current measurements is plotted as a function of potential. Potential is applied in a series of small constant amplitudes with regular pulses. The base potential remains constant through one pulse period but varies from one pulse to the other with equal increments. The current measurement (denoted by 'sample period') is done before the application of pulse, after that the potential is stepped (denoted by 'Step E') and the current is measured again as shown in figure 3.3. Then, the difference between the two current measurements is used to obtain DPV characteristics (Rifkin & Evans (1976); Kounaves (1997)).

The sample periods are selected in such a way that allows the decaying of non-faradic (charging) current so that only faradic reactions are obtained, which makes DPV more sensitive than the CV technique (Scholz (2015); Simões & Xavier (2017)). Nevertheless, both CV an DPV techniques have been employed in this work because CV provides important information about process reversibility, the redox process in the analysis (analyte, matrix and electrode), diffusion coefficient of the electrolyte and transfer rate of electrons at the surface of electrode (Simões & Xavier (2017); Islam et al. (2018)). On the other hand, DPV is useful for quantitative measurements and has been used to measure low concentrations of

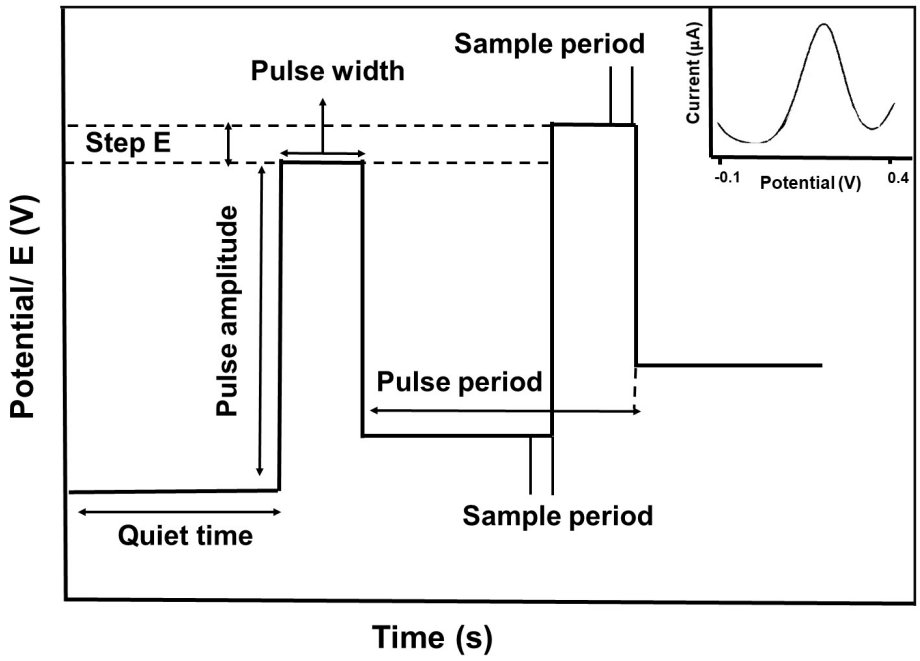

Figure 3.3: DPV measurement: (a) a typical voltammogram depicting change in current with respect to the potential (b) pulse sequence detail for a generic DPV experiment

analyte with high sensitivity (Li et al. (2015)). Both CV and DPV techniques were also used by Mars et al. (2018b) to assess the sensing performance of a novel curcumin-graphene quantum dots platform for ApoE4 detection. CV depicted a quasi-reversible redox process for the biosensor. DPV depicts a decrease in the current response with increase in target concentration and an LOD of 2.18 pg.mL^{-1} (buffer) and 18.6 pg.mL^{-1} (spiked human plasma) were obtained. Curcumin is an electroactive molecule, which facilitates the immobilisation of bio receptors. It is also an antioxidant polyphenol and is utilised for clinical purposes because of its anti-bacterial, anti-cancer and anti-inflammatory properties (Mars et al. (2018b)).

Measurements

Electrochemical biosensors were based on graphene or rGO modified SPEs provided by Metrohm Dropsens. The SPEs had graphene or rGO as working electrode, carbon as auxiliary electrode and silver as reference electrode. Both CV and DPV were carried out in an electrolyte containing 10 mM $K_3[Fe(CN)_6$ with 1 M potassium chloride (KCl) as the supporting electrolyte. CV was acquired at commonly used scan rate of 50 mV.s^{-1} within a potential range of -0.2 and 0.5 V without applying any pre-conditioning potential or accumulation time. DPV was also recorded at 50 mV.s^{-1} scan rate from a potential of $+0.15$

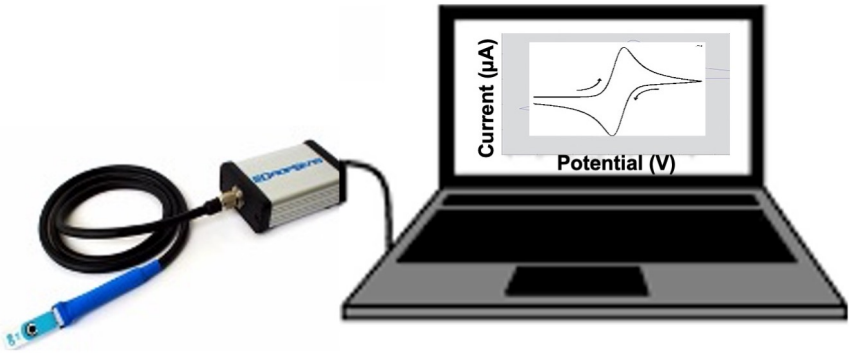

Figure 3.4: Portable electrochemical instrument by Dropsens

V to +0.45 V with a 50 mV pulse amplitude, 10 mV step potential and 0.4 s pulse period. The measurements were performed using an electrochemical instrument by DropSens (figure 3.4) with a portable bipotentiostat/galvanostat with a potential range of ±4 V DC and ±40 mA maximum measurable current.

3.4.2 Fourier Transform Infrared Spectroscopy (FTIR)

FTIR is an effective tool to obtain the chemical analysis of organic, inorganic and/or polymeric materials. It utilises infrared light for the scanning of samples. The collected data is processed using the fourier transform method and is translated into a spectrum (Shameer & Nishath (2019)). Infrared (IR) radiations of approximately 10,000–100 cm^{-1} are passed through the 'sample of interest' and only some of it is absorbed. The absorbed radiations are converted into rotational and vibrational energy by the sample. In general, resulting spectra obtained by the detector is between 4000- 400 cm^{-1}, which depicts molecular fingerprints of the sample. Every molecule carries a unique fingerprint making FTIR (Titus et al. (2019)) an extremely useful technique to confirm the changes in chemical structure and hence, successful modification of the SPEs.

FTIR instrument consists of a sample cell, an IR light source, a detector, an amplifier, an A/D converter and a computer as seen in figure 3.5. The IR radiations produced from the source passes through the sample and reaches the detector. The signal at the detector is processed, amplified followed by conversion into a digital signal with the help of an A/D converter. This processed signal is then sent to a computer, which performs the fourier transform process on it to generate the desired spectrum.

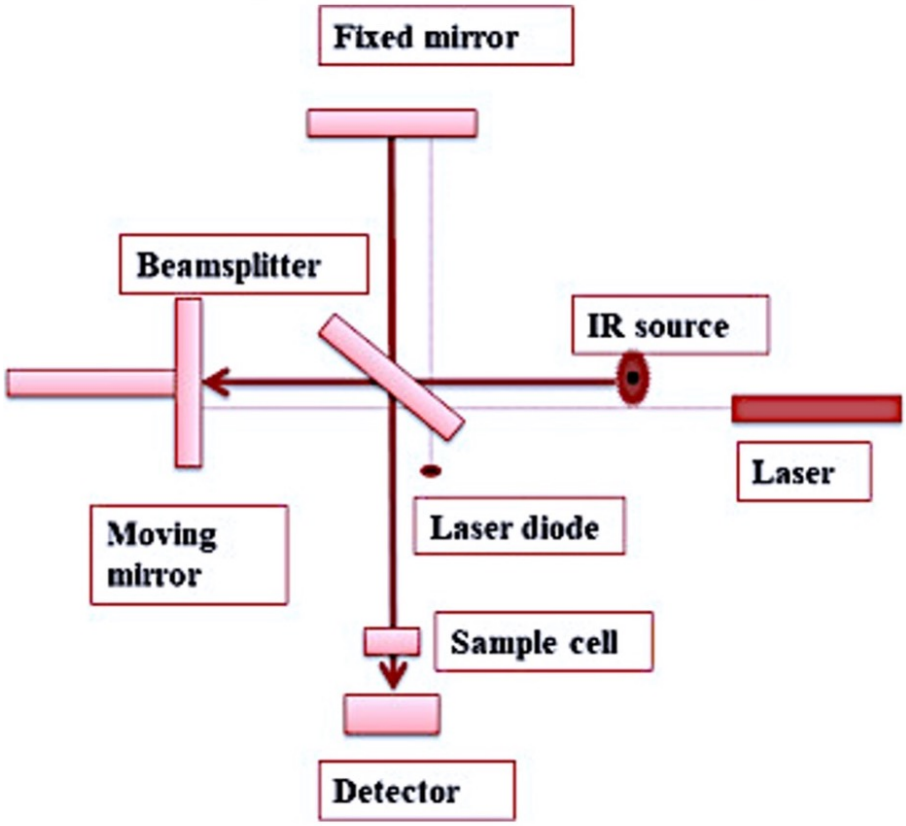

Figure 3.5: Working principle of a FTIR instrument (Titus et al. (2019))

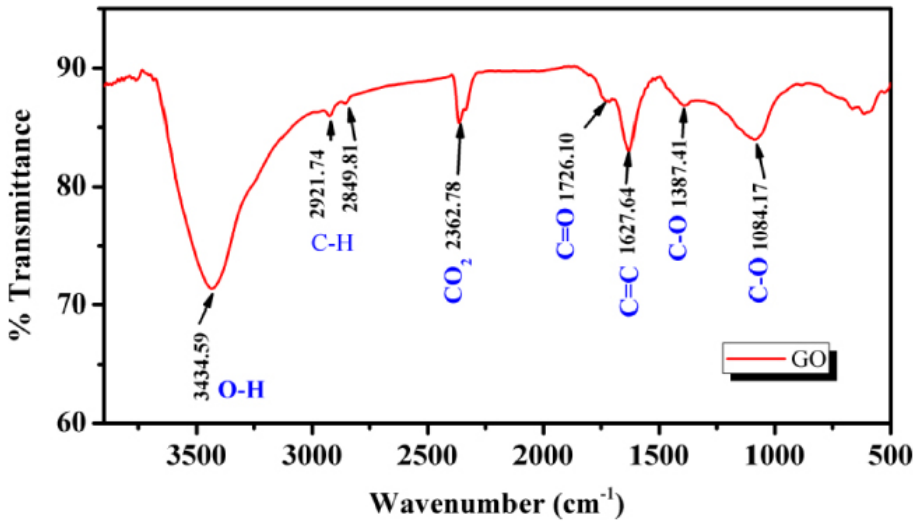

Figure 3.6: FTIR spectra of GO (Kumar et al. (2013))

In the present study, FTIR is used to characterise the surface of SPEs, before and after the ammonia treatment, during the fabrication process. Comparison of ammonia treated and untreated SPE's spectra give us the information about the newly attached functional groups on the surface. As an example, a typical GO spectrum is shown in figure 3.6. The spectrum is obtained between transmittance percentage (%) Transmittance) and wavenumber (cm^{-1}). The peaks represent the absorption of light by various molecules

present in the GO sample.

3.4.3 Raman Spectroscopy

Raman spectroscopy is an effective tool for determining quality, number of layers as well as doping/ impurity content of graphene. A typical system consists of optics, photo-detector, monochromator and an excitation light source. Laser excitation leads to the elastic scattering of most of the photons from the surface of graphene, nevertheless, a small portion gets inelastically scattered. Inelastic scattering is referred to as a change in the wavelength (Raman shift) of the photon after its interaction with graphene crystal. The molecules absorb the photon and get excited to a virtual state from where they either decay back to a level higher (stokes) or lower than their initial level (anti-stokes) as shown in figure 3.7. These changes in wavelength of the scattered light, caused by the molecular vibrations/ rotations, provide information about the chemical bond structures and defects of graphene (Tobias (1967); Ferrari (2007); Schrader (2008)).

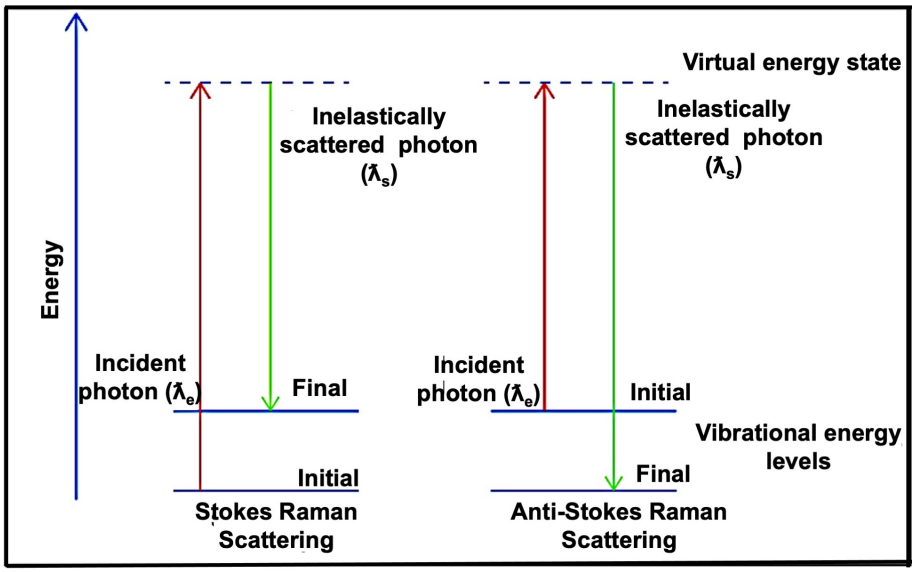

Figure 3.7: Schematic representation of Raman scattering with Stokes and Anti-Stokes Scatters (McGregor et al. (2016))

In this work, Raman analysis was performed using a XPLORA HORIBA system combined with an Olympus BX41 microscope (equipped with 10 X, 100 X objective lenses and 10 X eyepieces) (figure 3.8). The characterisation of graphene was achieved using a 532 nm green laser source with 100 mW power, 100 X objective lens, 1100 to 2000 cm^{-1} scan range and 5-60 s exposure time.

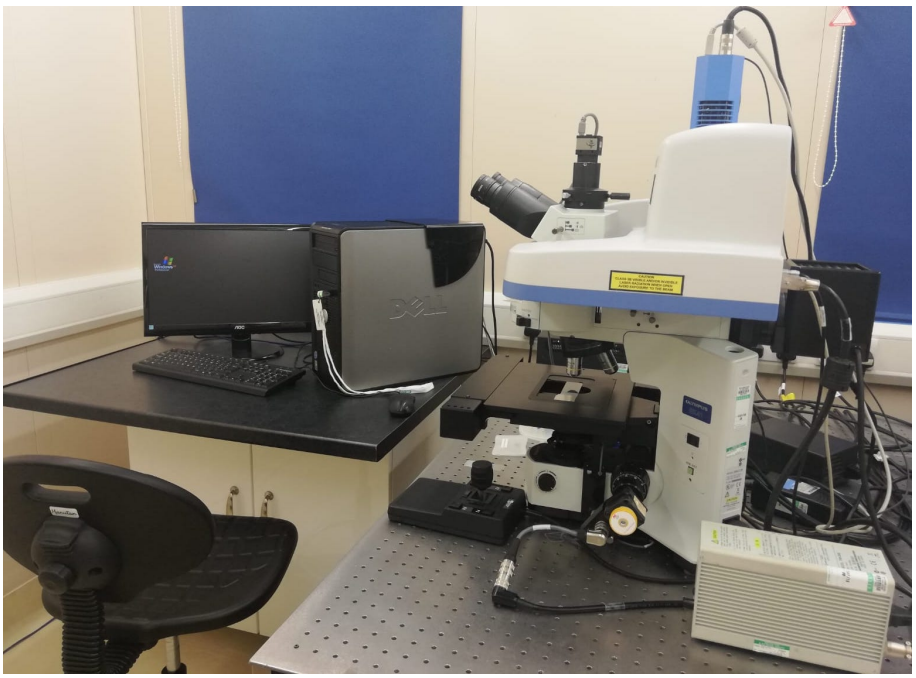

Figure 3.8: XPLORA HORIBA system combined with an Olympus BX41 microscope for Raman Spectroscopy

Raman spectroscopy is used to characterise the surface of graphene and rGO SPEs before and after the surface modifications. This is to see the changes induced into the graphene structure such as the introduction of defects, during the fabrication process. An example of a Raman spectrum of GO, plotted between intensity and Raman shift (cm^{-1}) is shown in figure 3.9. The two peaks are for D (1347 cm^{-1}) and G band (1596 cm^{-1}) respectively. The D band is an indication of disorder or edge sites present within the graphene plane and its intensity is related to the level of disorder. This band is formed due to second order Raman scattering process of sp^3 hybridised carbon bonds. On the other hand, G band is a result of in-plane vibrations of C-C and is therefore, extremely sensitive to stress changes induced by the variations in number, crystallinity and symmetry of graphene layers (Dresselhaus et al. (2008)). The ratio I_D/I_G indicates average distance between defective sites (Lucchese et al. (2010)). In this study, Raman spectra is collected from random points on the surface to make sure that the surface was modified completely which also eliminated the need for Raman mapping.

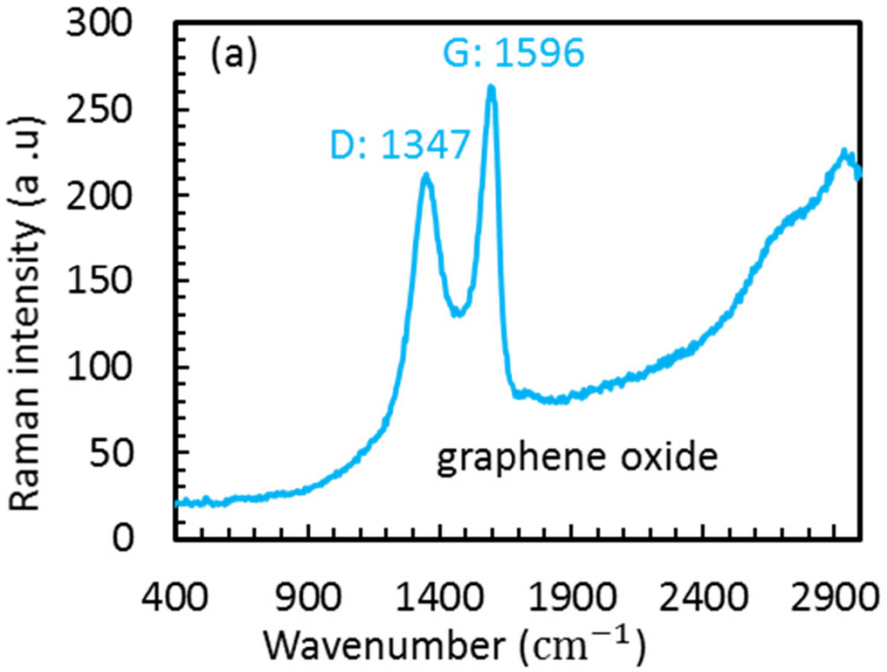

Figure 3.9: Raman spectrum of GO (Adewole et al. (2019))

3.4.4 X-ray photoelectron spectroscopy (XPS)

XPS is another effective tool for the characterisation of sample surfaces and gives detailed information regarding the elemental composition and chemical states. In principle, the 'sample of interest' is irradiated with X-rays, input photons are absorbed by the sample resulting in the emission of the photo electrons (figure 3.10) with characteristic binding energy for individual elements. The minimum amount of energy required for the ejection of electron from an atom is known as the work function and is a correction factor for the instrument. By analysing particular binding energies as well as their corresponding intensities, quantitative data about the elemental composition and chemical states can be obtained.

A Thermo Scientific™ Nexsa™ system was used for performing the XPS analysis using a monochromatic X-ray source (1486.68 eV). For the wide scan, pass energy was 200 eV with a step size of 1 eV and 10 scans. For the high-resolution scan, pass energy was 40 eV with a step size of 0.1 eV and 20 scans.

In this study, XPS is used to study the chemical states of the elements on rGO and graphene surface before and after the surface modification. This is to ensure the successful attachment of desired groups on the surface during the fabrication process. An example

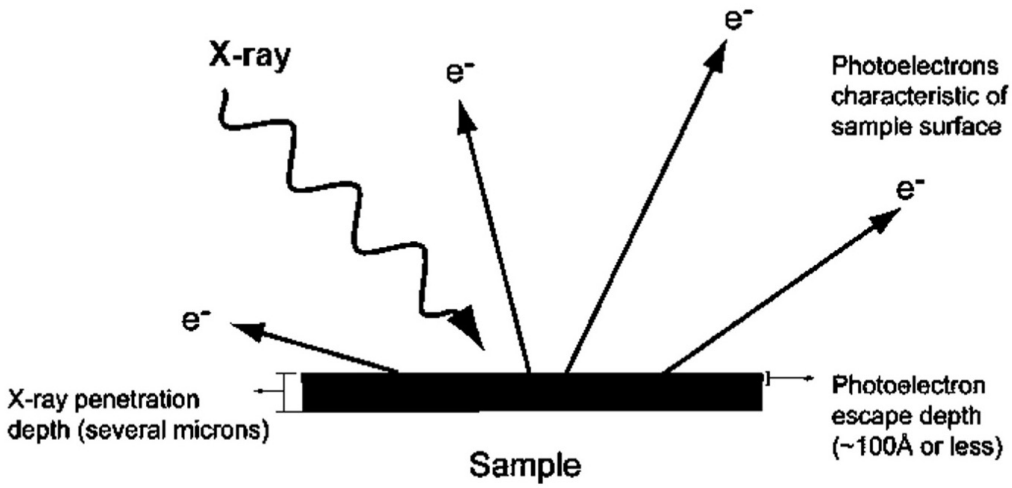

Figure 3.10: Working principle of XPS (EAG Laboratories (2015))

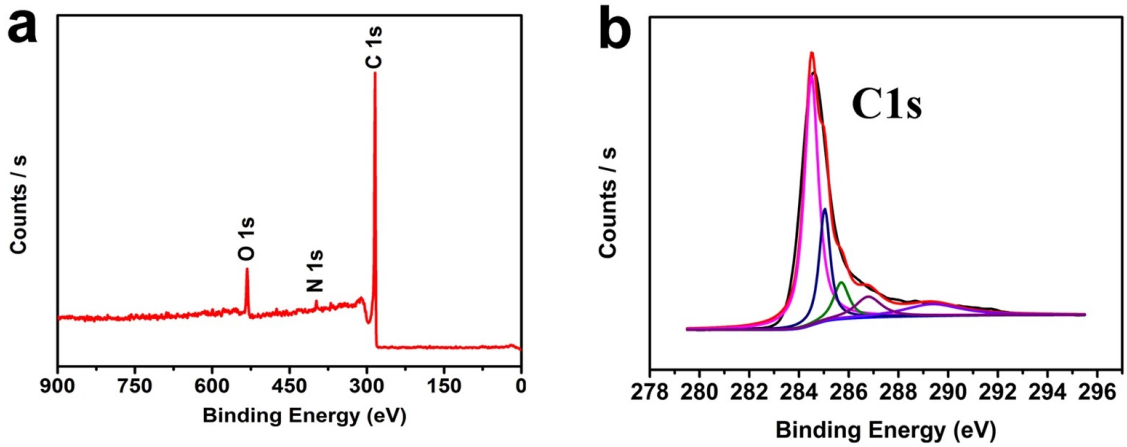

Figure 3.11: XPS analysis of a n doped graphene: (a) wide scan and (b) C1s spectra (Xing et al. (2016))

of a wide region and C1s spectra of a n-doped graphene obtained by Xing et al. (2016), plotted between count per second and binding energy (eV), is shown in figure 3.11. The wide region spectra provide information about the major elements and C1s spectra gives detailed information about the type of carbon bonds present on the surface (including C-C, C-N, C-O, C=O, and O=C-O groups) (Xing et al. (2016)). Other spectras such as O1s (information about oxygen bonds, obtained between 528- 540 eV) and N1s (information about nitrogen bonds, obtained between 394-406 eV) are also used in this work and are presented in section 4.1.4 (figure 4.6) and section 4.2.4 (figure 4.16(a,b,c)).

3.4.5 Scanning electron microscope (SEM)

SEM is performed to study morphology of the modified surfaces. Sample is loaded in a vacuum chamber and sample surface is scanned using a focused beam of electrons. This

leads to a generation of secondary electrons, which are detected to provide information about the topographical data.

SEM characterisation was performed using JEOL 6610 LV SEM from Oxford Instruments using acceleration voltage of 30 kV. An image of the instrument is shown in figure 3.12.

Figure 3.12: JEOL 6610 LV SEM from Oxford Instruments

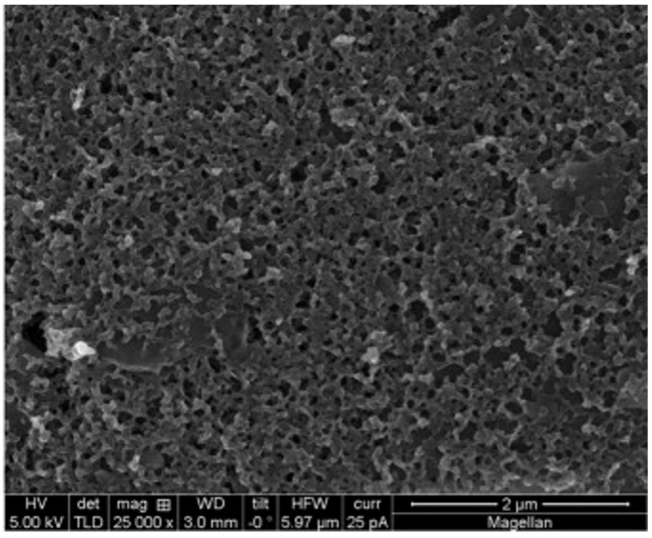

Figure 3.13: SEM image of a graphite SPE (Amin et al. (2014))

In this study, SEM analysis is used to study the changes in the morphology of graphene and rGO SPEs before and after the surface modification with desired groups. This is mainly to see whether the chemicals used during the fabrication process have any impact on the surface of graphene. As an example, SEM image of a graphite SPE is shown in figure

3.13 depicting a rough surface. A detailed explanation of the SEM images is provided in section 4.1.4 (figure 4.4) and section 4.2.4 (figure 4.15(a,b)).

3.4.6 Animal based studies

Blood and brain sampling

Blood and brain samples were obtained from 9 and 12 months old wildtype (WT) and transgenic (Tg) animals of the strain B6.Cg-Tg (APPswe/PSEN1dE9) 85Dbo/Mmjax, lab stock number 005864. Blood was drawn by submandibular bleeding methods using a sterile blood lancet. The blood droplets were collected by Microvette CB 300 K2E tubes. A novel standardized method of blood extraction and purification protocol was developed to obtain non-haemolytic plasma samples from rodents. It consisted of two centrifuge steps. The first centrifuge step (1500 $\times$g for 10 min at 15 °C) was performed soon after the blood collection, to separate the plasma fraction from red blood cells and buffy coat. Then, the plasma fraction was collected in Eppendorf® LoBind microcentrifuge tubes and directly placed on ice. The second centrifuge step (3500 $\times$g for 10 min at 4 °C) was carried out to separate additional red blood cell debris. Finally, the plasma was divided in aliquots and stored at -80°C for long-term preservation.

All the experiments related to the animals were performed in Centro de Investigación Biomédica en Red Enfermedades Neurodegenerativas (CIBERNED), Spain. The ethical approval was provided by the "Ethics Committee for Animal Experimentation" of the Instituto de Investigaciones Biomédicas (CSIC-UAM) and experiments were carried out in accordance with European Communities Council Directive (2010/63/EEC) and National regulations (Normative 53/2013). Plasma studies with biosensors were performed in University of Plymouth, UK with approval of local Ethics Committee.

Immunohistochemistry (IHC)

IHC is a powerful tool for the detection of target antigens in the animal tissues. It gives important information regarding the tissue distribution of target antigen using specific antibodies (Duraiyan et al. (2012)). Double-immunofluorescence analysis was performed with mice brain sections using a previously described protocol (Luna-Medina et al. (2007)). Briefly, animals were anesthetised followed by transcardial perfusion. After this, brains

were extracted and post-fixed with 4% paraformaldehyde and 30% sucrose solution overnight at 4°C. Subsequently, 30 µm coronal section were obtained using a cryostat. The selected free-floating cortical-hippocampal section was blocked in 0.1 M containing 3% normal goat Serum and 0.1% Triton X-100 for 1 hour at RT. It was then incubated with $A\beta_{1-42}$ primary antibody (H31L21), overnight at 4°C. Several washes were performed in 0.1M phosphate buffer containing 0.1% Triton X-100. Then, the sections were incubated for 1 hour with a secondary antibody, Alexa-fluor 546 goat anti-rabbit. Nuclei staining was performed using DAPI. Finally, the brain sections were mounted with Vectashield H-1200, fluorescence microscope images were collected using a Nikon Eclipse 90i microscope using Plan APO 4x objective, equipped with Nikon DS-Fi1 digital camera. It was connected to Nis-elements software (Preibisch et al. (2009)).

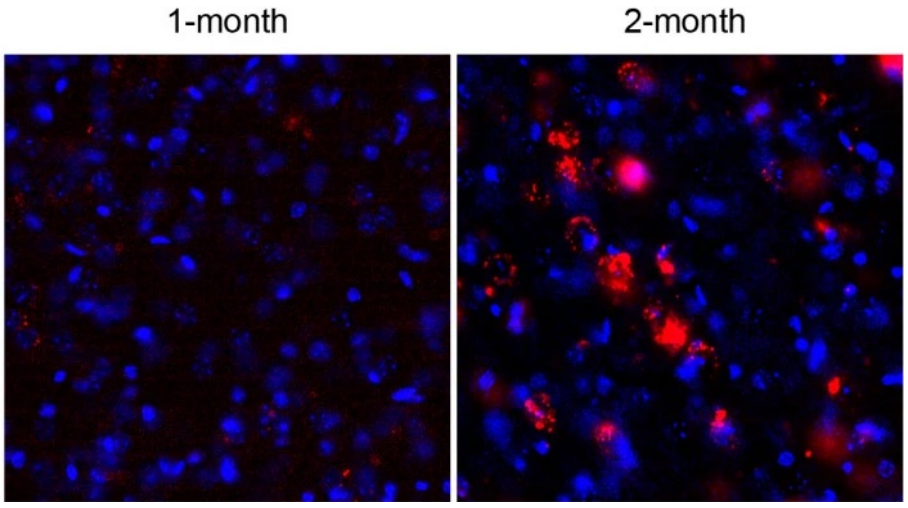

Figure 3.14: IHC images for the accumulation of Aβ (red) in the brain of 1 and 2 months old Tg mice (Youmans et al. (2012))

In this study, IHC is used to study the accumulation of $A\beta_{1-42}$ in the 9 and 12 months old WT and Tg mice. The is to see the changes that occur in the brain tissues of these mice with progression of AD. Correlation studies with the $A\beta_{1-42}$ levels in plasma help to validate the performance of biosensor for biofluidic analysis. An example of IHC image is shown in figure 3.14 and depicts an increased Aβ pathology (shown in red colour) in the brain of a 2 month old Tg mouse (with 5 familial AD mutations, two presenilin-1 and three APP) compared to 1 month old Tg mouse (Youmans et al. (2012); Maarouf et al. (2013)).

Magnetic resonance imaging (MRI)

MRI is a widely accepted technique and provides detailed anatomical information about the brain (Ogawa et al. (1990)). In the present work, it was used to obtain evidence

regarding Aβ load in the brain of 12 months old WT and Tg mice. It was performed on a Bruker Pharmascan Biospect system (Bruker Medical Gmbh, Ettlingen, Germany). The system was equipped with a 7.0-T horizontal-bore superconducting magnet, 1H receive-only mouse brain surface coil and volume transmission coil and a Bruker gradient insert (maximum intensity 36 G/cm). All data was acquired using a Hewlett-Packard console running on Paravision 5.1 software. Sensor with monitor system (SA Instruments, Stony Brook, NY) was used to measure the rate and depth of respiration of the animals. To perform the MRI, animals were anesthetized using a mixture of 2% isoflurane-oxygen, which was continuously regulated to retain a 60 +/- 40 bpm breathing rate. This was monitored with a respiration sensor placed under the abdomen of the animals. The mouse brain surface coil was mounted on the mouse cradle and placed over brain of the animal. Then, the animal was positioned in the magnet of the Bruker Pharmascan Biospect system. The acquisition of two sets of magnetization transfer contrast imaging were obtained. Finally, the MTR (magnetic transfer ratio) maps were evaluated using a homemade software application with Matlab (R2007a). The values were extracted from the maps using the region of interest (ROI) with the Image J software.

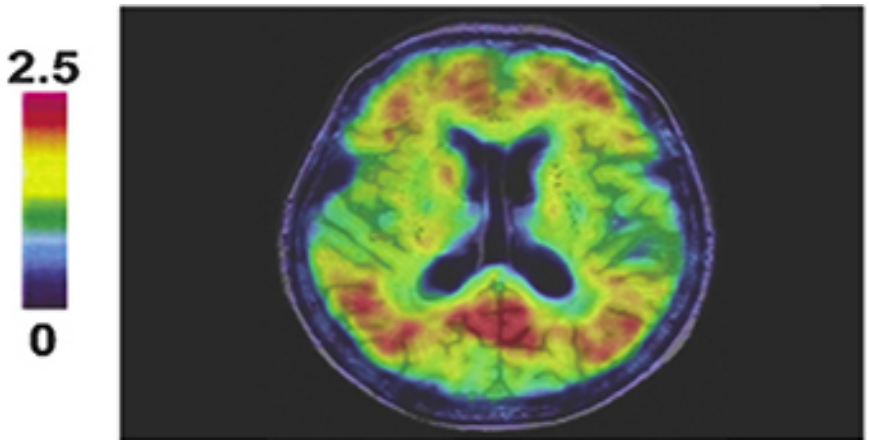

Figure 3.15: MRI image of the brain of an AD patient showing Aβ plaques accumulation (Adlard et al. (2014))

In this study, the MRI is used to see the accumulation of $A\beta_{1-42}$ in the brain of mice. This helps to confirm that a high level of AD pathology is observed in Tg mice in comparison to WT mice. An image of the amyloid deposition in the brain of an AD patient is shown in figure 3.15. The ration of Aβ plaques accumulation is illustrated by 0-2.5 (from blue to red magnetic resonance spectra).

Chapter 4

Results and discussion

4.1 A label-free biosensor based on graphene/rGO dual-layer for detection of beta-amyloid biomarkers

4.1.1 Introduction

In this section, a graphene/rGO dual-layer biosensor is demonstrated for detection of $A\beta_{1-42}$ biomarker. Most biosensors developed for detection of various AD biomarkers are either based on only graphene or only rGO (as discussed in section 2.3), however, a combination of the two is employed for the first time in the detection of protein biomarkers. Coupling of rGO and graphene provides a robust, highly conductive and sensitive platform with high number of available active sites that can enhance the electrochemical response, generate a higher redox current. In addition, the conductivity of rGO on graphene was found to be much higher than on other materials such as carbon (Su et al. (2009)). The rGO surface is chemically functionalised with Pyr-NHS to anchor antibodies without damaging/ degrading its properties. The interaction of Pyr-NHS with rGO on a dual-layer surface is reported for the first time. The immobilisation of H31L21 antibodies lead to high selectivity of the biosensor towards $A\beta_{1-42}$ peptides against $A\beta_{1-40}$ and ApoE ϵ4 interfering species. The biosensor has been successfully validated with both spiked human and mice plasma samples displaying its applicability for real-time analysis (Sethi et al. (2020)). Therefore, this dual-layer platform provides sensitive, selective, rapid and reliable detection of target biomarker and overcomes the shortcomings of existing biosensors discussed in section 2.3.3.

4.1.2 Fabrication process

Firstly, a solution of 0.15 mg.mL^{-1} monolayer GO was prepared in deionised (DI) water. This solution was carefully drop casted onto the surface of graphene SPEs and dried for 2 hrs at room temperature (RT) to promote strong bond formation between graphene and GO as shown in figure 4.1 (a).

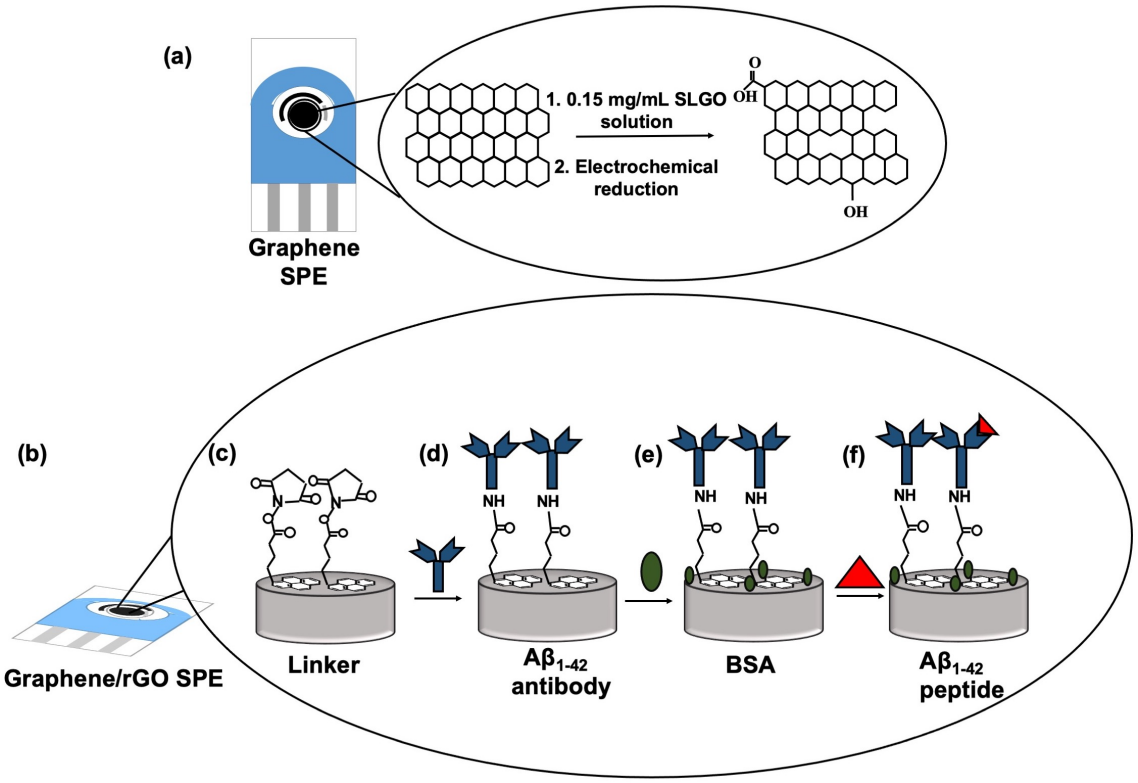

Figure 4.1: Fabrication steps involved in the development of the electrochemical system: (a) modification of graphene SPE with monolayer GO followed by its electrochemical reduction generating graphene/rGO dual-layer (b); modification of dual-layer with linker (c); Aβ_{1-42} antibody (d); BSA (e) and Aβ_{1-42} peptide (f)

Following this, modified SPEs were washed 3 times with DI water. Then, the GO layer was electrochemically reduced in the electrolyte solution using one CV cycle to obtain graphene/rGO dual-layer. The dual-layer SPEs were incubated in a 5 mM Pyr-NHS solution (in methanol) for 2 hrs at RT followed by washing with methanol to remove the unbound Pyr-NHS molecules. After that, SPEs were incubated overnight (16 hrs) with 20 µg.mL^{-1} of Aβ_{1-42} antibodies at 4°C. The antibodies were prepared according to the instructions provided by the supplier and diluted in a solution of PBS. Following the incubation, the SPEs were washed with PBS to remove any unbound antibodies and incubated with 2% BSA (in PBS) for 2 hrs at RT. After washing, the SPEs were ready to be used for the detection of the target and were incubated with desired dilutions of freshly

prepared $A\beta_{1-42}$ peptides in PBS solution for 60 minute at RT. The scheme of this process is shown in figure 4.1 (b). In order to avoid the aggregation, peptides were prepared fresh and kept on ice before putting them onto the sensor. Then, the sensors were washed 3 times with PBS before the measurements to remove any unbound peptide. The volume of the solution required for incubation was between 10-20 µl. Similarly, for real-time detection, human plasma was spiked with desired concentration of $A\beta_{1-42}$. Then, 20 µl of it was drop casted on to the biosensors for 60 min. Mice plasma samples were analysed in a similar way without any pretreatment.

4.1.3 Optimisation experiments

The effect of various linker concentrations (2, 3, 5, 7, 10, 20 and 40 mM) on the normalised current was studied (figure 4.2(a)). Here, the maximum normalised current values indicate the optimum immersion time at which the best performance of the biosensor was recorded. A steady increment in the normalised current is observed until it reaches its maximum value at 5 mM linker concentration, after which it steadily decreases and then saturates for a concentration beyond 20 mM. It can therefore, be hypothesized that below 5 mM, there are not enough linker molecules on the surface to attach 20 $\mu g.mL^{-1}$ concentration of antibody. The increase in linker concentration improves the performance of biosensor until the 5 mM concentration is reached. Increasing the concentration beyond this point leads to a decrease in current due to shielding of the electrode surface from the electrolyte which in turn leads to poor charge transfer with the surface. Another reason could be that the increase in linker molecules beyond 5 mM leads to non specific adsorption of the antigen on the surface which deteriorates the performance of the biosensor. Linker concentration above 20 mM, leads to a saturation of the electrode surface, deteriorating the charge transfer even further such that no change is observed in the current beyond this point. For further verification of the the above results, calibration plots for determination of $A\beta_{1-42}$ (0.2 pM-55nM) using sensors modified with different linker concentrations were plotted (figure 4.3). Biosensor with 40 mM linker concentration was so much saturated with molecules, that almost all the antigen concentrations gave similar response. The 5 mM linker concentration depicted reproducible results with small error bars (shown in figure 4.9) and hence, chosen as optimum for the present study.

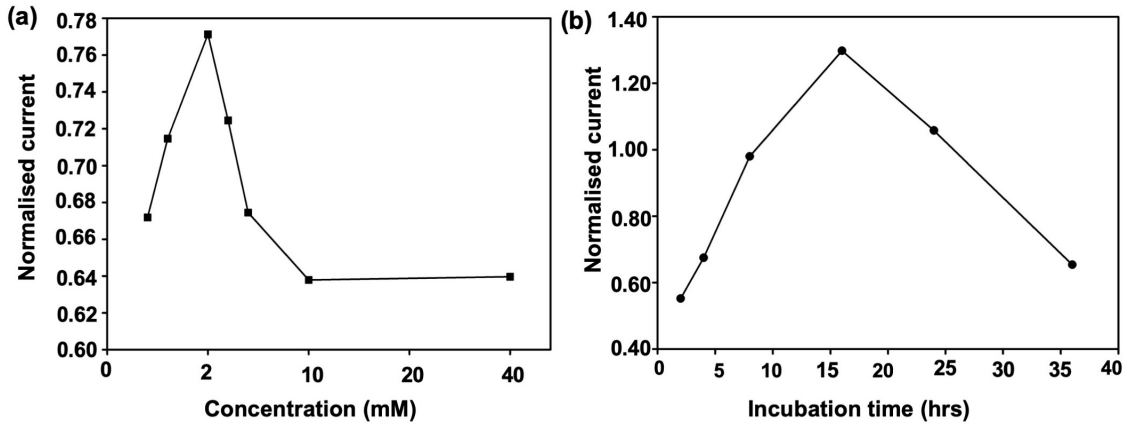

Figure 4.2: Effect of different linker concentration (2, 3, 5, 7, 10, 20 and 40 mM) (a) and antibody incubation time (2, 4, 8, 16, 24 and 36 hrs at 4°C) (b) on the normalised current response of the biosensor

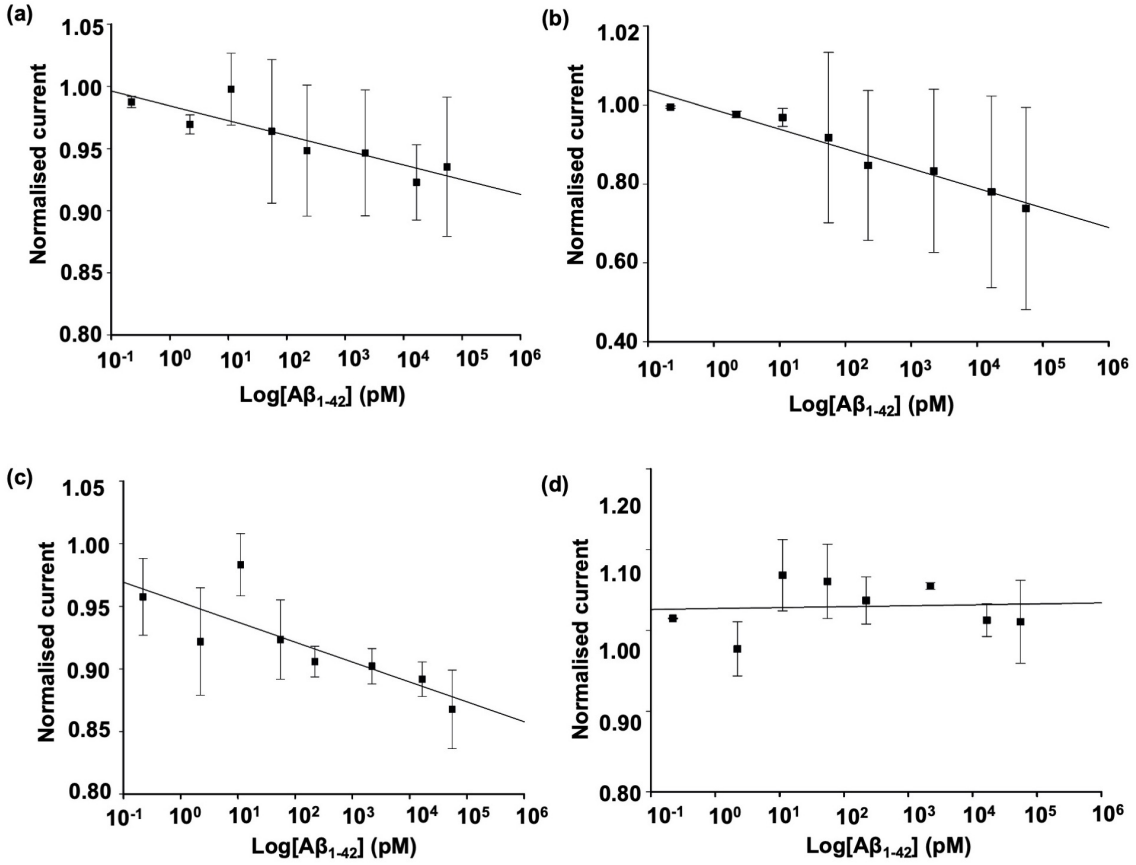

Figure 4.3: Detection of various $A\beta_{1-42}$ concentrations with biosensors modified with different linker concentrations namely, (a) 2mM; (b) 10mM; (c) 20mM; and (d) 40mM (n =3)

The effect of different incubation times of antibody (2, 4, 8, 16, 24 and 36 hrs at 4°C) on normalised current was also studied. As seen in figure 4.2(b), the current boosts drastically with the increment in time up to 16 hrs after which it starts decreasing. This indicate that the incubation times below 16 hours, leads to lower density of antibodies on the surface which are not enough to capture the given concentration of target molecules. Beyond this,

the surface gets shielded with antibody leading to poor charge transfer and ultimately, poor performance of the biosensor. Consequently, 16 hrs is chosen as the optimal time for incubation of antibody. All the data is based on DPV responses.

4.1.4 Characteristics of graphene/rGO dual-layer biosensor

In this section, the morphological, spectral and electrochemical properties of graphene and graphene/ rGO dual-layer were studied to understand the superiority of the latter structure.

SEM Analysis

The SEM images display surface morphologies of the graphene and graphene/rGO on carbon WE (figure 4.4). The images depict that modification of graphene with rGO did not effect the surface significantly and confirms that no structural damage was done. This contrasts with violent and deleterious chemical modification procedures used for graphene sensors such as the Fenton method by Teixeira et al. (2014) (discussed in section 2.3.3), which can damage the structure of graphene. As a result, the unique electrical properties of graphene remain unaltered and a high redox current is observed for graphene/rGO dual-layers as observed by CV analysis (figure 4.7(a)).

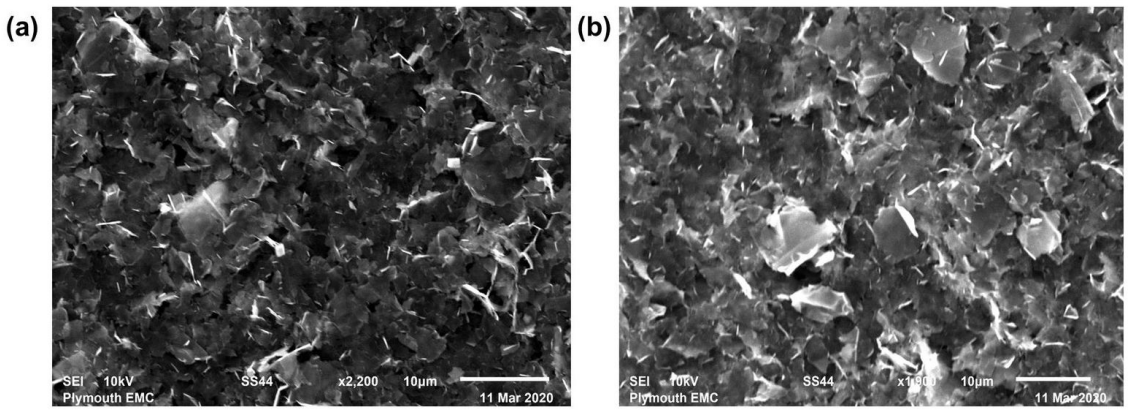

Figure 4.4: SEM analysis of graphene (blue) and graphene/rGO (black) dual-layer SPE

Raman Analysis

Raman spectra of graphene (blue) and graphene/rGO (black) is shown in figure 4.5. Graphene has a weak peak around 1346 cm^{-1} and a strong peak around 1574 cm^{-1}. The intensity ratio of D to G band (I_D/I_G) was found to be 0.1, which indicates low level of

defects. Formation of graphene/rGO dual-layer led to wider peaks around 1346 cm^{-1} and 1574 cm^{-1}. Also, a slight increase in the intensity of D band is observed compared to the G band. I_D/I_G ratio is increased to 1.05 due to increase in sp^3 planar carbon atoms (Su et al. (2016); Abdali & Ajji (2017)) from rGO. This confirms the successful adhesion of rGO on graphene surface to form the dual-layer structure.

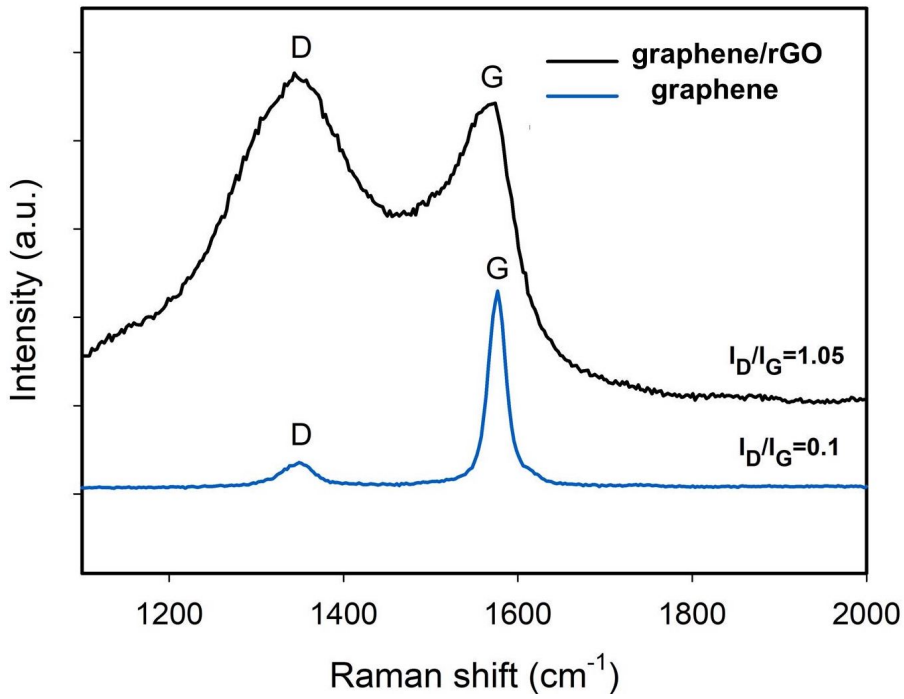

Figure 4.5: Raman spectra of graphene (blue) and graphene/rGO (black) dual-layer SPE

XPS Analysis

XPS analysis was employed to analyse chemical states of the elements on graphene WE before (black) and after modification with rGO (green) as shown in figure 4.6. The wide region spectra of graphene and graphene/rGO dual-layer surfaces show typical C (≈284.5 eV) and O (≈532 eV) peaks (figure 4.6(a)). The atomic percentage (at%) of oxygen on the surface was calculated by XPS elemental analysis. It increases from 1.40 to 2.62 after modification with rGO. For the analysis of the nature of C and O species, the C1s (figure 4.6(b)) and O1s (figure 4.6(c)) regional high resolution spectra were plotted. The C1s of graphene demonstrate four peaks emerging from C-C/C=C in aromatic rings (284.5 eV) , C-O (≈286.14), C=O (≈287.20 eV), and O-C=O (≈291.3 6 eV) bonds (Xing et al. (2016)). After modification with rGO, an increment in the peak intensity of C-O is seen whereas no significant shift is seen in C=O and O-C=O peaks. This can be attributed to the reduced number of oxygen functionalities in rGO (Li et al. (2015)). For further analysis,

the O1s spectrum of the two surfaces were compared. The graphene/rGO surface can be deconvoluted into two peaks, namely C=O/ O-C=O (≈531.5 eV) and C-O (≈533.2 eV) (Botas et al. (2012)) whereas graphene depicts a single lower intensity peak at ≈533.2 eV. These results confirm the successful modification of graphene with rGO.

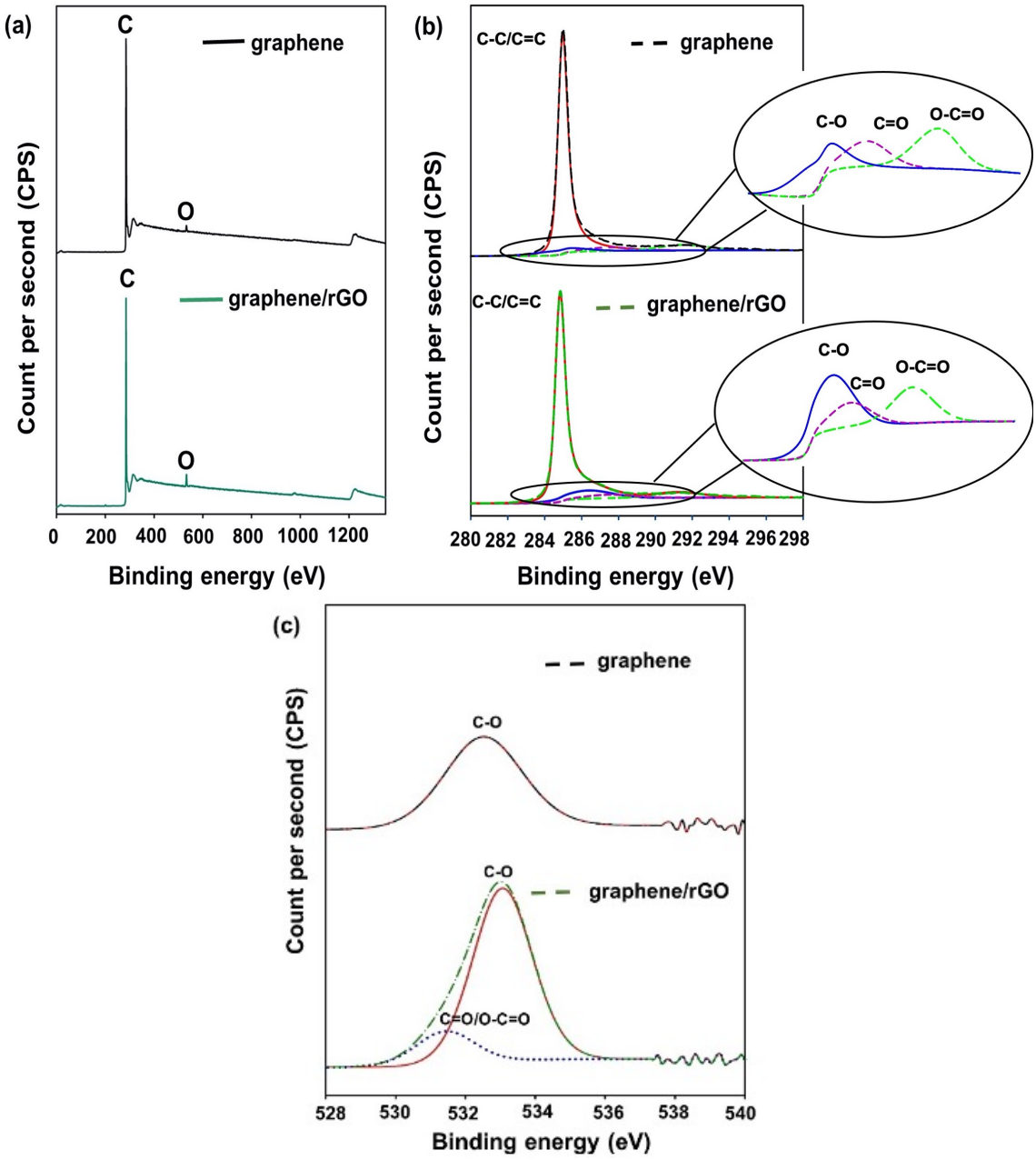

Figure 4.6: XPS analysis for graphene (black) and graphene/rGO (green) showing (a) wide scan; (b) C1s and (c) O1s spectra

Electrochemical analysis

Figure 4.7(a) shows a comparison in the voltammograms of graphene (blue), graphene/GO (red) and graphene/rGO dual-layer SPE (black). The modification of graphene with GO leads to a decrease in peak current. This is attributed to the long-range broken conjugated

network of GO due to many oxygen functional groups. Electrochemical reduction of GO leads to the formation of graphene/rGO dual-layer with higher peak currents compared with only graphene and graphene/GO modified SPE. This is due to a combination of inherited electroactive sites from rGO and high conductivity of graphene (Li et al. (2015)).

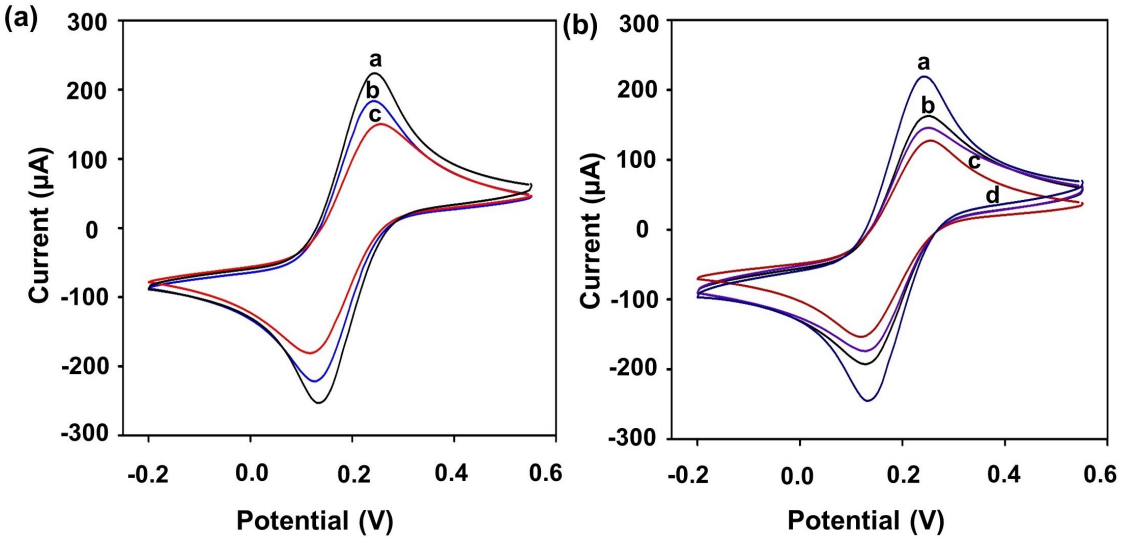

Figure 4.7: CV for the modification of SPE with **a** graphene/rGO (a), graphene (b) and graphene/GO (c); **b** graphene/rGO (a), antibody (b), BSA (c) and linker (d)

Then, the voltammograms were recorded after each surface modification step during the fabrication of the biosensor. This includes graphene/rGO (blue), linker (red), antibody (black) and BSA (purple) as shown in figure 4.7(b). It exhibit details relating to the kinetics of charge transfer of the redox probe $[Fe(CN)_6]^{3-/4-}$ from solution to the electrode. This provides information about the inter-facial properties of different layers on the surface. Assembly of linker decreases the anodic peak current (I_{pa}) or the positive peak current from 281.033 to 168.628 μA due to an increase in the electron transfer resistance. The pyrene moiety binds to the rGO surface via non-covalent bonding ($\pi - \pi$ interaction), whereas ester group forms an amide bond (covalent bonding) with the antibody (Islam et al. (2017)). The I_{pa} increases to 214.987 μA after the immobilisation of antibody. This is attributed to the presence of free NH^{3+} groups (epsilon amines) present on the antibody. These groups accelerate electron transfer between electrode and $[Fe(CN)_6]^{3-/4-}$ system. Immobilisation of BSA decreases the I_{pa} to 199.534 μA as it acquires free functional groups on the surface. This minimizes the chances of non-specific binding. The cathodic peak currents (I_{pc}) or the negative peak current displayed a similar trend after each surface modification step.

Scan rate studies (10 to 200 $mV.^{-1}$) of the biosensor were performed to study redox process

taking place at the surface. Peak to peak separation was found to be dependent on the scan rate indicating a quasi-reversible process. Both cathodic and anodic peak currents increase with an increment in scan rate (figure 4.8(a)). A linear correlation (R^2 =0.99) was obtained for current versus square root of scan rate (figure 4.8(b)). This is attributed to surface controlled diffusion of $[Fe(CN)_6]^{3-/4-}$ with no surface adsorption and is an important requirement for electrochemical biosensors (Li et al. (2015)). Randles-Sevcik equation (3.2) was used for calculating the diffusion coefficient and it was found to be 1.414×10^{-6} cm^2 s^{-1} which is in close agreement with the value of 7.26×10^{-6} cm^2 s^{-1} in the literature (Baur & Wightman (1991)). The value of heterogeneous rate constant (K_s) was found to be 0.23 s^{-1} at a scan rate of 50 $mV.s^{-1}$ and a peak to peak separation (m) of 0.12 V. This indicates fast electron transfer at the surface of SPE due to large electroactive sites and the high conductivity of the dual-layer.

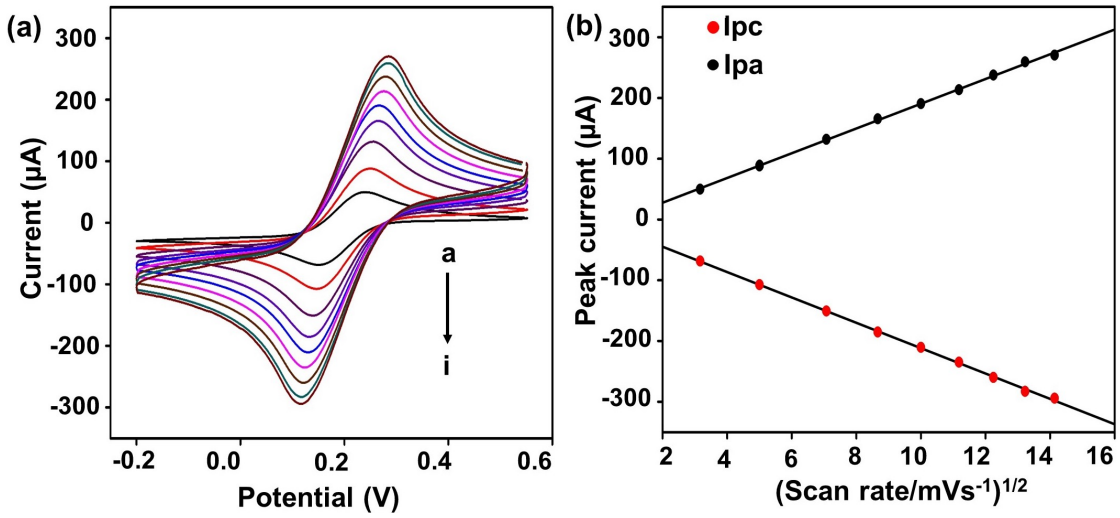

Figure 4.8: Scan rate studies of modified SPE (a) voltammograms under varying scan rates a-i (10, 25, 50, 75, 100, 125, 150, 175 and 200 mV s^{-1}); (b) anodic (I_{pa}) and cathodic (I_{pc}) peak currents versus the square root of corresponding scan rate

4.1.5 Analytical performance of the biosensor

For the optimised condition, sensitivity of the biosensor was evaluated against a wide range of concentrations from 0.2 pM to 55 nM using DPV. The current output of the biosensor is shown as a function of different concentrations of $A\beta_{1-42}$ in figure 4.9(a). The peak current decreased with the increase in concentration. The calibration plot of normalised current versus log of concentrations (in pM) is shown in figure 4.9(b) with R^2=0.97 (based on the 8 data points). The error bars were calculated based on 3 replicates of each experiment. The first two concentrations (0.2 pM, 2 pM), too low to be detected

by the biosensor, and last concentration (55 nM) represents the saturation region of the biosensor. The linear range of the biosensor is from 11 pM to 16.6 nM. The LOD was calculated as 2.4 pM. The high sensitivity was attributed to graphene that provides good electrocatalytic activity and electrochemical inertness, and rGO that provides a large number of electroactive sites (Li et al. (2015)). Pyr-NHS shows strong $\pi - \pi$ interaction with the graphene/rGO dual-layer due to its hydrophobic pyrenyl moiety base. Bioactive ester (NHS) groups form strong amide bonds with the H31L21 antibody resulting in a target-specific platform (Islam et al. (2018)).

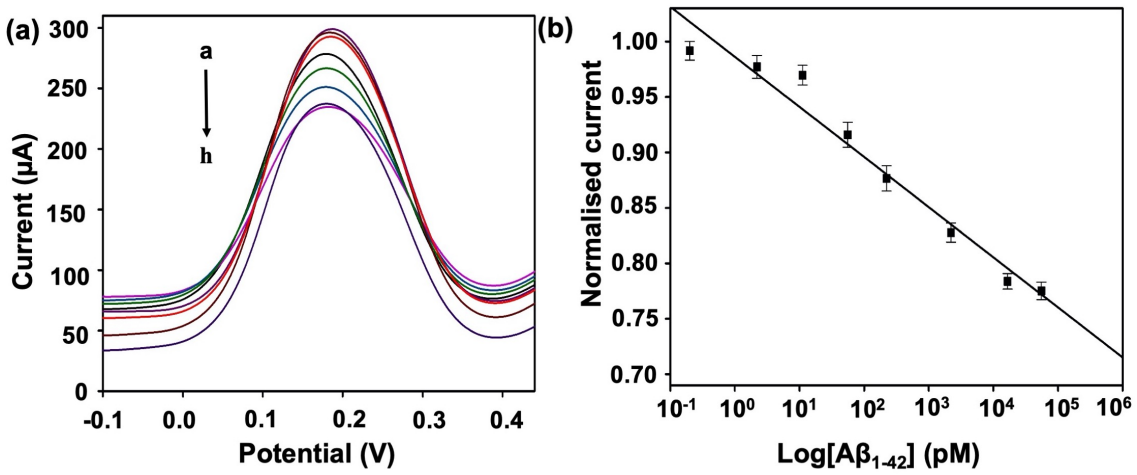

Figure 4.9: Analytical performance of the biosensor: (a) DPV curves obtained for the detection of different concentration of $A\beta_{1-42}$ from a-h (0.2, 2, 11, 50, 220, 2200, 16,600 and 55,000 pM); (b) Calibration plot representing normalised current of DPV data as a function of $A\beta_{1-42}$ concentration on a logarithmic scale (n =3)

4.1.6 Selectivity studies

The selectivity of the sensor towards $A\beta_{1-42}$ was analysed using DPV measurements. The modified SPE was incubated in blank (PBS buffer without protein), 50 pM of $A\beta_{1-42}$ and 500 nM of $A\beta_{1-40}$ and ApoE ϵ4 biomarkers. The higher concentration of interfering species was used to ensure the selectivity of sensor in complex fluids such as plasma. The bar graphs obtained from the normalised peak currents were plotted as shown in figure 4.10. Only $A\beta_{1-42}$ sample gave a significant decrease, whereas the interfering species were almost equivalent to the blank sample. These results illustrate high selectivity of the biosensor towards the $A\beta_{1-42}$ species.

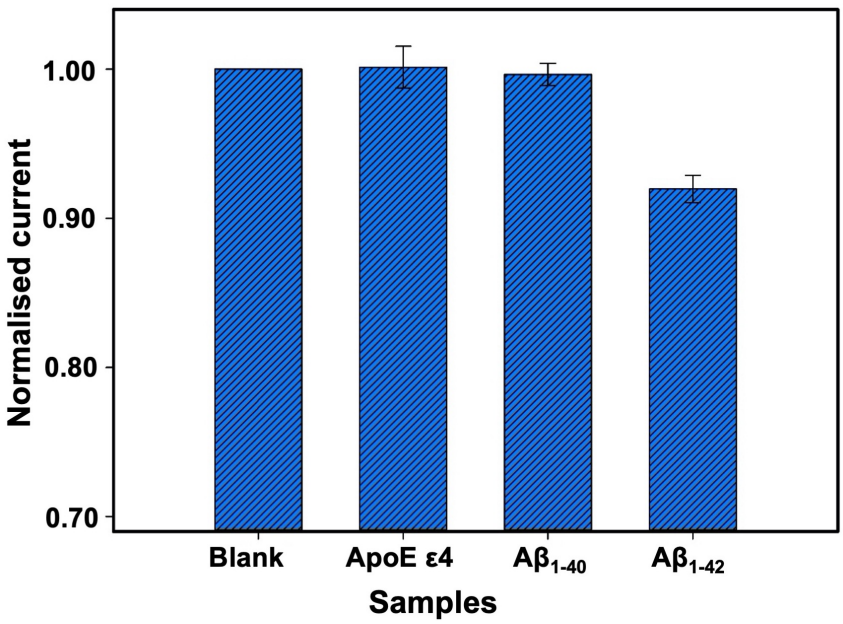

Figure 4.10: Specificity of the biosensor for the detection of 50 pM of $A\beta_{1-42}$ with 500 nM of interfering agents: $A\beta_{1-40}$ and ApoE $\epsilon 4$

4.1.7 Plasma analysis

The biosensor was validated with blood plasma (in a series of two experiments) to check the applicability for bio-fluid analysis. In the first experiment, human plasma was spiked with known concentrations (50, 220, 2200 and 16,600 pM) of $A\beta_{1-42}$, chosen from the linear range of biosensor. The DPV curves at varying concentration of spiked antigen and its calibration plot are shown in figure 4.11(a,b). The sensing platform displayed high linearity in human plasma (R^2 =0.98). In the second experiment, plasma samples obtained from 9 and 12-months-old WT and Tg mice were analysed without any pretreatment. The Tg mouse is an expression of a chimeric mouse and human amyloid precursor protein (Mo/HuAPP695swe). It also overexpresses a mutant human presenilin 1 (PS1-dE9) gene. Both mutations are associated with early-onset AD. Therefore, these animals are humanized models and produce human Aβ peptide species (e.g. $A\beta_{1-42}$). These $A\beta_{1-42}$ species can be detected by a specific antibody that either recognises human or mice sequence or both (Jankowsky et al. (2004)). For this reason, human $A\beta_{1-42}$ antibody (H31L21) was used for validation of mice samples using the biosensor. The DPV results shown in figure 4.11(c) display a much larger shift in peak current for Tg mice as opposed to WT mice. This indicates a higher $A\beta_{1-42}$ concentration in plasma of Tg mice. An age-based study was also performed with Tg mice as shown in figure 4.11(d). As seen, a higher normalised current is observed in case of 12 months in contrast to 9-month-old

mice plasma. This is attributed to the decrease in concentration of $A\beta_{1-42}$ in the plasma of older mice with the progression of AD. However, the decrease is not significant (p=0.347)

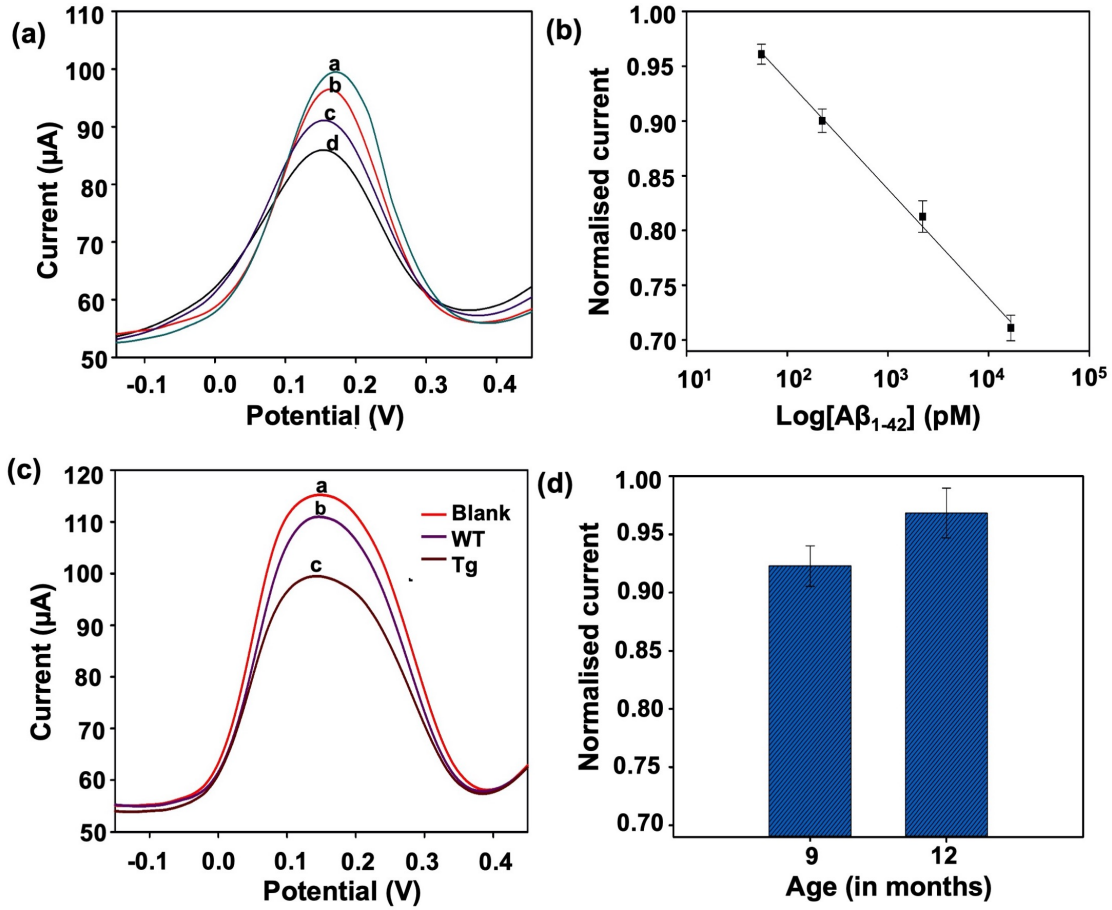

Figure 4.11: Plasma analysis **a** DPV responses from spiked concentration of $A\beta_{1-42}$ (50 (a), 220 (b), 2200 (c) and 16,600 (d) pM) in human plasma; **b** calibration plot of normalised current versus log of $A\beta_{1-42}$ concentration, **c** DPV responses for detection of WT (b) and Tg (c) mice compared with blank response (a); **d** an age-based study with the two groups (9 and 12 months) of Tg animals (n=3)

The IHC data shows a higher accumulation of $A\beta_{1-42}$ in both cortex and hippocampus regions. It increases with age for Tg mice compared with WT mice (figure 4.12). This increase in Aβ plaque burden leads to decrease in plasma $A\beta_{1-42}$ levels observed in figure 4.11(d) (Janelidze et al. (2016)). This correlation depicts the reliability of the platform for plasma analysis.

The MRI data of the 12-month-old WT and Tg mice is shown in figure 4.13. Similar to IHC, it depicts Aβ plaques accumulation in cortex and hippocampus area of the brain.

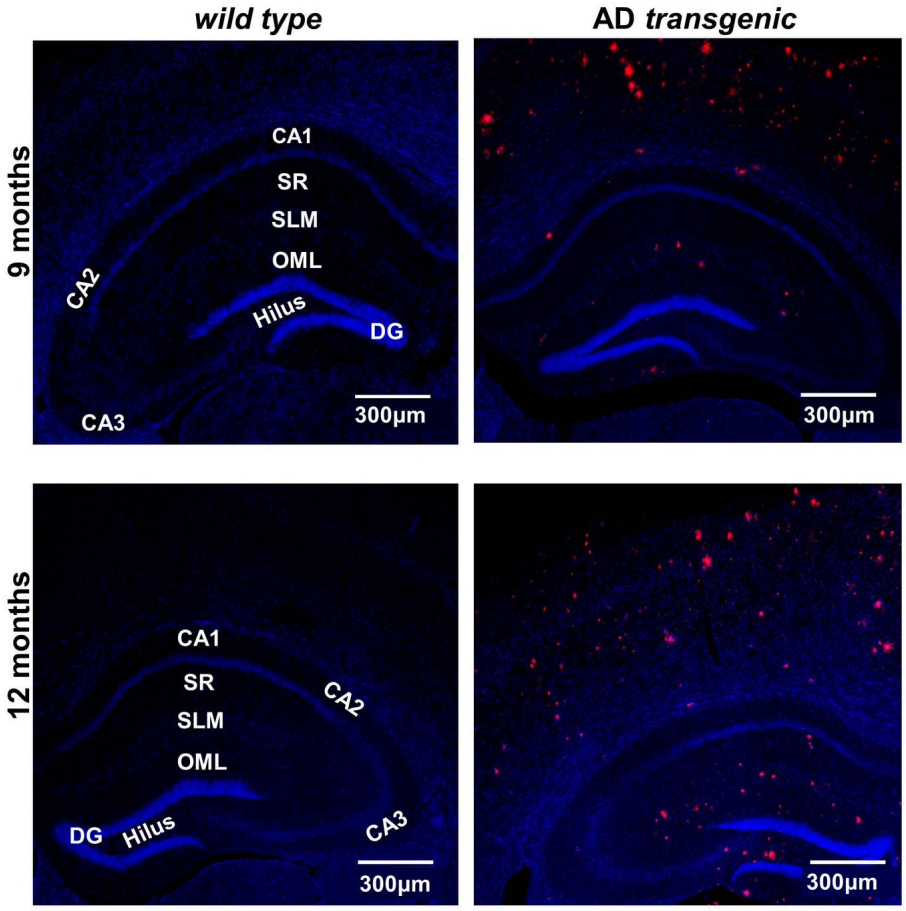

Figure 4.12: IHC data for the progression of AD pathology: An increase of human-specific $A\beta_{1-42}$ (red) aggregation in cortex and hippocampal area from 9 to 12-months-old Tg compared with E littermates; nuclei staining is in blue

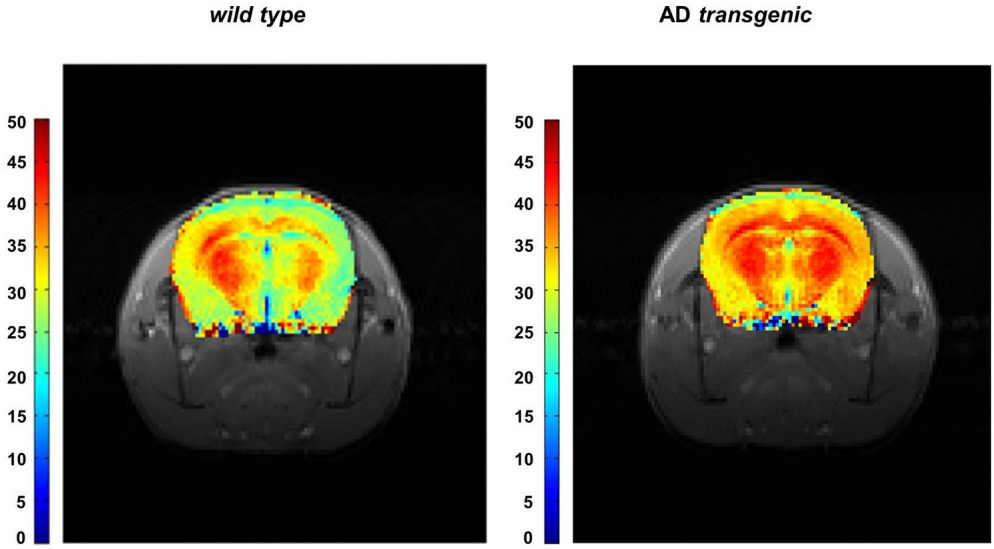

Figure 4.13: MRI depicting an increase of Aβ plaques accumulation in cortex and hippocampus of 12 months old Tg (right) compared to WT (left). The ration of Aβ plaques accumulation is illustrated by a percentage value from 0-100% (from blue to red magnetic resonance spectra)

4.1.8 Conclusion

In conclusion, graphene/rGO dual-layer SPE was developed for label-free detection of $A\beta_{1-42}$. The immobilisation of antibodies was achieved via Pyr-NHS molecule. Its pyrene moiety binds to rGO via non-covalent bonding, and ester group forms strong amide bonds with antibody. The sensor depicted high sensitivity and selectivity towards $A\beta_{1-42}$ over interfering $A\beta_{1-40}$ and ApoE ϵ4 species. It shows excellent performance for plasma sample analysis. Age-based study of mice samples exhibited a decrease in levels of $A\beta_{1-42}$ with the disease progression (from 9 to 12 months old). This was attributed to the increased $A\beta_{1-42}$ accumulation in 12-month-old mice shown by the IHC and MRI studies.

4.2 Amine linker for femtomolar label-free detection with rGO SPEs

4.2.1 Introduction

In this section, a novel functionalisation technique for amine (NH_2) modification has been demonstrated. Direct approach of attaching NH_2 molecules known as amination, shows potential for the effective immobilisation of bio-receptors (Lai et al. (2011)). The NH_2 molecule is small and attaches to the graphene surfaces in higher numbers to provide a large number of binding sites (Ali et al. (2014)). This increases the probability of attaching higher numbers of bio-receptors to capture the target biomarker. This is contrary to the Pyr-NHS molecule, which is a bulky linker containing one amine group per molecule and thus, provides fewer binding sites (Kawata et al. (2018)). However, the amine functionalisation process is usually based on complex reactions, which are time consuming and involves complicated instruments (Lai et al. (2011); Wang et al. (2011); Ali et al. (2014)). Therefore, a novel approach of amination is developed for the fabrication of biosensors. The analysis of XPS and Raman data reveals that functionalisation chemistry is based on the chemisorption of NH_2 on the oxygenated and defect sites of rGO without damaging its structure (Tang & Cao (2012); Mattson et al. (2013); Rivera et al. (2019)). The antibodies are attached via protein G to improve their orientation on the sensing surface, which in turn improves their capture efficiency (Yang et al. (2019)). Femto-molar (fM) detection and high selectivity has been demonstrated for both $A\beta_{1-40}$ and $A\beta_{1-42}$ biomarkers. The biosensors are further validated with human plasma spiked with different target concentrations (Sethi et al. (2021)). Therefore, this platform overcomes the shortcomings of the existing biosensors including the dual-layer platform.

4.2.2 Fabrication process

Firstly, rGO SPEs were immersed in ammonia solution (containing 28-30% NH_3) for about 30 min at RT, referred to as ammonia treatment. After that, the electrodes were gently dried with nitrogen and kept in a vacuum until further use. Then, the treated SPEs were kept in vacuum until further use. $A\beta_{1-42}$ antibody solution (20 $\mu g.mL^{-1}$) was mixed in the ratio of 70:30 with protein G (20 $\mu g.mL^{-1}$) using a vortex mixer. This mixture was kept

at RT for 30 minutes to encourage strong bond formation. $A\beta_{1-40}$ antibody (20 $\mu g.mL^{-1}$) and protein G (20 $\mu g.mL^{-1}$) mixture was prepared in the same ratio. Then, ammonia treated SPEs were incubated in the antibody and protein G (Ab + protein G) mixture for 6 hours at RT. After that, the SPEs were washed with PBS buffer for removing any unbound antibodies. 1% BSA (in PBS) was drop casted onto the SPEs for 15 minutes followed by rinsing with PBS to obtain the biosensors. Then, the sensors were incubated with desired dilutions of freshly prepared $A\beta_{1-42}$ and $A\beta_{1-40}$ peptides in PBS solution for 60 minutes at RT. In order to avoid the aggregation, peptides were prepared fresh and kept on ice before putting them onto the sensor. After that, sensors were washed 3 times with PBS before the measurements, to remove any unbound peptide. The volume of the solution required for incubation was between 10-20 μl. Similarly, human plasma was diluted in the ratio 1:100 using PBS. The desired dilutions of the two biomarkers were prepared in plasma by vortex mixing for 20 seconds. Then, the prepared biosensors were incubated with spiked samples for 60 minutes and washed with PBS before measurement.

4.2.3 Optimisation experiments

The crucial parameters such as immersion time in ammonia solution and antibody/antigen incubation time were optimised. Firstly, the SPEs were immersed in ammonia solution for different times (15, 25, 30, 35, 45, 60 and 120 min). Here, the maximum normalised current values indicate the optimum immersion time at which the best performance of the biosensor was recorded. As per the graph shown in figure 4.14(a), maximum value of normalised current is obtained at 30 min after which it decreases until 60 minutes and then saturates. Therefore, it can hypothesized that, immersion time below 30 minutes does not provide enough linker sites for the immobilisation of 20 $\mu g.mL^{-1}$ antibodies. At 30 minutes, maximum value of current response is observed suggesting an optimum concentration of linker sites on the electrode surface. Beyond this, the increased immersion time leads to an increased shielding of the electrode surface from the the electrolyte with poor charge transfer and/or increase in non-specific adsorption on the surface. Similarly, the incubation time for antibody and antigen were also optimised. The normalised current vs different incubation times of antibody (1, 2, 4, 6, 7, 9 and 12 hrs) and antigen (30, 45, 60, 75, 90, 105 and 120 min) are shown in figure 4.14(b) and figure 4.14(c) respectively. According to figure 4.14(b), the maximum current response (best performance of biosensor) was obtained at an antibody incubation time of 6 hrs. The incubation times below 6

hours, led to lower density of antibodies on the surface which are not enough to capture the given concentration of target molecules. Beyond this, the surface gets shielded with antibody leading to poor charge transfer and ultimately, poor performance of the biosensor. Similarly, figure 4.14(c) depicts an antigen incubation time of 60 minutes generates high normalised current and hence, best sensing performance. All the data was based on DPV responses.

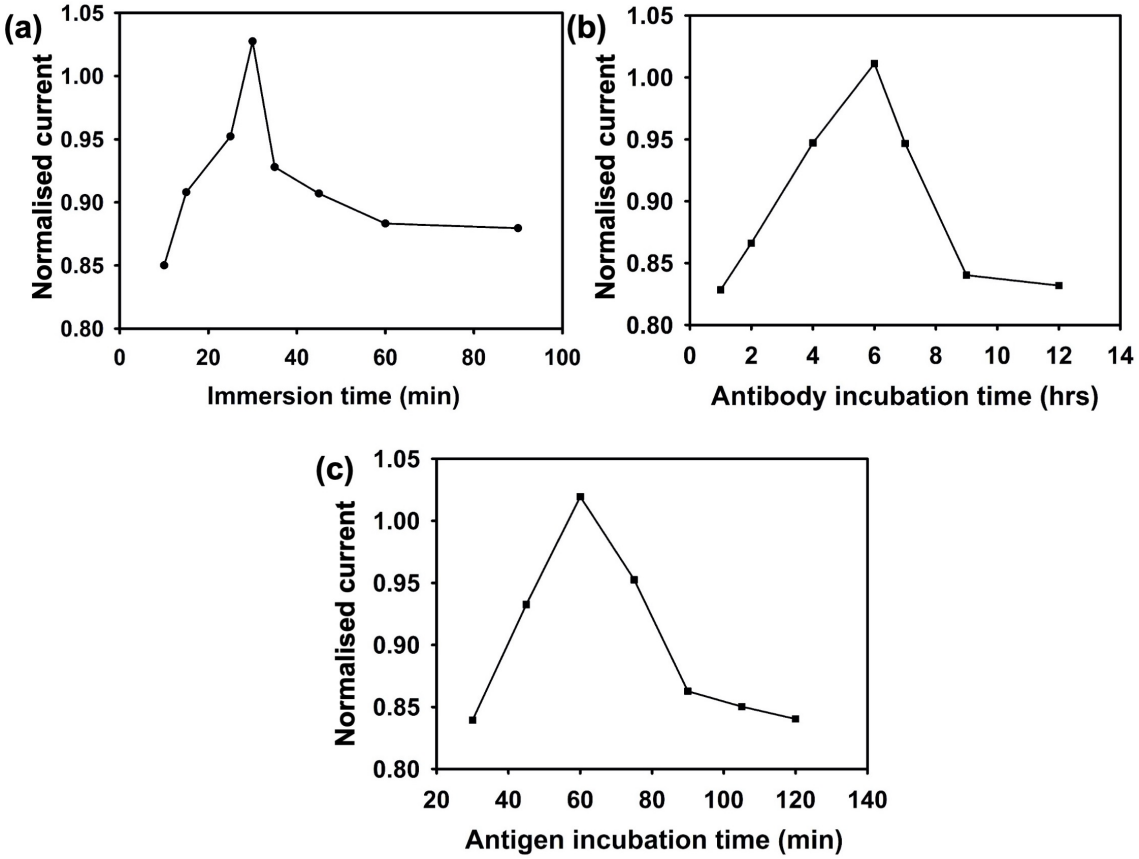

Figure 4.14: Optimisation of (a) immersion time in ammonia solution ((15, 25, 30, 35, 45, 60 and 120 mins), (b) incubation time for antibody ((1, 2, 4, 6, 7, 9 and 12 hrs), and (c) antigen (30, 45, 60, 75, 90, 105 and 120 min)

4.2.4 Characteristics of the biosensors

SEM Analysis

Morphological analysis of rGO WE was carried out using SEM before and after the ammonia treatment as shown in figure 4.15(a,b). Image of the bare electrode displays a rough surface. This can be attributed to the presence of rGO flakes on the WE. After ammonia treatment, the surface is slightly smoother, however, no significant change is observed which confirms that no structural damage was done to rGO. This shows the

superiority of the method over existing techniques that are based on complex reactions with deleterious chemicals over a prolonged period of time (Lai et al. (2011); Wang et al. (2011); Ali et al. (2014); Li et al. (2015)).

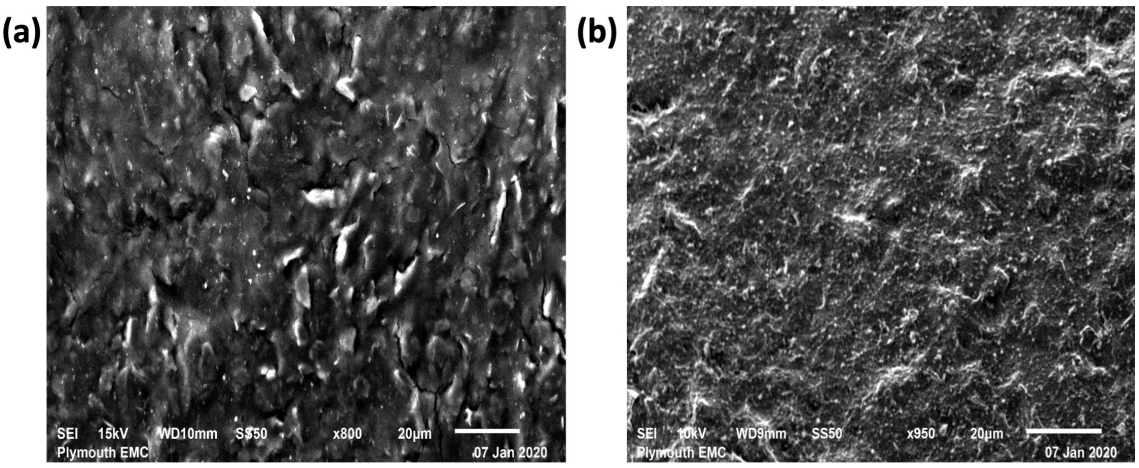

Figure 4.15: SEM images of rGO working electrode (a) before and (b) after ammonia treatment

XPS analysis

XPS analysis was performed to estimate chemical states and atomic ratios of bare rGO (black) and ammonia treated rGO (red). The wide region spectra of both surfaces show carbon (C) (≈284 eV), nitrogen (N) (≈400 eV) and oxygen (O) (≈532 eV) peaks (figure 4.16(a)). The presence of N peak in bare rGO can be attributed to the chemicals involved in the reduction of graphene oxide (Li et al. (2015)). The atomic percentage (at%) of the samples calculated using CasaXPS software. After the ammonia treatment, at% of N increases from 0.6 to 1.2, which indicates the chemisorption of N comprising functional groups on the rGO surface (Petit et al. (2009)). To further confirm the chemisorption of NH_3 or NH_2, nature of C and N species were analysed. The C1s high resolution spectra of ammonia treated rGO (figure 4.16(b)) demonstrate three peaks emerging from C-C/C=C in aromatic rings (≈284.5 eV), C-O/C-N (≈286.6 eV) and O-C=O (≈288.6 eV) bonds (Li et al. (2015); Xing et al. (2016); Bîru et al. (2018)). The C-N peaks appear at the same ranges as C-O, which is the reason for a significant increase in the peak at 286.6 eV compared to bare rGO electrode (Petit et al. (2009); Sobon et al. (2012);Shi et al. (2021)). The N1s high resolution spectra, shown in figure 4.16(c), can be deconvoluted into two peaks, namely C-N (≈400 eV) from amines (NH_2) and C-N^+ (≈402 eV) from quaternary nitrogen (Petit et al. (2009)). After the treatment, the peak height of C-N doubled while no significant

shift was seen in C-N^+ peak compared to bare rGO (Petit et al. (2009); Chen et al. (2012)). These results indicate that the ammonia treatment causes the loading of NH_2 molecules on the surface of rGO via chemisorption.

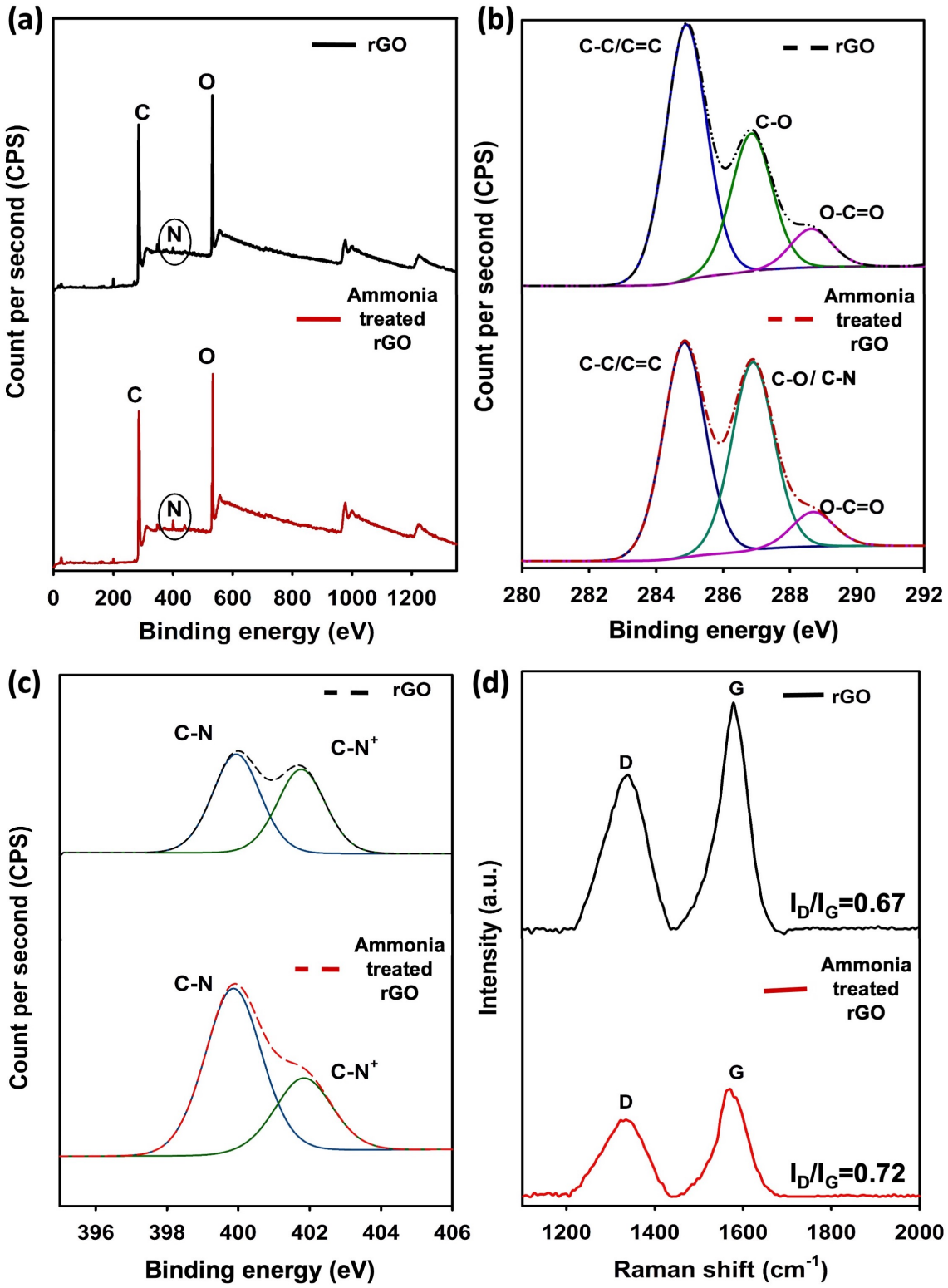

Figure 4.16: Spectral analysis of the SPE before and after the ammonia treatment (a) overall scan; (c) C1s scan; (c) N1s scan and (d) Raman Spectra

Raman analysis

Raman spectra of rGO and ammonia treated rGO is displayed in figure 4.16(d) with signature D and G bands. After the ammonia treatment, D band remains at ≈1340 cm^{-1}, however, a slight shift in the G band from ≈1580 cm^{-1} to ≈1575 cm^{-1} is observed. Similar shifts have been observed in the literature for amine functionalised graphene materials (Wang et al. (2011); Abdali & Ajji (2017)). Further, I_D/I_G increases from 0.67 for bare rGO to 0.72 for ammonia treated rGO. This suggests that the chemisorption of NH_2 introduces some defects in rGO lattice due to the chemical bonding, which leads to an increase in sp^3 planar carbon atoms (Su et al. (2016); Abdali & Ajji (2017)). However, the increase is not significant, which confirms that no major defects were introduced into the rGO structure indicating that the NH_2 groups get attached on available active sites on rGO without affecting its honeycomb lattice. In addition, a slight increase is also observed in full width at half maximum (FWHM) for ammonia treated rGO. All of these changes are a confirmation for the successful attachment of amine groups on the rGO surface (Baldovino et al. (2016); Abdali & Ajji (2017)).

FTIR analysis

FTIR analysis of the rGO working electrode before and after ammonia treatment was performed as shown in figure 4.17(a,b). Before ammonia treatment, the rGO spectrum depicts an intense and broad absorption at 3296 cm^{-1}, which is due to the vibration of -OH. Peak observed at 1618 cm^{-1} and 1723 cm^{-1} are attributed to the C=C groups and C=O (from -COOH) group respectively. The peaks at 1428, 1280 and 1059 cm^{-1} are because of the carboxy, epoxy and alkoxy (C-O) groups respectively. The peaks are assigned in accordance with the literature (Jang et al. (2014); Nath et al. (2018); Kang et al. (2019)). After ammonia treatment, the broad peak shifted to 3371 cm^{-1} exhibiting two peaks, one can be assigned to N-H stretching vibrations (from amines) (Kong & Yu (2007); Zhang et al. (2016); Guler et al. (2017)) and other to the -OH vibrations. The small peak at approximately 1100 cm^{-1} is assigned to C-N stretching (Kong & Yu (2007); Badertscher et al. (2009); Zhang et al. (2016); Milella & Mazzotti (2019)). A shift of the peak at 1059 cm^{-1} to 1066 cm^{-1} was also observed after the ammonia treatment, which is associated to the C-N stretch (Zhang et al. (2016); Kang et al. (2019)). Small peaks at approx. 2360 cm^{-1} in both graphs are due to CO_2 molecule Souza et al. (2009), which arises from the

measuring conditions.

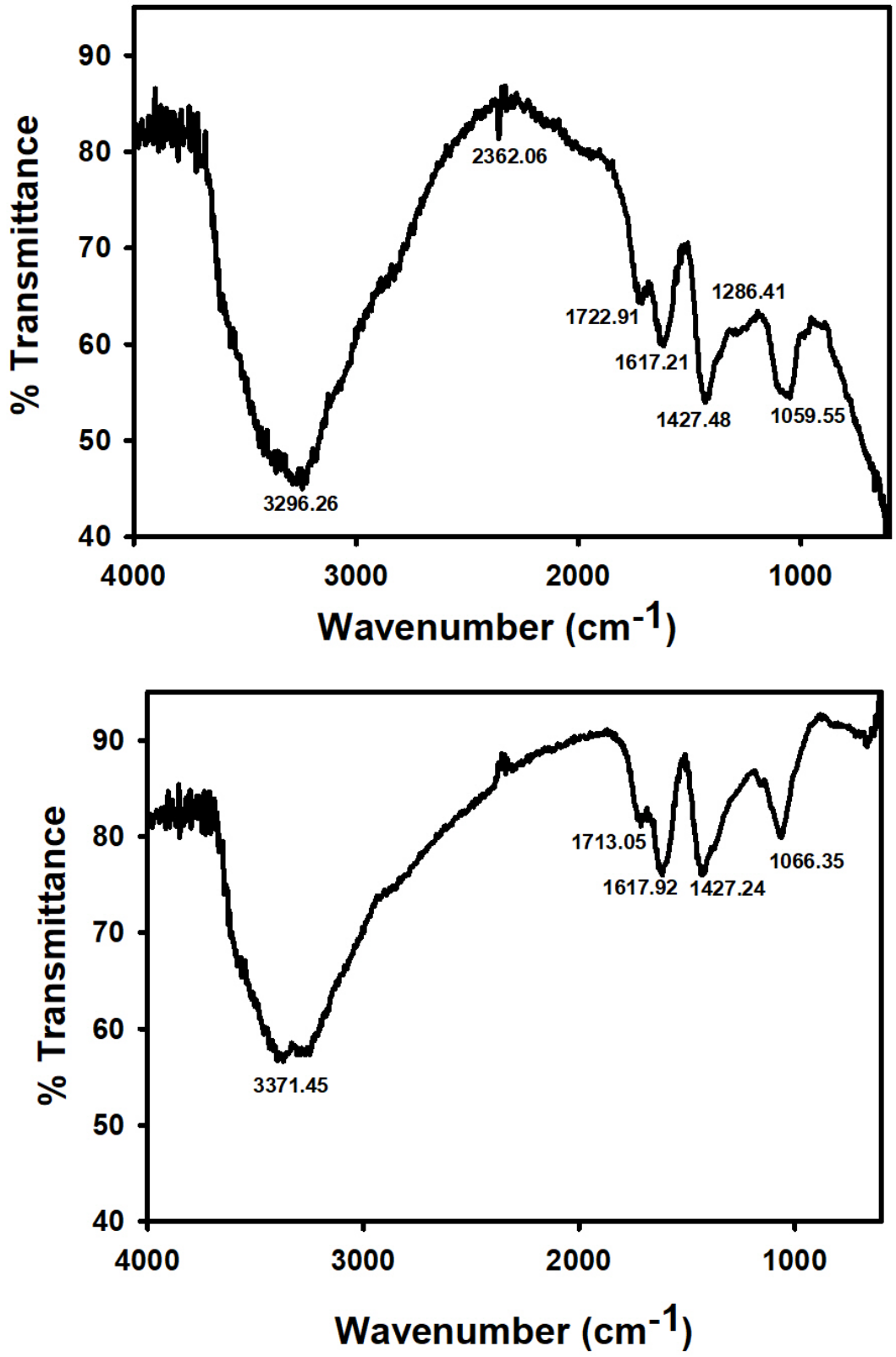

Figure 4.17: FTIR spectra of rGO before (a) and (b) after ammonia treatment

Reaction Mechanism

Surface chemistry of functionalisation of rGO is proposed based on the XPS and Raman analysis. The reaction of ammonia solution ($NH_3.H_2O$) with rGO can take place either by chemisorption (adsorption via covalent bonds)of NH_2 groups on the defect sites and oxygen functionalities (Tang & Cao (2012)) or by replacement of carbon (C) atoms in the lattice with nitrogen (N) atom (Baldovino et al. (2016)). However, the latter is not possible without the application of high temperature and pressure (Baldovino et al. (2016)). Therefore, the chemisorption of NH_2 is the only possibility for the present study, which can occur in one of the following ways:

Case 1: NH_2/ defect sites or carbon vacancy: This is the most plausible mechanism as rGO has many vacant/ defect sites (Veluswamy et al. (2018)). The electrode material is made up of stacked rGO flakes due to which there are many available sites for the attachment of NH_2. The NH_3/NH_4^+ present in ammonia solution can interact with C atoms resulting in adjacent C-NH_2 and C-H bonds (Kumar et al. (2019)). The defect sites create a state of non-equilibrium in the structural network, therefore, readily bond with NH_2 to stabilise it (Rivera et al. (2019)). This is a common phenomenon observed in case of CNTs where the defect site chemistry has been quite useful for attachment of functional groups on the surface (Banerjee et al. (2005)). The successful functionalisation is confirmed by C1s and N1s high resolution spectra (figure 4.16(b, c)) showing an increase in the C-N peak intensity from amines at ≈286.6 eV and ≈400 eV respectively. All these surface reactions occur without adversely affecting the honeycomb structure of rGO as seen in figure 4.18. This agrees with the Raman spectra (figure 4.16(d)) that shows that no major defects were introduced during the functionalisation of NH_2. Further, FTIR analysis (figure 4.17) shows the peaks at 3371, 1100 and 1066 cm^{-1} exhibiting N–H stretch vibrations and C–N stretch.

Case 2: NH_2/ oxygen functionalities: This is another possible mechanism for functionalisation of rGO. The highly electronegative oxygen atoms present in epoxide (C-O-C), carboxyl (O-C=O) and hydroxyl (O-H) groups in rGO, attract the H atoms from NH_3/NH_4^+ when immersed in the ammonia solution. In case of epoxide, NH_2 and H atoms get chemisorbed on the C and O atoms respectively, resulting in the forming of C-OH and C-NH_2. The newly formed O-H groups interact with NH_2 via hydrogen bonding (OH—N) and lead to better chemisorption of NH_2 on rGO (Tang & Cao (2012)). In case of carboxyl and hydroxyl groups, there is a formation O=C-NH_2 and C-NH_2

respectively along with the formation H-O-H (Tang & Cao (2012); Mattson et al. (2013)). Due to reduced number of functionalities in rGO and absence of high temperature (Shazali et al. (2018)) this mechanism is less likely than Case 1. There is also a chance of physisorption (adsorption via weak Van Der Waals force) of NH_3 on the surface of rGO. However, these interactions are quite weak (Kumar et al. (2019)) and can be washed away in the next steps.

Since one SPE consists of numerous rGO flakes, therefore, there are many NH_2 groups attached on the SPE. As a result, there are a large number of binding sites for antibodies, which improves the overall sensitivity of the biosensor.

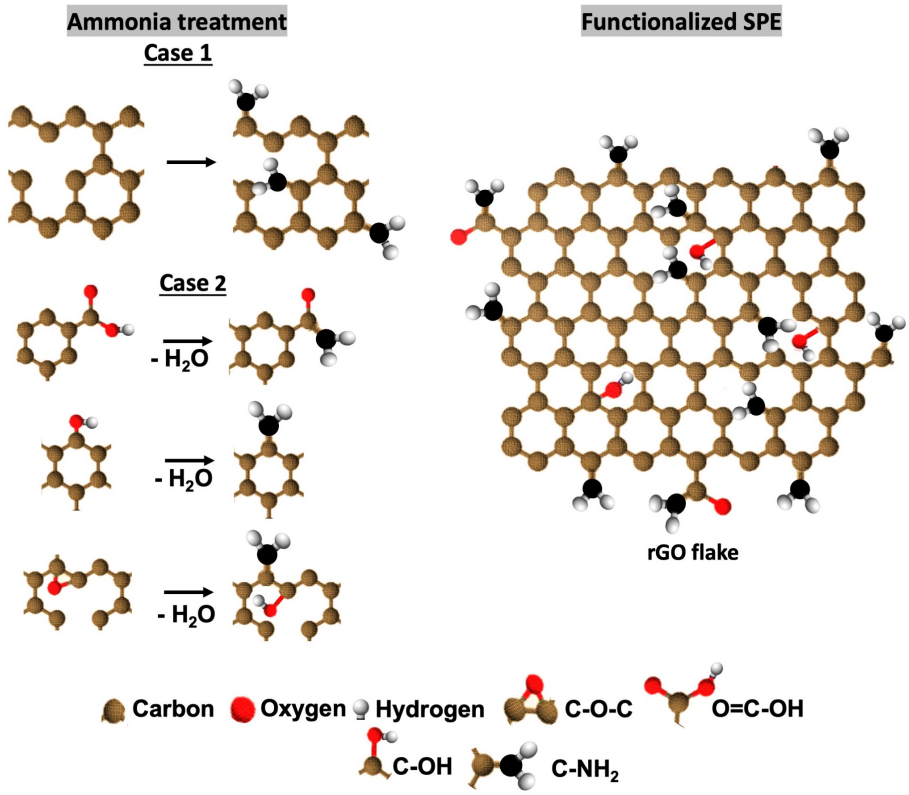

Figure 4.18: Chemisorption based reaction mechanism proposed for the NH_2 functionalisation of rGO SPE

Electrochemical analysis

The schematic of functionalisation steps involved in the preparation of biosensor are shown in figure 4.19 (a-e). The corresponding voltammograms for the bare (purple), NH_2 (green), antibody (brown) and BSA (red) functionalised rGO SPE are shown in figure 4.19 (f).

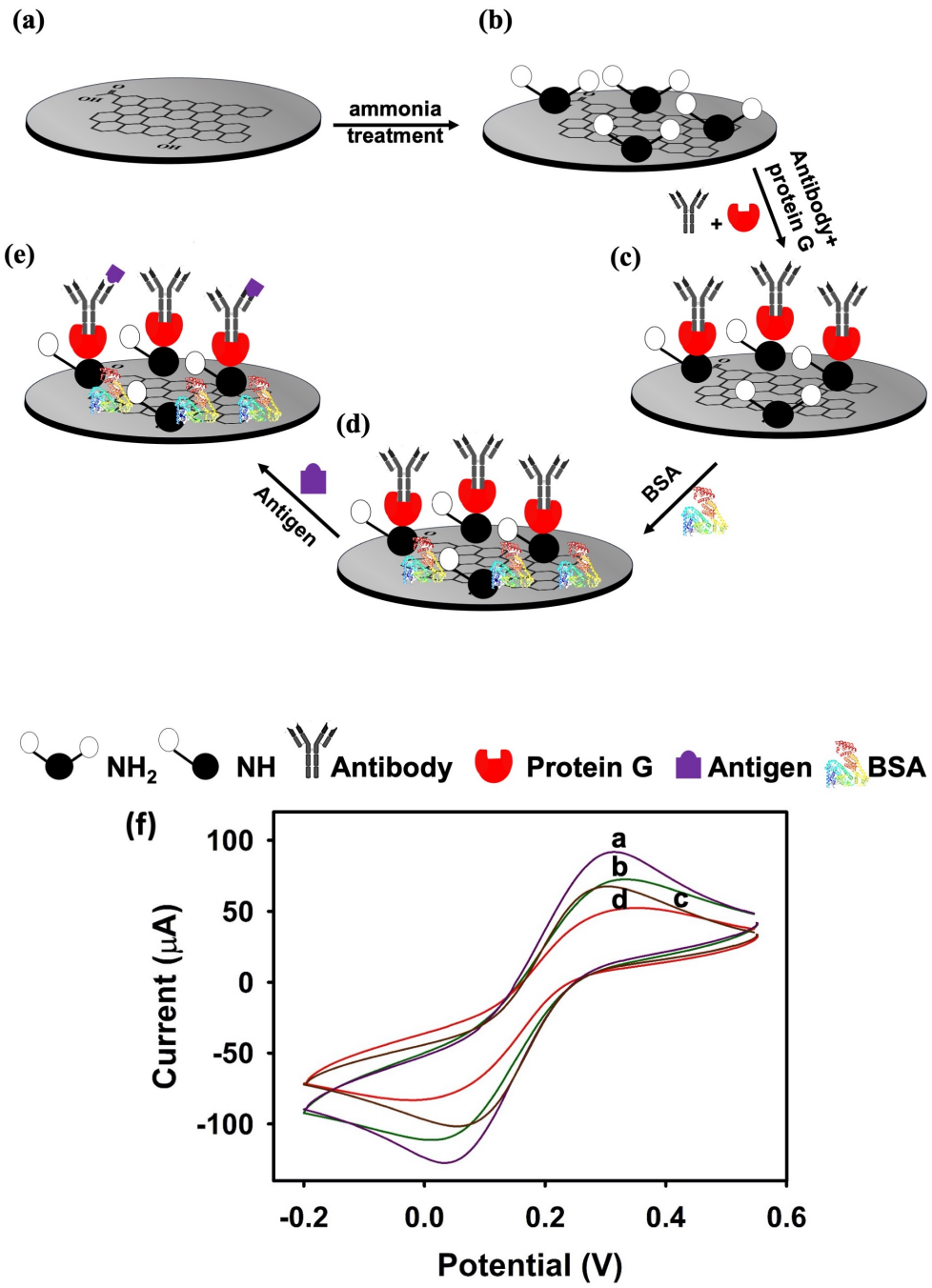

Figure 4.19: Fabrication steps involved in the development of electrochemical system: (a) commercial rGO SPE; (b) modification with amines; (c) incubation in antibody and protein G mixture; (d) blocking by BSA; (e) attachment of antigen and (f) voltammograms depicting each surface functionalisation step (a-d)

Chemisorption of NH_2 on rGO decreases the anodic peak current (I_{pa}) or the positive peak current from 91.969 μA to 72.25 μA. This is attributed to the increased electron transfer resistance due to the acquirement of the available electroactive sites on rGO by NH_2 groups. Immobilisation of antibody and protein G mixture (Ab + protein G) decreases the current further to 67.646 μA. This is due to the blocking of the modified area from the electrolyte/redox probe, which affects the charge transfer (Baradoke et al. (2019)). Lastly,

the attachment of BSA decreases the current to 50.594 μA as it binds to the free functional groups on surface to prevent non-specific binding (Islam et al. (2018)). The cathodic peak currents (I_{pc}) or the negative peak current displayed a similar trend after each surface modification step.

Scan rate studies of the biosensor were performed in 10 mM $[Fe(CN)_6]^{3-/4-}$ in 1 M KCl electrolyte. As seen in figure 4.20(a), the peak to peak separation was found to be dependent on the scan rates (10 $mV.s^{-1}$ to 300 $mV.s^{-1}$) showing a quasi-reversible process (Islam et al. (2018)). The increase in scan rate leads to an increase in both cathodic and anodic peak currents. The current and square root of scan rate displays a linear association (R^2=0.99) as shown in figure 4.20(b). This indicates a surface controlled diffusion of $[Fe(CN)_6]^{3-/4-}$ with no adsorption on electrode surface (Li et al. (2015)). The diffusion coefficient of the redox couple was calculated as 0.96 x 10^{-6} using Randles-Sevcik equation that is in close agreement with literature (Baur & Wightman (1991)). The K_s was calculated as 0.29 s^{-1} at scan rate of 50 $mV.s^{-1}$ and a peak to peak separation of 0.15 V, which indicates a fast electron transfer at the surface of biosensor. Surface density of the NH_2 groups were found to be 4.5 X 10^{21} and antibodies were found to be 3.9 X 10^{21} using eq3.4.

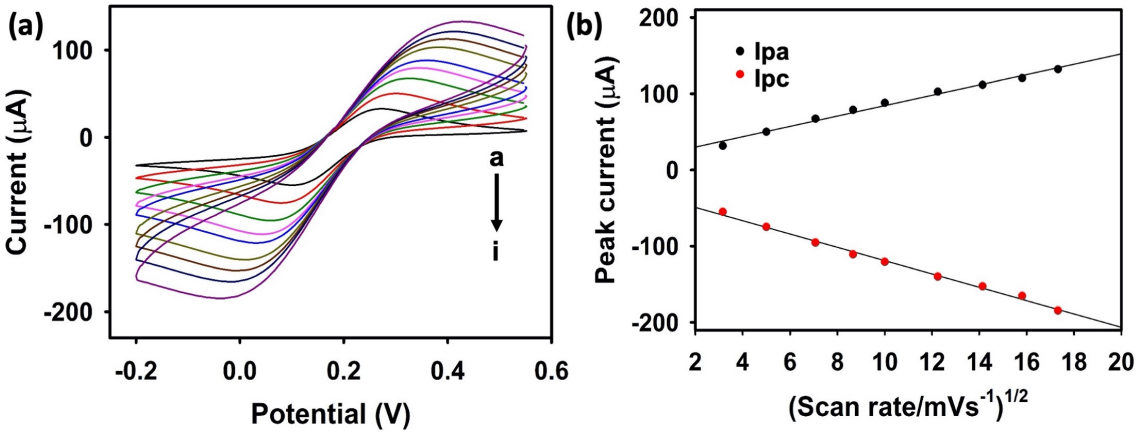

Figure 4.20: Scan rate studies of biosensor: (a) voltammogram obtained for varied scan rates from a-i (10, 25, 50, 75, 100, 150, 200, 250 and 300 $mV.s^{-1}$); (b) anodic and cathodic peak current vs the square root of scan

4.2.5 Analytical performance of biosensor

DPV was used to evaluate the detection limit of biosensor against a wide range of Aβ concentrations. Figure 4.21 (a, c) shows the output current as a function of various $A\beta_{1-40}$ and $A\beta_{1-42}$ concentrations. The calibration plot for the normalised current versus log of concentrations (in fM) are shown in Figure 4.21 (b, d). Normalised current reduced

linearly with the increment in concentration for both biomarkers (R^2=0.98).

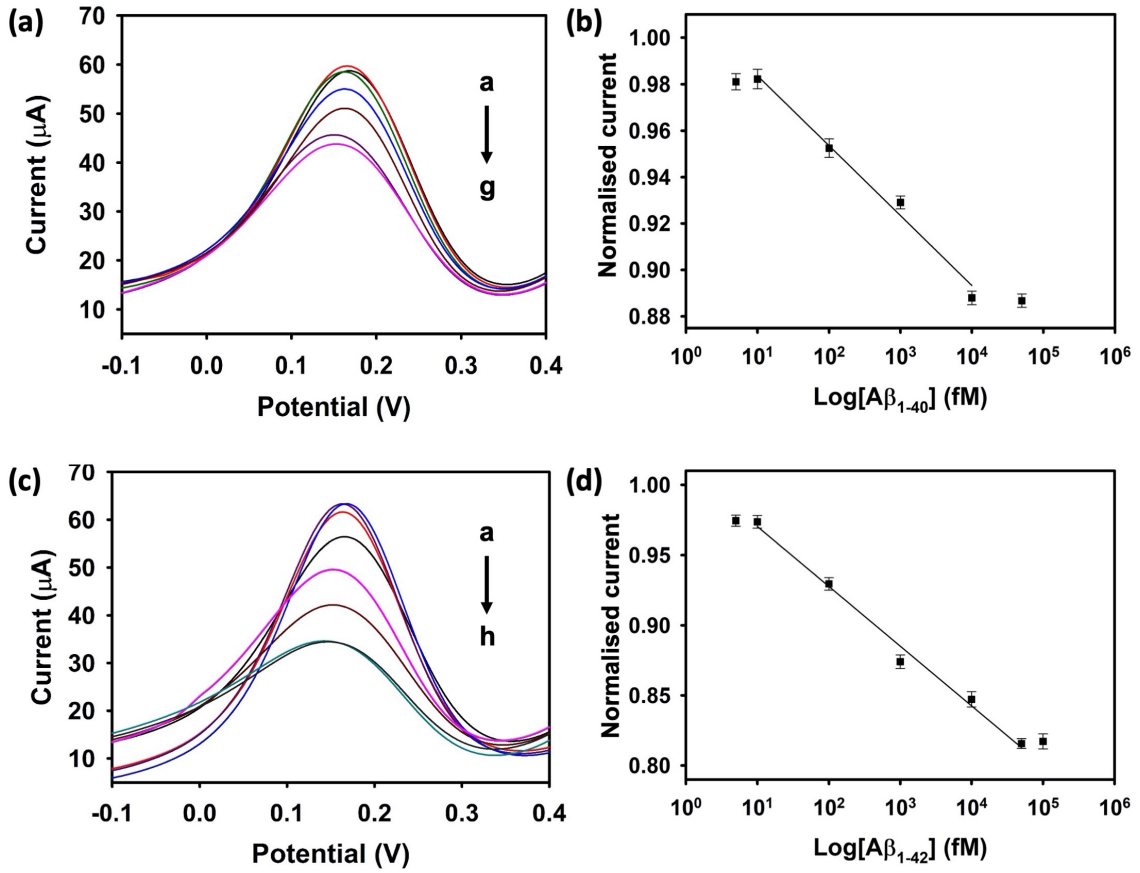

Figure 4.21: Analytical performance of the NH_2/rGO biosensor (a) DPV curves as a function of different concentration of $A\beta_{1-40}$ from a-g (0, 5, 10, 100, 1000, 10000, 50000 fM); (b) calibration plot for $A\beta_{1-40}$ for normalised current vs concentration on a logarithmic scale (n=3); (c) DPV curves as a function of different concentration of $A\beta_{1-42}$ from a-h (0, 5, 10, 100, 1000, 10000, 50000, 100000 fM)); (d) calibration plot for $A\beta_{1-42}$ for normalised current vs concentration on a logarithmic scale (n=3)

The outliers in the graph represent the saturation values for the biosensor. The saturation was obtained after 10 pM for $A\beta_{1-40}$ and 50 pM for $A\beta_{1-42}$ attributed to the lack of antibodies left on the surface to capture any more antigen. The linear range of the biosensor is from 5 fM to 10 pM for $A\beta_{1-40}$ and 5 fM to 50 pM for $A\beta_{1-42}$. The biosensor exhibited excellent repeatability (n=3) with a LOD of 9.51 fM for $A\beta_{1-40}$ and 8.65 fM for $A\beta_{1-42}$. This excellent performance is due to the chemisorption of NH_2 groups on the surface of rGO, which provide a higher number of binding sites for antibodies. Use of pro G leads to an optimal surface orientation of antibodies, which improves the capture efficiency (Yang et al. (2019)). The carboxyl terminal of pro G binds to the Fc site of the antibody making antigen binding (Fab) regions available for the target biomarkers (Welch et al. (2017)). Each protein G has two carboxyl terminals and even if one terminal is engaged with the Fc region of the antibody, the other one is free to bind to the amines on

the sensor surface generating strong amide bonds (Sjöbring et al. (1991); Sohn & Lee (2014). However, due to the absence of an activator (Kim & Herr (2013)), it is also likely that the protein G/antibody mixture was immobilized on the surface through hydrophobic and/or electrostatic interactions.

Comparison studies

Direct attachment of bio receptors such as DNA, has been achieved on the rGO surface because of the presence of electroactive sites and oxygen functionalities (Li et al. (2015)). To highlight the importance of aminated surfaces, a comparative study using unmodified rGO was performed. Figure 4.22 (a,b,c) shows the results obtained for the sensing of $A\beta_{1-42}$.

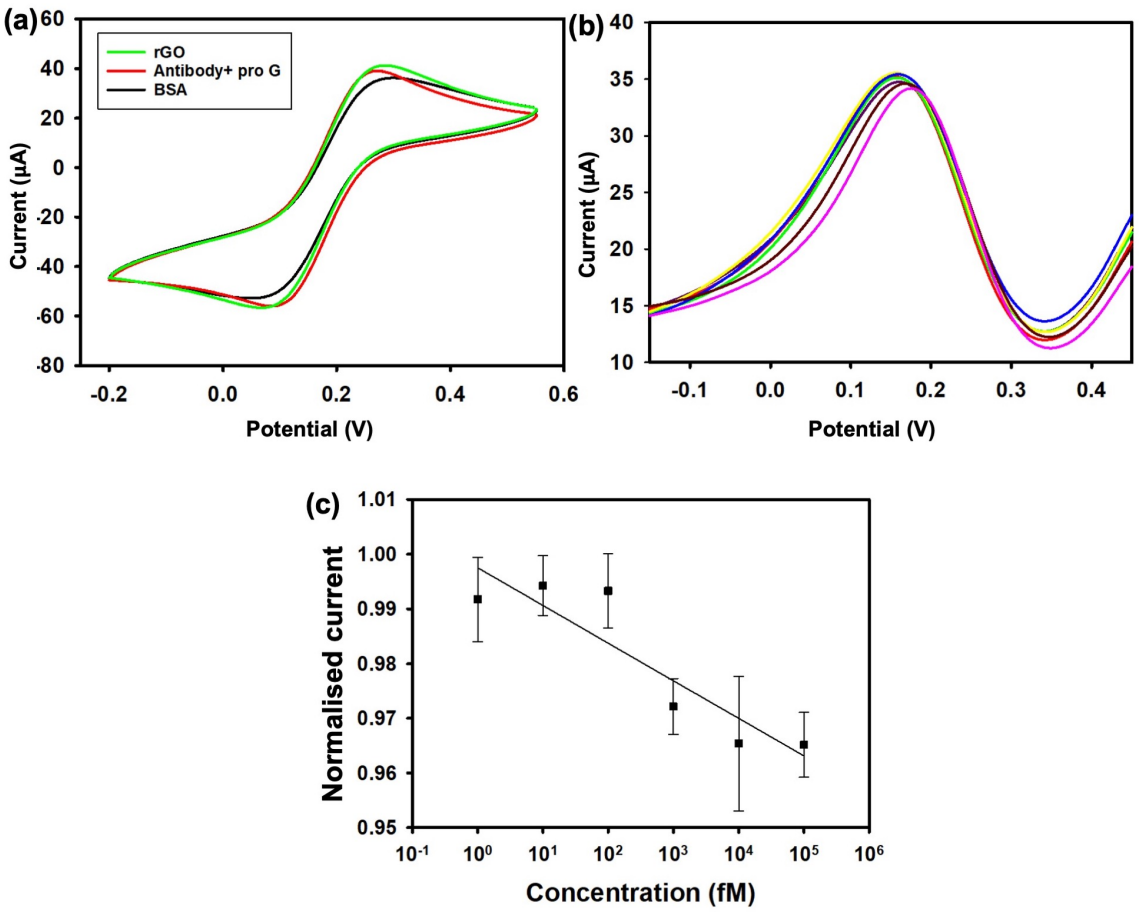

Figure 4.22: Detection with unmodified rGO biosensor: **(a)** CV responses for (a) rGO working electrode; (b) incubation with antibody and protein G mixture; (c) blocking with BSA, **(b)** DPV curves obtained as a function of different concentration of $A\beta_{1-42}$ from 0-100 pM (0, 5, 10, 100, 1000, 10000, 50000, 100000 fM) and **(c)** corresponding calibration plot for normalised current vs concentration on a logarithmic scale (n=3)

It can be clearly seen in figure 4.22 (a) that no major shift in the current was observed after attachment of antibodies and pro G mixture, which can be due to their poor

immobilisation. Figure 4.22 (b) depicts the analytical performance of the biosensor against various concentration of $A\beta_{1-42}$ from 0-100 pM. In DPV data, no major shifts in the current were obtained upto 10 pM after which slight shifts were obtained, however, they were negligible to be considered. This confirms that the aminated rGO leads to improved immobilisation and hence, improved detection sensitivity. The corresponding calibration plot of the biosensor is seen in figure 4.22 (c).

4.2.6 Selectivity studies

The selectivity towards $A\beta_{1-40}$ and $A\beta_{1-42}$ biosensors were evaluated with DPV measurements. The respective biosensors were incubated in 1 nM of interfering agents and 100 fM of target protein under similar experimental conditions. Figure 4.23(a,b) shows the bar graphs obtained from the normalised peak current values. The target protein shows a significantly lower response than the interfering species, which confirms the high selectivity of the biosensor.

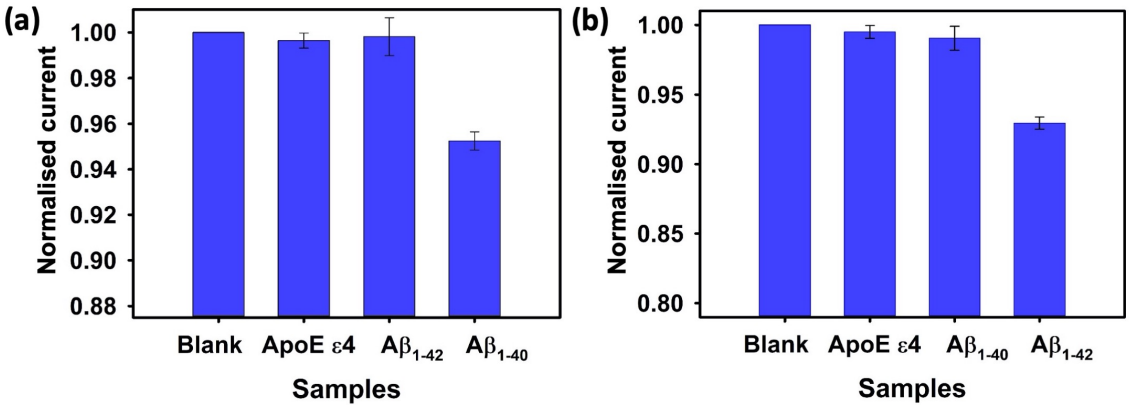

Figure 4.23: Specificity of the biosensor for the detection of 100 fM of $A\beta_{1-40}$ (a) and $A\beta_{1-42}$ (b) as compared to interfering agents at 1nM concentration

4.2.7 Spiked plasma analysis

The human plasma was spiked with known concentrations (in linear range of biosensor) including 10, 100, 1000 and 1000 fM for $A\beta_{1-40}$ and $A\beta_{1-42}$. The normalised current vs log of concentration (fM) for each biomarker is shown in Figure 4.24(a, b) to show the applicability in bio-fluids. The calibration plot obtained in PBS were replotted here to display a comparison with plasma results. The platform depicted a similar linear relationship with R^2=0.98 in the two matrices for $A\beta_{1-40}$ and slightly higher (R^2=0.99) for $A\beta_{1-42}$. The detection sensitivity was obtained by dividing the slope of calibration plot

with the area of electrode (normalised current/concentration (fM) /area (cm^2)) (Zakaria et al. (2018)). The value of sensitivity for $A\beta_{1-40}$ was obtained as 0.1032 in PBS and 0.0873 in plasma. The slight decrease can be attributed to the matrix effects of plasma. Similarly, value of sensitivity for $A\beta_{1-42}$ was found to be 0.1508 in PBS and 0.1349 in plasma.

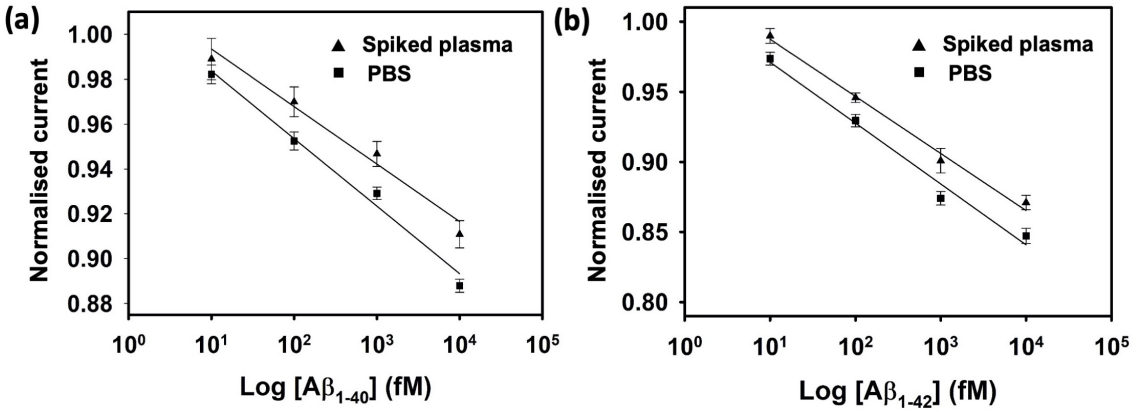

Figure 4.24: Calibration plot depicting the linear responses in PBS and human plasma for (a) $A\beta_{1-40}$ and (b) $A\beta_{1-42}$

4.2.8 Comparison with other graphene based biosensors

When compared to other biosensors discussed in Chapter 2, the performance of NH_2 functionalised rGO electrode was found to be relatively superior in terms of sensing chemistry, ease of fabrication and applicability. The ultra sensitive biosensors developed for sensing of Aβ biomarkers either depend on expensive labels such as the ones developed by Han et al. (2017), Diba et al. (2017), Gao et al. (2019), Negahdary & Heli (2019b) and Negahdary & Heli (2019a) or depend on nanoparticles for the signal enhancement such as the ones developed by Wu et al. (2014), Moreira et al. (2018), Sun et al. (2018), Qin et al. (2019b). The biosensor developed by Özcan et al. (2020) achieved an LOD of 44 aM, however, the biosensor was not validated with biofluids putting the selectivity in question. On the other hand, the NH_2/rGO biosensor presented here provides LOD in low fM ranges without the use of expensive labels or nanoparticles. It is based on simple sensing chemistry with fewer incubation steps and mass produced screen printed electrode.

4.2.9 Conclusion

In conclusion, a rGO SPEs modified with NH_2 linker have been developed for the detection of $A\beta_{1-40}$ and $A\beta_{1-42}$ biomarkers. The functionalisation occurs via chemisorption of NH_2 groups predominantly on the edge and defects sites of rGO without damaging its structure,

as confirmed by XPS, FTIR, and Raman analysis. The NH_2 linker provides a higher number of binding sites for the antibodies, which considerably enhances the sensitivity of the biosensor. It also displayed good selectivity for the target and was successfully validated with spiked human plasma. Therefore, the proposed biosensor provides a simple, low cost and time-effective approach for highly sensitive detection of AD biomarkers without using signal enhancers or labels.

Chapter 5

Conclusion and future work

5.1 Conclusion

This project has investigated the use of graphene based biosensors for detection of Aβ biomarkers of AD. Two biosensors were developed based on graphene and rGO SPEs respectively. The first biosensor was fabricated by modifying the graphene SPEs with electrochemically reduced rGO followed by Pyr-NHS linker and $A\beta_{1-42}$ antibodies. Raman, XPS and CV analysis before and after modification with rGO were used to confirm the formation of dual layer. Scan rate studies revealed a quasi-reversible process and a fast electron transfer with a heterogeneous rate transfer of 0.23 s^{-1}. The biosensor provided detection of target in lower pM ranges with high selectivity. It was effectively validated with both the spiked human and mice plasma to show its applicability for blood-based analysis. The age-based study with samples from 9 and 12 months mice revealed that the concentration of $A\beta_{1-42}$ in plasma decrease with a progression of AD due to an increase in Aβ plaque load in the brain. The cost of the biosensor was estimated to be £6.41, in which £5 is the price of one graphene SPE. Despite its excellent performance, the dual layer biosensors had few limitations. Firstly, Pyr-NHS linker provides low binding sites on the sensing surface because of its bulkiness and presence of one functional group per molecule. Secondly, the surface orientation of antibodies is random, which can have a negative effect on the capture efficiency and hence, sensitivity of the biosensor. Thirdly, the platform has a prolonged fabrication process with extended incubation times. These limitations were addressed by developing the rGO/NH_2 biosensor, which was employed for the detection of both $A\beta_{1-40}$ and $A\beta_{1-42}$. The surface

chemistry was based on the functionalisation of predominantly the edge and defect sites of rGO with NH_2 via chemisorption, as revealed by XPS, FTIR and Raman analysis, followed by immobilisation of the specific antibodies. Similar to the dual layer, the biosensor demonstrated a quasi-reversible process with a heterogeneous rate transfer of 29 s^{-1} as revealed by scan rate studies. Besides high selectivity for the targets, it depicted high sensitivity in the fM ranges with lowest reported LOD by a label free graphene based biosensor. This improvement was due to more binding sites provided by the NH_2 groups. Additionally, the orientation of the antibodies were improved by the use of protein G that binds to the Fc sites making the antigen binding regions readily available for the targets. Also, the fabrication of the rGO/NH_2 was achieved in half the time as opposed to the dual-layer platform. In terms of bio-fluidic sample analysis, the rGO/NH_2 platform was validated with spiked human plasma. It depicted a similar linear relationship in both PBS and plasma, however, a slight decrease in the sensitivity was observed due to the matrix effects. The cost of the biosensor was estimated to be £7.07, in which £5 is the price of one rGO SPE.

Conclusively, both graphene/rGO dual layer and rGO/NH_2 SPEs provide a rapid, sensitive and selective approach for real-time detection of Aβ biomarkers. Both the platforms are label-free and provide a cost-effective alternative to the platforms discussed in section 2.3 based on expensive labels and/or nanoparticles. Additionally, both are based on commercially available SPEs, which leads to an inexpensive fabrication process, less complexity and increases the likelihood of large scale mass production. Since they are single use electrodes, no maintenance cost is required. Lastly, due to the simple architecture/fabrication, these platforms can be easily adapted for other AD biomarkers depending on their levels (fM/pM) in plasma.

5.2 Future work

This work lays the foundation for developing highly sensitive and reliable graphene based biosensors for detection of disease biomarkers from bio-fluids. However, future work is required to improve the fabrication and application of these devices to ensure implementation in a clinical setting. In terms of fabrication, the biosensors developed in this work are based on commercially available SPEs. But for the industrial applications, reproducibility and scalability needs to be improved by printing the electrodes in house, as

it provides control over the quality of graphene. The stability of biosensors over a period of time also needs to be investigated before they can be commercialised. The fabrication process and testing of biosensors is carried out in an optimised setting inside a clean room. Therefore, effect of the environmental changes such as in temperature and/or humidity on the performance of biosensor still needs to be investigated. Furthermore, the effect of amination of graphene/rGO dual-layer structure needs to be studied to see the effect on the sensitivity of the biosensor. Detailed studies related to the effect of analyte affinity, diffusion distances, electrostatic interactions and on/off rate on the performance of the biosensor also needs to be conducted.

In terms of application, both graphene/rGO and rGO/NH_2 biosensors have been validated only with $A\beta_{1-40}$ and $A\beta_{1-42}$ biomarkers. However, AD is caused by a multi factorial pathway, which means several factors are responsible for disease progression. Therefore, the platforms need to be validated with other important clinical/preclinical AD biomarkers to check the feasibility/applicability for their detection. In addition, a multiplexing electronics is needed to allow simultaneous detection of multiple AD biomarkers, which is an important requirement for reliable and early diagnosis. Finally, both biosensors show potential for reliable real sample analysis, however, an extensive clinical validation with larger sample size is still needed before these sensors can be developed into POC diagnostics.

Appendices

Appendix A

Materials and Suppliers

$A\beta_{1-40}$ antibody, Biolegend (UK)

$A\beta_{1-40}$ peptide, Tocris (UK)

$A\beta_{1-42}$ antibody (H31L21), Thermo Fisher Scientific (UK)

$A\beta_{1-42}$ peptides, Sigma-Aldrich (UK)

ApoE ϵ4 peptides, Tocris (UK)

Ammonium hydroxide solution/Ammonia solution (28-30% NH3 basis), ACS reagents (UK)

Alexa Fluor 546 goat anti-rabbit secondary antibody, Thermo Fisher Scientific (Spain)

Bovine serum albumin (BSA), Sigma-Aldrich (UK)

Single-layer graphene oxide dispersion in water, Graphene Supermarket (USA)

4,6-Diamidino-2-Phenylindole (DAPI), Thermo Fisher Scientific (Spain)

Eppendorf® LoBind Microcentrifuge Tubes, Sigma-Aldrich (UK)

Human plasma, Sigma-Aldrich (UK)

Microvette® CB 300 K2E tubes, Sarstedt (Spain)

Normal Goat Serum (NGS), Vector Laboratories (Spain)

Paraformaldehyde (PFA), Merck (Spain)

Phosphate buffered saline (PBS), Sigma-Aldrich (UK)

Pierce® recombinant protein G, Thermofischer Scientific (UK)

Potassium ferricyanide ($K_3Fe(CN)_6$), Sigma-Aldrich (UK)

Potassium chloride (KCl), Sigma-Aldrich (UK)

1-Pyrenebutyric acid N-hydroxysuccinimide ester (Pyr-NHS), Sigma-Aldrich (UK)

Sucrose, Sigma-Aldrich (Spain)

Triton X-100, Sigma-Aldrich (Spain)

Vectashield H-1200, Vector Laboratories (Spain)

Bibliography

Abdali, H., & Ajji, A. (2017). Preparation of electrospun nanocomposite nanofibers of polyaniline/poly (methyl methacrylate) with amino-functionalized graphene. *Polymers*, *9*(9), 453.

Adewole, M., Cui, J., Lowell, D., Hassan, S., Jiang, Y., Singh, A., Ding, J., Zhang, H., Philipose, U., & Lin, Y. (2019). Electrically tunable, sustainable, and erasable broadband light absorption in graphene sandwiched in al 2 o 3 oxides. *Optical Materials Express*, *9*(3), 1095–1104.

Adlard, P. A., Tran, B. A., Finkelstein, D. I., Desmond, P. M., Johnston, L. A., Bush, A. I., & Egan, G. F. (2014). A review of β-amyloid neuroimaging in alzheimer's disease. *Frontiers in neuroscience*, *8*, 327.

Albert, M. S., DeKosky, S. T., Dickson, D., Dubois, B., Feldman, H. H., Fox, N. C., Gamst, A., Holtzman, D. M., Jagust, W. J., Petersen, R. C., Snyder, P. J., Carrillo, M. C., Thies, B., & Phelps, C. H. (2011). The diagnosis of mild cognitive impairment due to alzheimer's disease: Recommendations from the national institute on aging-alzheimer's association workgroups on diagnostic guidelines for alzheimer's disease. *Alzheimer's & Dementia*, *7*(3), 270–279.
URL `https://alz-journals.onlinelibrary.wiley.com/doi/abs/10.1016/j.jalz.2011.03.008`

Ali, M. A., Kamil Reza, K., Srivastava, S., Agrawal, V. V., John, R., & Malhotra, B. D. (2014). Lipid–lipid interactions in aminated reduced graphene oxide interface for biosensing application. *Langmuir*, *30*(14), 4192–4201.

Amin, S., Soomro, M. T., Memon, N., Solangi, A. R., Qureshi, T., Behzad, A. R., et al. (2014). Disposable screen printed graphite electrode for the direct electrochemical determination of ibuprofen in surface water. *Environmental Nanotechnology, Monitoring & Management*, *1*, 8–13.

Amor-Gutiérrez, O., Costa-Rama, E., Arce-Varas, N., Martínez-Rodríguez, C., Novelli, A., Fernández-Sánchez, M. T., & Costa-García, A. (2020). Competitive electrochemical immunosensor for the detection of unfolded p53 protein in blood as biomarker for alzheimer's disease. *Analytica chimica acta*, *1093*, 28–34.

Apweiler, R., Aslanidis, C., Deufel, T., Gerstner, A., Hansen, J., Hochstrasser, D., Kellner, R., Kubicek, M., Lottspeich, F., Maser, E., et al. (2009). Approaching clinical proteomics: current state and future fields of application in fluid proteomics. *Clinical Chemistry and Laboratory Medicine (CCLM)*, *47*(6), 724–744.

Arevalo-Rodriguez, I., Smailagic, N., i Figuls, M. R., Ciapponi, A., Sanchez-Perez, E., Giannakou, A., Pedraza, O. L., Cosp, X. B., & Cullum, S. (2015). Mini-mental state examination (mmse) for the detection of alzheimer's disease and other dementias in people with mild cognitive impairment (mci). *Cochrane Database of Systematic Reviews*, (3).

Aristov, N., & Habekost, A. (2015). Cyclic voltammetry-a versatile electrochemical method investigating electron transfer processes. *World J. Chem. Educ*, *3*(5), 115–119.

Armbruster, D. A., & Pry, T. (2008). Limit of blank, limit of detection and limit of quantitation. *The clinical biochemist reviews*, *29*(Suppl 1), S49.

Arnaout, R., Lee, R. A., Lee, G. R., Callahan, C., Yen, C. F., Smith, K. P., Arora, R., & Kirby, J. E. (2020). Sars-cov2 testing: the limit of detection matters. *bioRxiv*.

Ashley, J., Shahbazi, M.-A., Kant, K., Chidambara, V. A., Wolff, A., Bang, D. D., & Sun, Y. (2017). Molecularly imprinted polymers for sample preparation and biosensing in food analysis: Progress and perspectives. *Biosensors and Bioelectronics*, *91*, 606–615.

Azimzadeh, M., Nasirizadeh, N., Rahaie, M., & Naderi-Manesh, H. (2017). Early detection of alzheimer's disease using a biosensor based on electrochemically-reduced graphene oxide and gold nanowires for the quantification of serum microrna-137. *RSC advances*, *7*(88), 55709–55719.

Baca, G., & Dennis, A. L. (1978). Electrochemistry in a nutshell a general chemistry experiment. *Journal of Chemical Education*, *55*(12), 804.

Badertscher, M., Bühlmann, P., & Pretsch, E. (2009). *Structure Determination of Organic Compounds: Tables of Spectral Data*. Springer.

Balaji, A., & Zhang, J. (2017). Electrochemical and optical biosensors for early-stage cancer diagnosis by using graphene and graphene oxide. *Cancer nanotechnology*, *8*(1), 10.

Balandin, A. A., Ghosh, S., Bao, W., Calizo, I., Teweldebrhan, D., Miao, F., & Lau, C. N. (2008). Superior thermal conductivity of single-layer graphene. *Nano letters*, *8*(3), 902–907.

Balasubramanian, K., & Kern, K. (2014). 25th anniversary article: Label-free electrical biodetection using carbon nanostructures. *Advanced Materials*, *26*(8), 1154–1175. URL `https://onlinelibrary.wiley.com/doi/abs/10.1002/adma.201304912`

Baldovino, F., Quitain, A., Dugos, N. P., Roces, S. A., Koinuma, M., Yuasa, M., & Kida, T. (2016). Synthesis and characterization of nitrogen-functionalized graphene oxide in high-temperature and high-pressure ammonia. *RSC advances*, *6*(115), 113924–113932.

Banerjee, S., Hemraj-Benny, T., & Wong, S. S. (2005). Covalent surface chemistry of single-walled carbon nanotubes. *Advanced Materials*, *17*(1), 17–29.

Bao, Q., & Loh, K. P. (2012). Graphene photonics, plasmonics, and broadband optoelectronic devices. *ACS nano*, *6*(5), 3677–3694.

Baradoke, A., Jose, B., Pauliukaite, R., & Forster, R. J. (2019). Properties of anti-ca125 antibody layers on screen-printed carbon electrodes modified by gold and platinum nanostructures. *Electrochimica Acta*, *306*, 299–306.

Baryeh, K., Takalkar, S., Lund, M., & Liu, G. (2017). Introduction to medical biosensors for point of care applications. In *Medical Biosensors for Point of Care (POC) Applications*, (pp. 3–25). Elsevier.

Baur, J. E., & Wightman, R. M. (1991). Diffusion coefficients determined with microelectrodes. *Journal of electroanalytical chemistry and interfacial electrochemistry*, *305*(1), 73–81.

Beck, F., Horn, C., & Baeumner, A. J. (2022). Ag nanoparticles outperform au nanoparticles for the use as label in electrochemical point-of-care sensors. *Analytical and Bioanalytical Chemistry*, *414*(1), 475–483.

Berkowitz, C., Mosconi, L., Rahman, A., Scheyer, O., Hristov, H., & Isaacson, R. S. (2018). Clinical application of apoe in alzheimer's prevention: a precision medicine approach. *The journal of prevention of Alzheimer's disease*, *5*(4), 245–252.

Bîru, E. I., Gârea, S. A., Nicolescu, A., Vasile, E., & Iovu, H. (2018). Advanced polybenzoxazine structures based on modified reduced graphene oxide. *Polymers*, *10*(9), 941.

Blennow, K. (2004). Cerebrospinal fluid protein biomarkers for alzheimer's disease. *NeuroRx*, *1*(2), 213–225.

Blennow, K. (2010). Biomarkers in alzheimer's disease drug development. *Nature medicine*, *16*(11), 1218–1222.

Blennow, K., Dubois, B., Fagan, A. M., Lewczuk, P., De Leon, M. J., & Hampel, H. (2015). Clinical utility of cerebrospinal fluid biomarkers in the diagnosis of early alzheimer's disease. *Alzheimer's & Dementia*, *11*(1), 58–69.

Bo, Y., Yang, H., Hu, Y., Yao, T., & Huang, S. (2011). A novel electrochemical dna biosensor based on graphene and polyaniline nanowires. *Electrochimica Acta*, *56*(6), 2676–2681.

Boesl, U. (2017). Time-of-flight mass spectrometry: introduction to the basics. *Mass spectrometry reviews*, *36*(1), 86–109.

Bonhommeau, S., Talaga, D., Hunel, J., Cullin, C., & Lecomte, S. (2017). Tip-enhanced raman spectroscopy to distinguish toxic oligomers from aβ1–42 fibrils at the nanometer scale. *Angewandte Chemie*, *129*(7), 1797–1800.

Botas, C., Álvarez, P., Blanco, C., Gutiérrez, M. D., Ares, P., Zamani, R., Arbiol, J., Morante, J. R., & Menéndez, R. (2012). Tailored graphene materials by chemical reduction of graphene oxides of different atomic structure. *RSC advances*, *2*(25), 9643–9650.

Boukhvalov, D., & Katsnelson, M. (2008). Chemical functionalization of graphene with defects. *Nano letters*, *8*(12), 4373–4379.

Buizza, L., Prandelli, C., Bonini, S., Delbarba, A., Cenini, G., Lanni, C., Buoso, E., Racchi, M., Govoni, S., Memo, M., et al. (2013). Conformational altered p53 affects neuronal function: relevance for the response to toxic insult and growth-associated protein 43 expression. *Cell death & disease*, *4*(2), e484–e484.

Buxton, G. V., Greenstock, C. L., Helman, W. P., & Ross, A. B. (1988). Critical review of rate constants for reactions of hydrated electrons, hydrogen atoms and hydroxyl radicals ($\cdot$oh/$\cdot$o$^-$ in aqueous solution. *Journal of physical and chemical reference data*, *17*(2), 513–886.

Byrne, B., Stack, E., Gilmartin, N., & O'Kennedy, R. (2009). Antibody-based sensors: principles, problems and potential for detection of pathogens and associated toxins. *Sensors*, *9*(6), 4407–4445.

Calero, O., García-Albert, L., Rodríguez-Martín, A., Veiga, S., & Calero, M. (2018). A fast and cost-effective method for apolipoprotein e isotyping as an alternative to apoe genotyping for patient screening and stratification. *Scientific reports*, *8*(1), 1–8.

Carneiro, P., Loureiro, J., Delerue-Matos, C., Morais, S., & do Carmo Pereira, M. (2017). Alzheimer's disease: Development of a sensitive label-free electrochemical immunosensor for detection of amyloid beta peptide. *Sensors and Actuators B: Chemical*, *239*, 157–165.

Carneiro, P., Morais, S., & Pereira, M. C. (2019). Nanomaterials towards biosensing of alzheimer's disease biomarkers. *Nanomaterials*, *9*(12), 1663.

Chaki, N. K., & Vijayamohanan, K. (2002). Self-assembled monolayers as a tunable platform for biosensor applications. *Biosensors and Bioelectronics*, *17*(1-2), 1–12.

Chang, J., Zhou, G., Christensen, E. R., Heideman, R., & Chen, J. (2014). Graphene-based sensors for detection of heavy metals in water: a review. *Analytical and bioanalytical chemistry*, *406*(16), 3957–3975.

Chaubey, A., & Malhotra, B. (2002a). Mediated biosensors. *Biosensors and Bioelectronics*, *17*(6), 441 – 456.
URL `http://www.sciencedirect.com/science/article/pii/S095656630100313X`

Chaubey, A., & Malhotra, B. (2002b). Mediated biosensors. *Biosensors and bioelectronics*, *17*(6-7), 441–456.

Chauhan, N., Balayan, S., & Jain, U. (2020). Sensitive biosensing of neurotransmitter: 2d material wrapped nanotubes and mno2 composites for the detection of acetylcholine. *Synthetic Metals*, *263*, 116354.

Chauhan, N., Chawla, S., Pundir, C., & Jain, U. (2017). An electrochemical sensor for detection of neurotransmitter-acetylcholine using metal nanoparticles, 2d material and conducting polymer modified electrode. *Biosensors and Bioelectronics*, *89*, 377–383.

Chauhan, N., & Pundir, C. (2014). Amperometric determination of acetylcholine—a neurotransmitter, by chitosan/gold-coated ferric oxide nanoparticles modified gold electrode. *Biosensors and Bioelectronics*, *61*, 1–8.

Chen, A., & Chatterjee, S. (2013). Nanomaterials based electrochemical sensors for biomedical applications. *Chemical Society Reviews*, *42*(12), 5425–5438.

Chen, C., Ridzon, D. A., Broomer, A. J., Zhou, Z., Lee, D. H., Nguyen, J. T., Barbisin, M., Xu, N. L., Mahuvakar, V. R., Andersen, M. R., et al. (2005). Real-time quantification of micrornas by stem–loop rt–pcr. *Nucleic acids research*, *33*(20), e179–e179.

Chen, C.-M., Zhang, Q., Zhao, X.-C., Zhang, B., Kong, Q.-Q., Yang, M.-G., Yang, Q.-H., Wang, M.-Z., Yang, Y.-G., Schlögl, R., et al. (2012). Hierarchically aminated graphene honeycombs for electrochemical capacitive energy storage. *Journal of Materials Chemistry*, *22*(28), 14076–14084.

Chen, L., Wang, L., Shuai, Z., & Beljonne, D. (2013). Energy level alignment and charge carrier mobility in noncovalently functionalized graphene. *The Journal of Physical Chemistry Letters*, *4*(13), 2158–2165.

Chen, L.-C., Wang, E., Tai, C.-S., Chiu, Y.-C., Li, C.-W., Lin, Y.-R., Lee, T.-H., Huang, C.-W., Chen, J.-C., & Chen, W. L. (2020). Improving the reproducibility, accuracy, and stability of an electrochemical biosensor platform for point-of-care use. *Biosensors and Bioelectronics*, *155*, 112111.

Chen, T.-B., Lee, Y.-J., Lin, S.-Y., Chen, J.-P., Hu, C.-J., Wang, P.-N., & Cheng, I. H. (2019). Plasma aβ42 and total tau predict cognitive decline in amnestic mild cognitive impairment. *Scientific reports*, *9*(1), 1–10.

Cheng, X. R., Hau, B. Y., Endo, T., & Kerman, K. (2014). Au nanoparticle-modified dna sensor based on simultaneous electrochemical impedance spectroscopy and localized surface plasmon resonance. *Biosensors and Bioelectronics*, *53*, 513–518.

Chertkow, H., Feldman, H. H., Jacova, C., & Massoud, F. (2013). Definitions of dementia and predementia states in alzheimer's disease and vascular cognitive impairment: consensus from the canadian conference on diagnosis of dementia. *Alzheimer's research & therapy*, *5*(1), 1–8.

Chou, I.-H., Benford, M., Beier, H. T., Coté, G. L., Wang, M., Jing, N., Kameoka, J., & Good, T. A. (2008). Nanofluidic biosensing for β-amyloid detection using surface enhanced raman spectroscopy. *Nano letters*, *8*(6), 1729–1735.

Coleman, R. E. (2007). Positron emission tomography diagnosis of alzheimer's disease. *PET Clinics*, *2*(1), 25 – 34. Neurologic Applications of PET.
URL http://www.sciencedirect.com/science/article/pii/S1556859807000247

Colvin, V. L. (2003). The potential environmental impact of engineered nanomaterials. *Nature biotechnology*, *21*(10), 1166–1170.

Congur, G., Eksin, E., & Erdem, A. (2015). Impedimetric detection of microrna at graphene oxide modified sensors. *Electrochimica Acta*, *172*, 20–27.

Connolly, A., Gaehl, E., Martin, H., Morris, J., & Purandare, N. (2011). Underdiagnosis of dementia in primary care: variations in the observed prevalence and comparisons to the expected prevalence. *Aging & mental health*, *15*(8), 978–984.

Cooper, D. R., D'Anjou, B., Ghattamaneni, N., Harack, B., Hilke, M., Horth, A., Majlis, N., Massicotte, M., Vandsburger, L., Whiteway, E., et al. (2012). Experimental review of graphene. *ISRN Condensed Matter Physics*, *2012*.

Crous-Bou, M., Minguillón, C., Gramunt, N., & Molinuevo, J. L. (2017). Alzheimer's disease prevention: from risk factors to early intervention. *Alzheimer's Research & Therapy*, *9*(1), 71.

Dai, Y., Molazemhosseini, A., & Liu, C. C. (2017). In vitro quantified determination of β-amyloid 42 peptides, a biomarker of neuro-degenerative disorders, in pbs and human serum using a simple, cost-effective thin gold film biosensor. *Biosensors*, *7*(3), 29.

de Almeida, S. M., Shumaker, S. D., LeBlanc, S. K., Delaney, P., Marquie-Beck, J., Ueland, S., Alexander, T., & Ellis, R. J. (2011). Incidence of post-dural puncture headache in research volunteers. *Headache: The Journal of Head and Face Pain*, *51*(10), 1503–1510.

De Picciotto, S., Imperiali, B., Griffith, L. G., & Wittrup, K. D. (2014). Equilibrium and dynamic design principles for binding molecules engineered for reagentless biosensors. *Analytical biochemistry*, *460*, 9–15.

Demeritte, T., Viraka Nellore, B. P., Kanchanapally, R., Sinha, S. S., Pramanik, A., Chavva, S. R., & Ray, P. C. (2015). Hybrid graphene oxide based plasmonic-magnetic multifunctional nanoplatform for selective separation and label-free identification of alzheimer's disease biomarkers. *ACS applied materials & interfaces*, *7*(24), 13693–13700.

Derkus, B., Bozkurt, P. A., Tulu, M., Emregul, K. C., Yucesan, C., & Emregul, E. (2017). Simultaneous quantification of myelin basic protein and tau proteins in cerebrospinal fluid and serum of multiple sclerosis patients using nanoimmunosensor. *Biosensors and Bioelectronics*, *89*, 781–788.

Devi, R., Gogoi, S., Dutta, H. S., Bordoloi, M., Sanghi, S. K., & Khan, R. (2020). Au/nife 2 o 4 nanoparticle-decorated graphene oxide nanosheets for electrochemical immunosensing of amyloid beta peptide. *Nanoscale Advances*, *2*(1), 239–248.

Diba, F. S., Kim, S., & Lee, H. J. (2017). Electrochemical immunoassay for amyloid-beta 1–42 peptide in biological fluids interfacing with a gold nanoparticle modified carbon surface. *Catalysis Today*, *295*, 41–47.

Ding, S., Xu, Y., Liu, Q., Gu, H., Zhu, A., & Shi, G. (2020). Interface engineering of microelectrodes toward ultrasensitive monitoring of β-amyloid peptides in cerebrospinal fluid in alzheimer's disease. *Analyst*, *145*(6), 2331–2338.

Dong, H., Yan, F., Ji, H., Wong, D. K., & Ju, H. (2010). Quantum-dot-functionalized poly (styrene-co-acrylic acid) microbeads: step-wise self-assembly, characterization, and applications for sub-femtomolar electrochemical detection of dna hybridization. *Advanced Functional Materials*, *20*(7), 1173–1179.

Dresselhaus, M., Dresselhaus, G., & Hofmann, M. (2008). Raman spectroscopy as a probe of graphene and carbon nanotubes. *Philosophical Transactions of the Royal Society A: Mathematical, Physical and Engineering Sciences*, *366*(1863), 231–236.

Dryhurst, G. (2012). *Electrochemistry of biological molecules*. Elsevier.

Duong, T., Nikolaeva, M., & Acton, P. J. (1997). C-reactive protein-like immunoreactivity in the neurofibrillary tangles of alzheimer's disease. *Brain research*, *749*(1), 152–156.

Duraiyan, J., Govindarajan, R., Kaliyappan, K., & Palanisamy, M. (2012). Applications of immunohistochemistry. *Journal of pharmacy & bioallied sciences*, *4*(Suppl 2), S307.

Duthey, B. (2013). Priority medicines for europe and the world" a public health approach to innovation. *WHO Background paper*, *6*.

EAG Laboratories, E. C. (2015). X-ray photoelectron spectroscopy (xps spectroscopy) or electron spectroscopy for chemical analysis (esca).
URL `https://www.eag.com/techniques/spectroscopy/x-ray-photoelectron-spectroscopy-xps-esca/`

Eisele, Y. S. (2013). From soluble aβ to progressive aβ aggregation: Could prion-like templated misfolding play a role? *Brain Pathology*, *23*(3), 333–341.
URL `https://onlinelibrary.wiley.com/doi/abs/10.1111/bpa.12049`

Elgrishi, N., Rountree, K. J., McCarthy, B. D., Rountree, E. S., Eisenhart, T. T., & Dempsey, J. L. (2018). A practical beginner's guide to cyclic voltammetry. *Journal of Chemical Education*, *95*(2), 197–206.

Evans, D. H. (1972). Theory for a homogeneous reaction following a quasireversible electrode reaction. *The Journal of Physical Chemistry*, *76*(8), 1160–1165.

Fei, Y., Sun, Y.-S., Li, Y., Lau, K., Yu, H., Chokhawala, H. A., Huang, S., Landry, J. P., Chen, X., & Zhu, X. (2011). Fluorescent labeling agents change binding profiles of glycan-binding proteins. *Molecular BioSystems*, *7*(12), 3343–3352.

Fenton, H. (1894). Lxxiii.—oxidation of tartaric acid in presence of iron. *Journal of the Chemical Society, Transactions*, *65*, 899–910.

Ferrari, A. C. (2007). Raman spectroscopy of graphene and graphite: Disorder, electron–phonon coupling, doping and nonadiabatic effects. *Solid state communications*, *143*(1-2), 47–57.

Gabin, J. M., Saltvedt, I., Tambs, K., & Holmen, J. (2018). The association of high sensitivity c-reactive protein and incident alzheimer disease in patients 60 years and older: The hunt study, norway. *Immunity & Ageing*, *15*(1), 4.

Gaggelli, E., Janicka-Klos, A., Jankowska, E., Kozlowski, H., Migliorini, C., Molteni, E., Valensin, D., Valensin, G., & Wieczerzak, E. (2008). Nmr studies of the zn2+ interactions with rat and human β-amyloid (1- 28) peptides in water-micelle environment. *The journal of physical chemistry B*, *112*(1), 100–109.

Gao, L., Zhao, H., Li, T., Huo, P., Chen, D., & Liu, B. (2018). Atomic force microscopy based tip-enhanced raman spectroscopy in biology. *International journal of molecular sciences*, *19*(4), 1193.

Gao, Z., Li, Y., Zhang, C., Zhang, S., Jia, Y., Li, F., Ding, H., Li, X., Chen, Z., & Wei, Q. (2019). Aucu x o-embedded mesoporous ceo2 nanocomposites as a signal probe for electrochemical sensitive detection of amyloid-beta protein. *ACS applied materials & interfaces*, *11*(13), 12335–12341.

Ge, C., Li, Y., Yin, J.-J., Liu, Y., Wang, L., Zhao, Y., & Chen, C. (2012). The contributions of metal impurities and tube structure to the toxicity of carbon nanotube materials. *NPG Asia Materials*, *4*(12), e32–e32.

Geekiyanage, H., Jicha, G. A., Nelson, P. T., & Chan, C. (2012). Blood serum mirna: non-invasive biomarkers for alzheimer's disease. *Experimental neurology*, *235*(2), 491–496.

Geim, A. K., & Novoselov, K. S. (2010). The rise of graphene. In *Nanoscience and technology: a collection of reviews from nature journals*, (pp. 11–19). World Scientific.

Georgakilas, V., Bourlinos, A. B., Zboril, R., Steriotis, T. A., Dallas, P., Stubos, A. K., & Trapalis, C. (2010). Organic functionalisation of graphenes. *Chemical Communications*, *46*(10), 1766–1768.

Georgakilas, V., Otyepka, M., Bourlinos, A. B., Chandra, V., Kim, N., Kemp, K. C., Hobza, P., Zboril, R., & Kim, K. S. (2012). Functionalization of graphene: covalent and non-covalent approaches, derivatives and applications. *Chemical reviews*, *112*(11), 6156–6214.

Ghaderi, N., & Peressi, M. (2010). First-principle study of hydroxyl functional groups on pristine, defected graphene, and graphene epoxide. *The Journal of Physical Chemistry C*, *114*(49), 21625–21630.

Gilje, S., Dubin, S., Badakhshan, A., Farrar, J., Danczyk, S. A., & Kaner, R. B. (2010). Photothermal deoxygenation of graphene oxide for patterning and distributed ignition applications. *Advanced Materials*, *22*(3), 419–423.

Gilje, S., Han, S., Wang, M., Wang, K. L., & Kaner, R. B. (2007). A chemical route to graphene for device applications. *Nano letters*, *7*(11), 3394–3398.

Gill, A. A., Singh, S., Thapliyal, N., & Karpoormath, R. (2019). Nanomaterial-based optical and electrochemical techniques for detection of methicillin-resistant staphylococcus aureus: a review. *Microchimica Acta*, *186*(2), 114.

Gisslén, M., Price, R. W., Andreasson, U., Norgren, N., Nilsson, S., Hagberg, L., Fuchs, D., Spudich, S., Blennow, K., & Zetterberg, H. (2016). Plasma concentration of the neurofilament light protein (nfl) is a biomarker of cns injury in hiv infection: A cross-sectional study. *EBioMedicine*, *3*, 135 – 140.
URL `http://www.sciencedirect.com/science/article/pii/S235239641530219X`

Gómez-Navarro, C., Weitz, R. T., Bittner, A. M., Scolari, M., Mews, A., Burghard, M., & Kern, K. (2007). Electronic transport properties of individual chemically reduced graphene oxide sheets. *Nano letters*, *7*(11), 3499–3503.

Graff-Radford, N. R., Crook, J. E., Lucas, J., Boeve, B. F., Knopman, D. S., Ivnik, R. J., Smith, G. E., Younkin, L. H., Petersen, R. C., & Younkin, S. G. (2007). Association of low plasma aβ42/aβ40 ratios with increased imminent risk for mild cognitive impairment and alzheimer disease. *Archives of neurology*, *64*(3), 354–362.

Grieshaber, D., MacKenzie, R., Vörös, J., & Reimhult, E. (2008). Electrochemical biosensors-sensor principles and architectures. *Sensors*, *8*(3), 1400–1458.

Gross, J. H. (2006). *Mass spectrometry: a textbook*. Springer Science & Business Media.

Growdon, J. H. (1999). Biomarkers of alzheimer disease. *Archives of neurology*, *56*(3), 281–283.

Gui, R., Jin, H., Guo, H., & Wang, Z. (2018). Recent advances and future prospects in molecularly imprinted polymers-based electrochemical biosensors. *Biosensors and Bioelectronics*, *100*, 56–70.

Guler, M., Turkoglu, V., & Basi, Z. (2017). Determination of malation, methidathion, and chlorpyrifos ethyl pesticides using acetylcholinesterase biosensor based on nafion/ag@ rgo-nh2 nanocomposites. *Electrochimica Acta*, *240*, 129–135.

Gupta, V. B., Sundaram, R., & Martins, R. N. (2013). Multiplex biomarkers in blood. *Alzheimer's research & therapy*, *5*(3), 31.

Ha, M., & Kim, V. N. (2014). Regulation of microrna biogenesis. *Nature reviews Molecular cell biology*, *15*(8), 509–524.

Hale, J. E. (2013). Advantageous uses of mass spectrometry for the quantification of proteins. *International journal of proteomics*, *2013*.

Hampel, H., O'Bryant, S. E., Molinuevo, J. L., Zetterberg, H., Masters, C. L., Lista, S., Kiddle, S. J., Batrla, R., & Blennow, K. (2018). Blood-based biomarkers for alzheimer disease: mapping the road to the clinic. *Nature Reviews Neurology*, *14*(11), 639–652.

Hampel, H., Shen, Y., Walsh, D. M., Aisen, P., Shaw, L. M., Zetterberg, H., Trojanowski, J. Q., & Blennow, K. (2010). Biological markers of amyloid β-related mechanisms in alzheimer's disease. *Experimental Neurology*, *223*(2), 334 – 346. Beta-amyloid and tau protein abnormalities in Alzheimer's disease.
URL http://www.sciencedirect.com/science/article/pii/S0014488609004117

Han, J., Zhang, M., Chen, G., Zhang, Y., Wei, Q., Zhuo, Y., Xie, G., Yuan, R., & Chen, S. (2017). Ferrocene covalently confined in porous mof as signal tag for highly sensitive electrochemical immunoassay of amyloid-β. *Journal of Materials Chemistry B*, *5*(42), 8330–8336.

Han, K., Liang, Z., & Zhou, N. (2010). Design strategies for aptamer-based biosensors. *Sensors*, *10*(5), 4541–4557.

Hanon, O., Vidal, J.-S., Lehmann, S., Bombois, S., Allinquant, B., Tréluyer, J.-M., Gelé, P., Delmaire, C., Blanc, F., Mangin, J.-F., Buée, L., Touchon, J., Hugon, J., Vellas, B., Galbrun, E., Benetos, A., Berrut, G., Paillaud, E., Wallon, D., Castelnovo, G., Volpe-Gillot, L., Paccalin, M., Robert, P.-H., Godefroy, O., Dantoine, T., Camus, V., Belmin, J., Vandel, P., Novella, J.-L., Duron, E., Rigaud, A.-S., Schraen-Maschke, S., Gabelle, A., & on behalf of the BALTAZAR study group (2018). Plasma amyloid levels within the alzheimer's process and correlations with central biomarkers. *Alzheimer's & Dementia*, *14*(7), 858–868.
URL https://alz-journals.onlinelibrary.wiley.com/doi/abs/10.1016/j.jalz.2018.01.004

Hardy, J., & Selkoe, D. J. (2002). The amyloid hypothesis of alzheimer's disease: Progress and problems on the road to therapeutics. *Science*, *297*(5580), 353–356.
URL https://science.sciencemag.org/content/297/5580/353

Hassan, Q., & Kerman, K. (2019). Electrochemical approaches for the detection of amyloid-β, tau, and α-synuclein. *Current Opinion in Electrochemistry*, *14*, 89–95.

Helmerhorst, E., Chandler, D. J., Nussio, M., & Mamotte, C. D. (2012). Real-time and label-free bio-sensing of molecular interactions by surface plasmon resonance: a laboratory medicine perspective. *The Clinical Biochemist Reviews*, *33*(4), 161.

Henriksen, K., O'Bryant, S. E., Hampel, H., Trojanowski, J. Q., Montine, T. J., Jeromin, A., Blennow, K., Lönneborg, A., Wyss-Coray, T., Soares, H., et al. (2014). The future of blood-based biomarkers for alzheimer's disease. *Alzheimer's & Dementia*, *10*(1), 115–131.

Hölttä, M., Hansson, O., Andreasson, U., Hertze, J., Minthon, L., Nägga, K., Andreasen, N., Zetterberg, H., & Blennow, K. (2013). Evaluating amyloid-β oligomers in cerebrospinal fluid as a biomarker for alzheimer's disease. *PloS one*, *8*(6), e66381.

Huang, Y., Xu, J., Liu, J., Wang, X., & Chen, B. (2017). Disease-related detection with electrochemical biosensors: a review. *Sensors*, *17*(10), 2375.

Hunt, H. K., & Armani, A. M. (2010). Label-free biological and chemical sensors. *Nanoscale*, *2*(9), 1544–1559.

Hwang, S. S., Chan, H., Sorci, M., Van Deventer, J., Wittrup, D., Belfort, G., & Walt, D. (2019). Detection of amyloid β oligomers toward early diagnosis of alzheimer's disease. *Analytical Biochemistry*, *566*, 40 – 45.
URL `http://www.sciencedirect.com/science/article/pii/S0003269718304408`

Iglesias-Mayor, A., Amor-Gutiérrez, O., Novelli, A., Fernández-Sánchez, M.-T., Costa-García, A., & de la Escosura-Muñiz, A. (2020). Bifunctional au@ pt/au core@ shell nanoparticles as novel electrocatalytic tags in immunosensing: Application for alzheimer's disease biomarker detection. *Analytical Chemistry*, *92*(10), 7209–7217.

Ishigami, M., Chen, J., Cullen, W., Fuhrer, M., & Williams, E. (2007). Atomic structure of graphene on sio2. *Nano letters*, *7*(6), 1643–1648.

Islam, K., Damiati, S., Sethi, J., Suhail, A., & Pan, G. (2018). Development of a label-free immunosensor for clusterin detection as an alzheimer's biomarker. *Sensors*, *18*(1), 308.

Islam, K., Suhail, A., & Pan, G. (2017). A label-free and ultrasensitive immunosensor for detection of human chorionic gonadotrophin based on graphene fets. *Biosensors*, *7*(3), 27.

Islam, M. N., & Channon, R. B. (2020). Electrochemical sensors. In *Bioengineering Innovative Solutions for Cancer*, (pp. 47–71). Elsevier.

Iwamoto, N., Nishiyama, E., Ohwada, J., & Arai, H. (1994). Demonstration of crp immunoreactivity in brains of alzheimer's disease: immunohistochemical study using formic acid pretreatment of tissue sections. *Neuroscience letters*, *177*(1-2), 23–26.

Jack Jr, C. R., Bennett, D. A., Blennow, K., Carrillo, M. C., Dunn, B., Haeberlein, S. B., Holtzman, D. M., Jagust, W., Jessen, F., Karlawish, J., et al. (2018). Nia-aa research framework: toward a biological definition of alzheimer's disease. *Alzheimer's & Dementia*, *14*(4), 535–562.

Janelidze, S., Berron, D., Smith, R., Strandberg, O., Proctor, N. K., Dage, J. L., Stomrud, E., Palmqvist, S., Mattsson-Carlgren, N., & Hansson, O. (2021). Associations of plasma phospho-tau217 levels with tau positron emission tomography in early alzheimer disease. *JAMA neurology*, *78*(2), 149–156.

Janelidze, S., Stomrud, E., Palmqvist, S., Zetterberg, H., Van Westen, D., Jeromin, A., Song, L., Hanlon, D., Hehir, C. A. T., Baker, D., et al. (2016). Plasma β-amyloid in alzheimer's disease and vascular disease. *Scientific reports*, *6*(1), 1–11.

Jang, J., Pham, V. H., Hur, S. H., & Chung, J. S. (2014). Dispersibility of reduced alkylamine-functionalized graphene oxides in organic solvents. *Journal of colloid and interface science*, *424*, 62–66.

Jankowsky, J. L., Fadale, D. J., Anderson, J., Xu, G. M., Gonzales, V., Jenkins, N. A., Copeland, N. G., Lee, M. K., Younkin, L. H., Wagner, S. L., et al. (2004). Mutant presenilins specifically elevate the levels of the 42 residue β-amyloid peptide in vivo: evidence for augmentation of a 42-specific γ secretase. *Human molecular genetics*, *13*(2), 159–170.

Jennings, V., Forster, T., & Williams, J. (1970). Study of the voltammetric behaviour of 2-ethylanthraquinone by using a vitreous carbon electrode. *Analyst*, *95*(1133), 718–721.

Jiang, Z., Wang, Y., Sun, L., Yuan, B., Tian, Y., Xiang, L., Li, Y., Li, Y., Li, J., & Wu, A. (2019). Dual atp and ph responsive zif-90 nanosystem with favorable biocompatibility and facile post-modification improves therapeutic outcomes of triple negative breast cancer in vivo. *Biomaterials*, *197*, 41–50.

Joe, H. (2004). Everitt bs 2002: The cambridge dictionary of statistics, cambridge: Cambridge university press. 420 pp.£ 30.00 (us 50.00)(hb). isbn 05218 1099 x.

Justino, C. I., Gomes, A. R., Freitas, A. C., Duarte, A. C., & Rocha-Santos, T. A. (2017). Graphene based sensors and biosensors. *TrAC Trends in Analytical Chemistry*, *91*, 53–66.

Kampeera, J., Pasakon, P., Karuwan, C., Arunrut, N., Sappat, A., Sirithammajak, S., Dechokiattawan, N., Sumranwanich, T., Chaivisuthangkura, P., Ounjai, P., Chankhamhaengdecha, S., Wisitsoraat, A., Tuantranont, A., & Kiatpathomchai, W. (2019). Point-of-care rapid detection of vibrio parahaemolyticus in seafood using loop-mediated isothermal amplification and graphene-based screen-printed electrochemical sensor. *Biosensors and Bioelectronics*, *132*, 271 – 278.
URL `http://www.sciencedirect.com/science/article/pii/S0956566319301800`

Kang, S., Qiao, S., Hu, Z., Yu, J., Wang, Y., & Zhu, J. (2019). Interfacial polymerized reduced graphene oxide covalently grafted polyaniline nanocomposites for high-performance electromagnetic wave absorber. *Journal of Materials Science*, *54*(8), 6410–6424.

Kawata, T., Ono, T., Kanai, Y., Ohno, Y., Maehashi, K., Inoue, K., & Matsumoto, K. (2018). Improved sensitivity of a graphene fet biosensor using porphyrin linkers. *Japanese Journal of Applied Physics*, *57*(6), 065103.

Keene, C. D., Wilson, A. M., Kilgore, M. D., Bruner, L. T., Postupna, N. O., & Darvas, M. (2018). Luminex-based quantification of alzheimer's disease neuropathologic change in formalin-fixed post-mortem human brain tissue. *Laboratory Investigation*, (p. 1).

Kim, D., & Herr, A. E. (2013). Protein immobilization techniques for microfluidic assays. *Biomicrofluidics*, *7*(4), 041501.

Kim, H. J., Kim, C.-D., & Sohn, Y.-S. (2019). Thiolated protein a-functionalized bimetallic surface plasmon resonance chip for enhanced determination of amyloid beta 42. *Applied Chemistry for Engineering*, *30*(3), 379–383.

Kim, S., Wark, A. W., & Lee, H. J. (2016). Femtomolar detection of tau proteins in undiluted plasma using surface plasmon resonance. *Analytical chemistry*, *88*(15), 7793–7799.

Kim, S.-E., Tieu, M. V., Hwang, S. Y., & Lee, M.-H. (2020). Magnetic particles: Their applications from sample preparations to biosensing platforms. *Micromachines*, *11*(3), 302.

Kim, S. H., Iwai, S., Araki, S., Sakakihara, S., Iino, R., & Noji, H. (2012). Large-scale femtoliter droplet array for digital counting of single biomolecules. *Lab on a Chip*, *12*(23), 4986–4991.

Kissinger, P., & Heineman, W. R. (2018). *Laboratory Techniques in Electroanalytical Chemistry, revised and expanded*. CRC press.

Kong, J., & Yu, S. (2007). Fourier transform infrared spectroscopic analysis of protein secondary structures. *Acta biochimica et biophysica Sinica*, *39*(8), 549–559.

Kounaves, S. P. (1997). Voltammetric techniques. *Handbook of instrumental techniques for analytical chemistry*, (pp. 709–726).

Krishnan, S., & Rani, P. (2014). Evaluation of selenium, redox status and their association with plasma amyloid/tau in alzheimer's disease. *Biological trace element research*, *158*(2), 158–165.

Krishnan, S. K., Singh, E., Singh, P., Meyyappan, M., & Nalwa, H. S. (2019). A review on graphene-based nanocomposites for electrochemical and fluorescent biosensors. *RSC advances*, *9*(16), 8778–8881.

Kuhle, J., Barro, C., Andreasson, U., Derfuss, T., Lindberg, R., Sandelius, Å., Liman, V., Norgren, N., Blennow, K., & Zetterberg, H. (2016). Comparison of three analytical platforms for quantification of the neurofilament light chain in blood samples: Elisa, electrochemiluminescence immunoassay and simoa. *Clinical Chemistry and Laboratory Medicine (CCLM)*, *54*(10), 1655–1661.

Kuila, T., Bose, S., Khanra, P., Mishra, A. K., Kim, N. H., & Lee, J. H. (2011). Recent advances in graphene-based biosensors. *Biosensors and bioelectronics*, *26*(12).

Kuila, T., Bose, S., Mishra, A. K., Khanra, P., Kim, N. H., & Lee, J. H. (2012). Chemical functionalization of graphene and its applications. *Progress in Materials Science*, *57*(7), 1061 – 1105.
URL `http://www.sciencedirect.com/science/article/pii/S0079642512000254`

Kumar, N., Das, S., Bernhard, C., Varma, G., et al. (2013). Effect of graphene oxide doping on superconducting properties of bulk mgb2. *Superconductor Science and Technology*, *26*(9), 095008.

Kumar, R., Kumar, A., Singh, R., Kashyap, R., Kumar, R., Kumar, D., & Kumar, M. (2019). Room temperature ammonia gas sensor using ester functionalization of graphene oxide. *Materials Research Express*, *6*(9), 095618.

Kwak, K., Kumar, S. S., Pyo, K., & Lee, D. (2014). Ionic liquid of a gold nanocluster: a versatile matrix for electrochemical biosensors. *ACS nano*, *8*(1), 671–679.

Lahoz, C., Schaefer, E. J., Cupples, L. A., Wilson, P. W., Levy, D., Osgood, D., Parpos, S., Pedro-Botet, J., Daly, J. A., & Ordovas, J. M. (2001). Apolipoprotein e genotype and cardiovascular disease in the framingham heart study. *Atherosclerosis*, *154*(3), 529–537.

Lai, L., Chen, L., Zhan, D., Sun, L., Liu, J., Lim, S. H., Poh, C. K., Shen, Z., & Lin, J. (2011). One-step synthesis of nh2-graphene from in situ graphene-oxide reduction and its improved electrochemical properties. *Carbon*, *49*(10), 3250–3257.

Lakhin, A., Tarantul, V., & Gening, L. (2013). Aptamers: problems, solutions and prospects. *Acta Naturae*, *5*(4 (19)).

Lambert, J.-C., Schraen-Maschke, S., Richard, F., Fievet, N., Rouaud, O., Berr, C., Dartigues, J.-F., Tzourio, C., Alperovitch, A., Buee, L., et al. (2009). Association of plasma amyloid β with risk of dementia: the prospective three-city study. *Neurology*, *73*(11), 847–853.

Laurent, V., Trausch, G., Bruot, O., Olivier, P., Felblinger, J., & Régent, D. (2010). Comparative study of two whole-body imaging techniques in the case of melanoma metastases: advantages of multi-contrast mri examination including a diffusion-weighted sequence in comparison with pet-ct. *European journal of radiology*, *75*(3), 376–383.

Laviron, E. (1979). General expression of the linear potential sweep voltammogram in the case of diffusionless electrochemical systems. *Journal of Electroanalytical Chemistry and Interfacial Electrochemistry*, *101*(1), 19–28.

Lawrence, M. S., Phillips, K. J., & Liu, D. R. (2007). Supercharging proteins can impart unusual resilience. *Journal of the American Chemical Society*, *129*(33), 10110–10112.

Le, H. T. N., Park, J., Chinnadayyala, S. R., & Cho, S. (2019a). Sensitive electrochemical detection of amyloid beta peptide in human serum using an interdigitated chain-shaped electrode. *Biosensors and Bioelectronics*, *144*, 111694.
URL `http://www.sciencedirect.com/science/article/pii/S0956566319307730`

Le, H. T. N., Park, J., Chinnadayyala, S. R., & Cho, S. (2019b). Sensitive electrochemical detection of amyloid beta peptide in human serum using an interdigitated chain-shaped electrode. *Biosensors and Bioelectronics*, *144*, 111694.

Lee, C., Wei, X., Kysar, J. W., & Hone, J. (2008). Measurement of the elastic properties and intrinsic strength of monolayer graphene. *science*, *321*(5887), 385–388.

Lee, E. J., Choi, J.-H., Um, S. H., & Oh, B.-K. (2017). Electrochemical sensor for selective detection of norepinephrine using graphene sheets-gold nanoparticle complex modified electrode. *Korean Journal of Chemical Engineering*, *34*(4), 1129–1132.

Lee, H. H., Dineva, M. A., Chua, Y. L., Ritchie, A., Ushiro-Lumb, I., & Wisniewski, C. A. (2010). Simple amplification-based assay: a nucleic acid-based point-of-care platform for hiv-1 testing. *Journal of Infectious Diseases*, *201*(Supplement_1), S65–S71.

Leeman, M., Choi, J., Hansson, S., Storm, M. U., & Nilsson, L. (2018). Proteins and antibodies in serum, plasma, and whole blood—size characterization using asymmetrical flow field-flow fractionation (af4). *Analytical and bioanalytical chemistry*, *410*(20), 4867–4873.

Leidinger, P., Backes, C., Deutscher, S., Schmitt, K., Mueller, S. C., Frese, K., Haas, J., Ruprecht, K., Paul, F., Stähler, C., et al. (2013). A blood based 12-mirna signature of alzheimer disease patients. *Genome biology*, *14*(7), R78.

Lewczuk, P., Ermann, N., Andreasson, U., Schultheis, C., Podhorna, J., Spitzer, P., Maler, J. M., Kornhuber, J., Blennow, K., & Zetterberg, H. (2018). Plasma neurofilament light as a potential biomarker of neurodegeneration in alzheimer's disease. *Alzheimer's research & therapy*, *10*(1), 71.

Lewczuk, P., & Kornhuber, J. (2016). Do we still need positron emission tomography for early alzheimer's disease diagnosis? *Brain*, *139*(11), e60–e60.

Li, B., Pan, G., Avent, N. D., Lowry, R. B., Madgett, T. E., & Waines, P. L. (2015). Graphene electrode modified with electrochemically reduced graphene oxide for label-free dna detection. *Biosensors and Bioelectronics*, *72*, 313 – 319.
URL `http://www.sciencedirect.com/science/article/pii/S0956566315301305`

Li, B.-R., Hsieh, Y.-J., Chen, Y.-X., Chung, Y.-T., Pan, C.-Y., & Chen, Y.-T. (2013a). An ultrasensitive nanowire-transistor biosensor for detecting dopamine release from living pc12 cells under hypoxic stimulation. *Journal of the American Chemical Society*, *135*(43), 16034–16037.

Li, H., Xie, H., Cao, Y., Ding, X., Yin, Y., & Li, G. (2013b). A general way to assay protein by coupling peptide with signal reporter via supermolecule formation. *Analytical chemistry*, *85*(2), 1047–1052.

Li, S.-S., Lin, C.-W., Wei, K.-C., Huang, C.-Y., Hsu, P.-H., Liu, H.-L., Lu, Y.-J., Lin, S.-C., Yang, H.-W., & Ma, C.-C. M. (2016). Non-invasive screening for early alzheimer's disease diagnosis by a sensitively immunomagnetic biosensor. *Scientific reports*, *6*(1), 1–11.

Li, X., Jiang, M., Cheng, J., Ye, M., Zhang, W., Jaffrezic-Renault, N., & Guo, Z. (2020). Signal multi-amplified electrochemical biosensor for voltammetric determination of tau-441 protein in biological samples using carbon nanomaterials and gold nanoparticles to hint dementia. *Microchimica Acta*, *187*, 1–8.

Liang, K. Y., Mintun, M. A., Fagan, A. M., Goate, A. M., Bugg, J. M., Holtzman, D. M., Morris, J. C., & Head, D. (2010). Exercise and alzheimer's disease biomarkers in cognitively normal older adults. *Annals of Neurology*, *68*(3), 311–318.
URL `https://onlinelibrary.wiley.com/doi/abs/10.1002/ana.22096`

Lien, T. T., Takamura, Y., Tamiya, E., & Mun'delanji, C. V. (2015). Modified screen printed electrode for development of a highly sensitive label-free impedimetric immunosensor to detect amyloid beta peptides. *Analytica chimica acta*, *892*, 69–76.

Lipiec, E., Perez-Guaita, D., Kaderli, J., Wood, B. R., & Zenobi, R. (2018). Direct nanospectroscopic verification of the amyloid aggregation pathway. *Angewandte Chemie*, *130*(28), 8655–8660.

Lippow, S. M., Wittrup, K. D., & Tidor, B. (2007). Computational design of antibody-affinity improvement beyond in vivo maturation. *Nature biotechnology*, *25*(10), 1171–1176.

Liu, L., He, Q., Zhao, F., Xia, N., Liu, H., Li, S., Liu, R., & Zhang, H. (2014). Competitive electrochemical immunoassay for detection of β-amyloid (1–42) and total β-amyloid peptides using p-aminophenol redox cycling. *Biosensors and bioelectronics*, *51*, 208–212.

Liu, T.-C., Lee, Y.-C., Ko, C.-Y., Liu, R.-S., Ke, C.-C., Lo, Y.-C., Hong, P.-S., Chu, C.-Y., Chang, C.-W., Wu, P.-W., et al. (2018). Highly sensitive/selective 3d nanostructured immunoparticle-based interface on a multichannel sensor array for detecting amyloid-beta in alzheimer's disease. *Theranostics*, *8*(15), 4210.

Liu, Y., He, G., Liu, H., Yin, H., Gao, F., Chen, J., Zhang, S., & Yang, B. (2020). Electrochemical immunosensor based on aubp@ pt nanostructure and aupd-pda nanozyme for ultrasensitive detection of apoe4. *RSC Advances*, *10*(13), 7912–7917.

Liu, Y., Xu, L.-P., Wang, S., Yang, W., Wen, Y., & Zhang, X. (2015). An ultrasensitive electrochemical immunosensor for apolipoprotein e4 based on fractal nanostructures and enzyme amplification. *Biosensors and bioelectronics*, *71*, 396–400.

Liu, Y., Yu, D., Zeng, C., Miao, Z., & Dai, L. (2010). Biocompatible graphene oxide-based glucose biosensors. *Langmuir*, *26*(9), 6158–6160.

Lonkar, S. P., Deshmukh, Y. S., & Abdala, A. A. (2015). Recent advances in chemical modifications of graphene. *Nano Research*, *8*(4), 1039–1074.

Lu, H., Wu, L., Wang, J., Wang, Z., Yi, X., Wang, J., & Wang, N. (2018). Voltammetric determination of the alzheimer's disease-related apoe 4 gene from unamplified genomic dna extracts by ferrocene-capped gold nanoparticles. *Microchimica Acta*, *185*(12), 549.

Lucchese, M. M., Stavale, F., Ferreira, E. M., Vilani, C., Moutinho, M. V. d. O., Capaz, R. B., Achete, C. A., & Jorio, A. (2010). Quantifying ion-induced defects and raman relaxation length in graphene. *Carbon*, *48*(5), 1592–1597.

Luna-Medina, R., Cortes-Canteli, M., Sanchez-Galiano, S., Morales-Garcia, J. A., Martinez, A., Santos, A., & Perez-Castillo, A. (2007). Np031112, a thiadiazolidinone compound, prevents inflammation and neurodegeneration under excitotoxic conditions: potential therapeutic role in brain disorders. *Journal of Neuroscience*, *27*(21), 5766–5776.

Ma, H., Han, X. X., & Zhao, B. (2020). Enhanced raman spectroscopic analysis of protein post-translational modifications. *TrAC Trends in Analytical Chemistry*, (p. 116019).

Maarouf, C. L., Kokjohn, T. A., Whiteside, C. M., Macias, M. P., Kalback, W. M., Sabbagh, M. N., Beach, T. G., Vassar, R., & Roher, A. E. (2013). Molecular differences and similarities between alzheimer's disease and the 5xfad transgenic mouse model of amyloidosis. *Biochemistry insights*, *6*, BCI–S13025.

Mabbott, G. A. (1983). An introduction to cyclic voltammetry. *Journal of Chemical education*, *60*(9), 697.

Macchia, E., Manoli, K., Di Franco, C., Scamarcio, G., & Torsi, L. (2020). New trends in single-molecule bioanalytical detection. *Analytical and Bioanalytical Chemistry*, (pp. 1–10).

Mahley, R. W. (1988). Apolipoprotein e: cholesterol transport protein with expanding role in cell biology. *Science*, *240*(4852), 622–630.

Malima, A., Siavoshi, S., Musacchio, T., Upponi, J., Yilmaz, C., Somu, S., Hartner, W., Torchilin, V., & Busnaina, A. (2012). Highly sensitive microscale in vivo sensor enabled by electrophoretic assembly of nanoparticles for multiple biomarker detection. *Lab on a Chip*, *12*(22), 4748–4754.

Mandelkow, E. (1999). The tangled tale of tau. *Nature*, *402*(6762), 588–589.

Mao, H. Y., Lu, Y. H., Lin, J. D., Zhong, S., Wee, A. T. S., & Chen, W. (2013). Manipulating the electronic and chemical properties of graphene via molecular functionalization. *Progress in Surface Science*, *88*(2), 132–159.

Mars, A., Hamami, M., Bechnak, L., Patra, D., & Raouafi, N. (2018a). Curcumin-graphene quantum dots for dual mode sensing platform: Electrochemical and fluorescence detection of apoe4, responsible of alzheimer's disease. *Analytica chimica acta*, *1036*, 141–146.

Mars, A., Hamami, M., Bechnak, L., Patra, D., & Raouafi, N. (2018b). Curcumin-graphene quantum dots for dual mode sensing platform: Electrochemical and fluorescence detection of apoe4, responsible of alzheimer's disease. *Analytica Chimica Acta*, *1036*, 141 – 146.
URL http://www.sciencedirect.com/science/article/pii/S0003267018308407

Martínez-Morillo, E., Hansson, O., Atagi, Y., Bu, G., Minthon, L., Diamandis, E. P., & Nielsen, H. M. (2014). Total apolipoprotein e levels and specific isoform composition in cerebrospinal fluid and plasma from alzheimer's disease patients and controls. *Acta neuropathologica*, *127*(5), 633–643.

Masson, J.-F. (2020). Consideration of sample matrix effects and "biological" noise in optimizing the limit of detection of biosensors.

Mattson, E. C., Pande, K., Unger, M., Cui, S., Lu, G., Gajdardziska-Josifovska, M., Weinert, M., Chen, J., & Hirschmugl, C. J. (2013). Exploring adsorption and reactivity of nh3 on reduced graphene oxide. *The Journal of Physical Chemistry C*, *117*(20), 10698–10707.

Mattsson, N., Andreasson, U., Persson, S., Carrillo, M. C., Collins, S., Chalbot, S., Cutler, N., Dufour-Rainfray, D., Fagan, A. M., Heegaard, N. H., et al. (2013). Csf biomarker variability in the alzheimer's association quality control program. *Alzheimer's & Dementia*, *9*(3), 251–261.

Mayeux, R., Saunders, A. M., Shea, S., Mirra, S., Evans, D., Roses, A. D., Hyman, B. T., Crain, B., Tang, M.-X., & Phelps, C. H. (1998). Utility of the apolipoprotein e genotype in the diagnosis of alzheimer's disease. *New England Journal of Medicine*, *338*(8), 506–511.

Mayeux, R., Tang, M.-X., Jacobs, D. M., Manly, J., Bell, K., Merchant, C., Small, S. A., Stern, Y., Wisniewski, H. M., & Mehta, P. D. (1999). Plasma amyloid β-peptide 1–42 and incipient alzheimer's disease. *Annals of Neurology*, *46*(3), 412–416.
URL https://onlinelibrary.wiley.com/doi/abs/10.1002/1531-8249%28199909%2946%3A3%3C412%3A%3AAID-ANA19%3E3.0.CO%3B2-A

McGregor, H. C., Wang, W., Short, M. A., & Zeng, H. (2016). Clinical utility of raman spectroscopy: current applications and ongoing developments. *Adv. Health Care Technol.*, *2*, 13–29.

Medina-Sánchez, M., Miserere, S., Morales-Narváez, E., & Merkoçi, A. (2014). On-chip magneto-immunoassay for alzheimer's biomarker electrochemical detection by using quantum dots as labels. *Biosensors and Bioelectronics*, *54*, 279 – 284.
URL http://www.sciencedirect.com/science/article/pii/S0956566313007719

Mehta, P. D., Pirttilä, T., Mehta, S. P., Sersen, E. A., Aisen, P. S., & Wisniewski, H. M. (2000). Plasma and cerebrospinal fluid levels of amyloid β proteins 1-40 and 1-42 in alzheimer disease. *Archives of neurology*, *57*(1), 100–105.

Milella, F., & Mazzotti, M. (2019). Estimating speciation of aqueous ammonia solutions of ammonium bicarbonate: application of least squares methods to infrared spectra. *Reaction Chemistry & Engineering*, *4*(7), 1284–1302.

Mobed, A., & Hasanzadeh, M. (2020). Biosensing: The best alternative for conventional methods in detection of alzheimer's disease biomarkers. *International Journal of Biological Macromolecules*, *161*, 59 – 71.
URL http://www.sciencedirect.com/science/article/pii/S0141813020334243

Mokdad, A. H., Ballestros, K., Echko, M., Glenn, S., Olsen, H. E., Mullany, E., Lee, A., Khan, A. R., Ahmadi, A., Ferrari, A. J., et al. (2018). The state of us health, 1990-2016: burden of diseases, injuries, and risk factors among us states. *Jama*, *319*(14), 1444–1472.

Morales-Narváez, E., Baptista-Pires, L., Zamora-Gálvez, A., & Merkoçi, A. (2017). Graphene-based biosensors: Going simple. *Advanced Materials*, *29*(7), 1604905.
URL https://onlinelibrary.wiley.com/doi/abs/10.1002/adma.201604905

Moreira, F. T., Rodriguez, B. A., Dutra, R. A., & Sales, M. G. F. (2018). Redox probe-free readings of a β-amyloid-42 plastic antibody sensory material assembled on copper@ carbon nanotubes. *Sensors and Actuators B: Chemical*, *264*, 1–9.

Moreira, F. T., & Sales, M. G. F. (2017). Smart naturally plastic antibody based on poly (α-cyclodextrin) polymer for β-amyloid-42 soluble oligomer detection. *Sensors and Actuators B: Chemical*, *240*, 229–238.

Morris, J. C., Roe, C. M., Xiong, C., Fagan, A. M., Goate, A. M., Holtzman, D. M., & Mintun, M. A. (2010). Apoe predicts amyloid-beta but not tau alzheimer pathology in cognitively normal aging. *Annals of neurology*, *67*(1), 122–131.

Mosier-Boss, P. A. (2017). Review of sers substrates for chemical sensing. *Nanomaterials*, *7*(6), 142.

Mu, X., Wu, X., Zhang, T., Go, D. B., & Luo, T. (2014). Thermal transport in graphene oxide–from ballistic extreme to amorphous limit. *Scientific reports*, *4*(1), 1–9.

Murphy, M. P., & LeVine, H. (2010). Alzheimer's Disease and the Amyloid-β Peptide. *Journal of Alzheimer's Disease*, *19*(1), 311–323.
URL `https://www.medra.org/servlet/aliasResolver?alias=iospress&doi=10.3233/JAD-2010-1221`

Nakamura, A., Kaneko, N., Villemagne, V. L., Kato, T., Doecke, J., Doré, V., Fowler, C., Li, Q.-X., Martins, R., Rowe, C., et al. (2018). High performance plasma amyloid-β biomarkers for alzheimer's disease. *Nature*, *554*(7691), 249–254.

Nanotechnologies, I. (2015). vocabulary–part 1: Core terms. *International Stanardisation Organisation (ISO), Technical Specification ISO/TS*, (pp. 80004–1).

Nath, J., Chowdhury, A., & Dolui, S. K. (2018). Chitosan/graphene oxide-based multifunctional ph-responsive hydrogel with significant mechanical strength, self-healing property, and shape memory effect. *Advances in Polymer Technology*, *37*(8), 3665–3679.

Negahdary, M., & Heli, H. (2019a). An electrochemical peptide-based biosensor for the alzheimer biomarker amyloid-β (1–42) using a microporous gold nanostructure. *Microchimica Acta*, *186*(12), 766.

Negahdary, M., & Heli, H. (2019b). An ultrasensitive electrochemical aptasensor for early diagnosis of alzheimer's disease, using a fern leaves-like gold nanostructure. *Talanta*, *198*, 510–517.

Nicholson, R. S. (1965). Theory and application of cyclic voltammetry for measurement of electrode reaction kinetics. *Analytical chemistry*, *37*(11), 1351–1355.

Niemantsverdriet, E., Valckx, S., Bjerke, M., & Engelborghs, S. (2017). Alzheimer's disease csf biomarkers: Clinical indications and rational use. *Acta Neurologica Belgica*, *117*(3), 591–602.

Nikhil, B., Pawan, J., Nello, F., & Pedro, E. (2016). Introduction to biosensors. *Essays in Biochemistry*, *60*(1), 1–8.

Nimse, S. B., Sonawane, M. D., Song, K.-S., & Kim, T. (2016). Biomarker detection technologies and future directions. *Analyst*, *141*(3), 740–755.

Niyogi, S., Bekyarova, E., Itkis, M. E., Zhang, H., Shepperd, K., Hicks, J., Sprinkle, M., Berger, C., Lau, C. N., Deheer, W. A., et al. (2010). Spectroscopy of covalently functionalized graphene. *Nano letters*, *10*(10), 4061–4066.

Njagi, J. I., & Kagwanja, S. M. (2011). The interface in biosensing: improving selectivity and sensitivity. In *Interfaces and Interphases in Analytical Chemistry*, (pp. 225–247). ACS Publications.

Noh, I. (2018). *Biomimetic medical materials: from nanotechnology to 3D bioprinting*, vol. 1064. Springer.

Novoselov, K., Geim, A., Morozov, S., Dubonos, S., Zhang, Y., & Jiang, D. (2004a). Room-temperature electric field effect and carrier-type inversion in graphene films. *arXiv preprint cond-mat/0410631*.

Novoselov, K. S., Geim, A. K., Morozov, S. V., Jiang, D., Zhang, Y., Dubonos, S. V., Grigorieva, I. V., & Firsov, A. A. (2004b). Electric field effect in atomically thin carbon films. *science*, *306*(5696), 666–669.

O'Bryant, S. E., Johnson, L., Edwards, M., Soares, H., Devous, M. D., Ross, S., Rohlfing, G., Hall, J., Consortium, T. A. R. . C., et al. (2013). The link between c-reactive protein and alzheimer's disease among mexican americans. *Journal of Alzheimer's Disease*, *34*(3), 701–706.

O'Bryant, S. E., Mielke, M. M., Rissman, R. A., Lista, S., Vanderstichele, H., Zetterberg, H., Lewczuk, P., Posner, H., Hall, J., Johnson, L., et al. (2017). Blood-based biomarkers in alzheimer disease: current state of the science and a novel collaborative paradigm for advancing from discovery to clinic. *Alzheimer's & Dementia*, *13*(1), 45–58.

O'Bryant, S. E., Waring, S. C., Hobson, V., Hall, J. R., Moore, C. B., Bottiglieri, T., Massman, P., & Diaz-Arrastia, R. (2010). Decreased c-reactive protein levels in alzheimer disease. *Journal of geriatric psychiatry and neurology*, *23*(1), 49–53.

Oda, T., Wals, P., Osterburg, H. H., Johnson, S. A., Pasinetti, G. M., Morgan, T. E., Rozovsky, I., Stine, W. B., Snyder, S. W., Holzman, T. F., et al. (1995). Clusterin (apoj) alters the aggregation of amyloid β-peptide (aβ1-42) and forms slowly sedimenting aβ complexes that cause oxidative stress. *Experimental neurology*, *136*(1), 22–31.

Ogawa, S., Lee, T.-M., Kay, A. R., & Tank, D. W. (1990). Brain magnetic resonance imaging with contrast dependent on blood oxygenation. *proceedings of the National Academy of Sciences*, *87*(24), 9868–9872.

Oh, S.-B., Kim, M. S., Park, S., Son, H., Kim, S.-Y., Kim, M.-S., Jo, D.-G., Tak, E., & Lee, J.-Y. (2019). Clusterin contributes to early stage of alzheimer's disease pathogenesis. *Brain Pathology*, *29*(2), 217–231.

Ohyoshi, E., Hamada, Y., Nakata, K., & Kohata, S. (1999). The interaction between human and bovine serum albumin and zinc studied by a competitive spectrophotometry. *Journal of inorganic biochemistry*, *75*(3), 213–218.

Ortseifen, V., Viefhues, M., Wobbe, L., & Grünberger, A. (2020). Microfluidics for biotechnology: bridging gaps to foster microfluidic applications. *Frontiers in Bioengineering and Biotechnology*, *8*, 1324.

Özcan, N., Medetalibeyoglu, H., Akyıldırım, O., Atar, N., & Yola, M. L. (2020). Electrochemical detection of amyloid-β protein by delaminated titanium carbide mxene/multi-walled carbon nanotubes composite with molecularly imprinted polymer. *Materials Today Communications*, (p. 101097).

O'Connell, G. C., Alder, M. L., Smothers, C. G., Still, C. H., Webel, A. R., & Moore, S. M. (2020). Use of high-sensitivity digital elisa improves the diagnostic performance of circulating brain-specific proteins for detection of traumatic brain injury during triage. *Neurological research*, *42*(4), 346–353.

Palmqvist, S., Janelidze, S., Quiroz, Y. T., Zetterberg, H., Lopera, F., Stomrud, E., Su, Y., Chen, Y., Serrano, G. E., Leuzy, A., Mattsson-Carlgren, N., Strandberg, O., Smith, R., Villegas, A., Sepulveda-Falla, D., Chai, X., Proctor, N. K., Beach, T. G., Blennow, K., Dage, J. L., Reiman, E. M., & Hansson, O. (2020). Discriminative Accuracy of Plasma Phospho-tau217 for Alzheimer Disease vs Other Neurodegenerative Disorders. *JAMA*, *324*(8), 772–781.
URL `https://doi.org/10.1001/jama.2020.12134`

Panchaud, A., Hansson, J., Affolter, M., Rhlid, R. B., Piu, S., Moreillon, P., & Kussmann, M. (2008). Anibal, stable isotope-based quantitative proteomics by aniline and benzoic acid labeling of amino and carboxylic groups. *Molecular & Cellular Proteomics*, *7*(4), 800–812.

Panraksa, Y., Siangproh, W., Khampieng, T., Chailapakul, O., & Apilux, A. (2018). Paper-based amperometric sensor for determination of acetylcholinesterase using screen-printed graphene electrode. *Talanta*, *178*, 1017–1023.

Park, S., & Kim, Y. (2021). Bias-generating factors in biofluid amyloid-β measurements for alzheimer's disease diagnosis. *Biomedical Engineering Letters*, *11*(4), 287–295.

Patel, S., Shah, R. J., Coleman, P., & Sabbagh, M. (2011). Potential peripheral biomarkers for the diagnosis of alzheimer's disease. *International Journal of Alzheimer's Disease*, *2011*.

Peres, N. (2009). The transport properties of graphene. *Journal of Physics: Condensed Matter*, *21*(32), 323201.

Petit, C., Seredych, M., & Bandosz, T. J. (2009). Revisiting the chemistry of graphite oxides and its effect on ammonia adsorption. *Journal of Materials Chemistry*, *19*(48), 9176–9185.

Petry, F. R., Pelletier, J., Bretteville, A., Morin, F., Calon, F., Hébert, S. S., Whittington, R. A., & Planel, E. (2014). Specificity of anti-tau antibodies when analyzing mice models of alzheimer's disease: problems and solutions. *PloS one*, *9*(5), e94251.

Peveler, W. J., Yazdani, M., & Rotello, V. M. (2016). Selectivity and specificity: pros and cons in sensing. *ACS sensors*, *1*(11), 1282–1285.

Ping, J., Vishnubhotla, R., Vrudhula, A., & Johnson, A. C. (2016). Scalable production of high-sensitivity, label-free dna biosensors based on back-gated graphene field effect transistors. *ACS nano*, *10*(9), 8700–8704.

Poon, S., Rybchyn, M. S., Easterbrook-Smith, S. B., Carver, J. A., Pankhurst, G. J., & Wilson, M. R. (2002). Mildly acidic ph activates the extracellular molecular chaperone clusterin. *Journal of Biological Chemistry*, *277*(42), 39532–39540.

Pottathara, Y. B., Thomas, S., Kalarikkal, N., Grohens, Y., & Kokol, V. (2019). *Nanomaterials Synthesis: Design, Fabrication and Applications*. Elsevier.

Prabhulkar, S., Piatyszek, R., Cirrito, J. R., Wu, Z.-Z., & Li, C.-Z. (2012). Microbiosensor for alzheimer's disease diagnostics: detection of amyloid beta biomarkers. *Journal of Neurochemistry*, *122*(2), 374–381.
URL `https://onlinelibrary.wiley.com/doi/abs/10.1111/j.1471-4159.2012.07709.x`

Preibisch, S., Saalfeld, S., & Tomancak, P. (2009). Globally optimal stitching of tiled 3d microscopic image acquisitions. *Bioinformatics*, *25*(11), 1463–1465.

Puiu, M., Idili, A., Moscone, D., Ricci, F., & Bala, C. (2014). A modular electrochemical peptide-based sensor for antibody detection. *Chemical Communications*, *50*(64), 8962–8965.

Pumera, M. (2009). Electrochemistry of graphene: new horizons for sensing and energy storage. *The Chemical Record*, *9*(4), 211–223.

Pumera, M. (2011). Graphene in biosensing. *Materials today*, *14*(7-8), 308–315.

Pumera, M., Sanchez, S., Ichinose, I., & Tang, J. (2007). Electrochemical nanobiosensors. *Sensors and Actuators B: Chemical*, *123*(2), 1195–1205.

Purohit, B., Vernekar, P. R., Shetti, N. P., & Chandra, P. (2020). Biosensor nanoengineering: Design, operation, and implementation for biomolecular analysis. *Sensors International*, (p. 100040).

Qin, J., Cho, M., & Lee, Y. (2019a). Ferrocene-encapsulated zn zeolitic imidazole framework (zif-8) for optical and electrochemical sensing of amyloid-β oligomers and for the early diagnosis of alzheimer's disease. *ACS applied materials & interfaces*, *11*(12), 11743–11748.

Qin, J., Cho, M., & Lee, Y. (2019b). Ultrasensitive detection of amyloid-β using cellular prion protein on the highly conductive au nanoparticles–poly (3, 4-ethylene dioxythiophene)–poly (thiophene-3-acetic acid) composite electrode. *Analytical chemistry*, *91*(17), 11259–11265.

Rama, E. C., González-García, M. B., & Costa-Garcia, A. (2014). Competitive electrochemical immunosensor for amyloid-beta 1-42 detection based on gold nanostructurated screen-printed carbon electrodes. *Sensors and Actuators B: Chemical*, *201*, 567–571.

Ramos-Vara, J. (2005). Technical aspects of immunohistochemistry. *Veterinary pathology*, *42*(4), 405–426.

Randall, J., Mörtberg, E., Provuncher, G. K., Fournier, D. R., Duffy, D. C., Rubertsson, S., Blennow, K., Zetterberg, H., & Wilson, D. H. (2013). Tau proteins in serum predict neurological outcome after hypoxic brain injury from cardiac arrest: results of a pilot study. *Resuscitation*, *84*(3), 351–356.

Rapp, B. E., Gruhl, F. J., & Länge, K. (2010). Biosensors with label-free detection designed for diagnostic applications. *Analytical and bioanalytical chemistry*, *398*(6), 2403–2412.

Razzino, C. A., Serafín, V., Gamella, M., Pedrero, M., Montero-Calle, A., Barderas, R., Calero, M., Lobo, A. O., Yáñez-Sedeño, P., Campuzano, S., et al. (2020). An electrochemical immunosensor using gold nanoparticles-pamam-nanostructured screen-printed carbon electrodes for tau protein determination in plasma and brain tissues from alzheimer patients. *Biosensors and Bioelectronics*, (p. 112238).

Reina, G., González-Domínguez, J. M., Criado, A., Vázquez, E., Bianco, A., & Prato, M. (2017). Promises, facts and challenges for graphene in biomedical applications. *Chemical Society Reviews*, *46*(15), 4400–4416.

Rifkin, S. C., & Evans, D. H. (1976). Analytical evaluation of differential pulse voltammetry at stationary electrodes using computer-based instrumentation. *Analytical Chemistry*, *48*(14), 2174–2179.

Rissin, D. M., Kan, C. W., Campbell, T. G., Howes, S. C., Fournier, D. R., Song, L., Piech, T., Patel, P. P., Chang, L., Rivnak, A. J., et al. (2010). Single-molecule enzyme-linked immunosorbent assay detects serum proteins at subfemtomolar concentrations. *Nature biotechnology*, *28*(6), 595–599.

Rivas, L., de la Escosura-Muñiz, A., Pons, J., & Merkoçi, A. (2014). Alzheimer disease biomarker detection through electrocatalytic water oxidation induced by iridium oxide nanoparticles. *Electroanalysis*, *26*(6), 1287–1294.

Rivera, L., Betancur, A., Zarate, D., Torres, D. T., Hoyos, L., & Garcia, A. (2019). Reduction and simultaneous doping of graphene oxide to repel ldl in treatment of atherosclerosis disease. *arXiv preprint arXiv:1902.01850*.

Rivnay, J., Inal, S., Salleo, A., Owens, R. M., Berggren, M., & Malliaras, G. G. (2018). Organic electrochemical transistors. *Nature Reviews Materials*, *3*(2), 1–14.

Ronald, T., on Aging Working Group, N. I., et al. (1998). Consensus report of the working group on:"molecular and biochemical markers of alzheimer's disease". *Neurobiology of Aging*, *19*(2), 109–116.

Ronkainen, N. J., Halsall, H. B., & Heineman, W. R. (2010). Electrochemical biosensors. *Chem. Soc. Rev.*, *39*, 1747–1763.
URL http://dx.doi.org/10.1039/B714449K

Sakamoto, S., Putalun, W., Vimolmangkang, S., Phoolcharoen, W., Shoyama, Y., Tanaka, H., & Morimoto, S. (2018). Enzyme-linked immunosorbent assay for the quantitative/qualitative analysis of plant secondary metabolites. *Journal of natural medicines*, *72*(1), 32–42.

Saltzgaber, G., Wojcik, P. M., Sharf, T., Leyden, M. R., Wardini, J. L., Heist, C. A., Adenuga, A. A., Remcho, V. T., & Minot, E. D. (2013). Scalable graphene field-effect sensors for specific protein detection. *Nanotechnology*, *24*(35), 355502.

Santin, M. D., Vandenberghe, M. E., Herard, A.-S., Pradier, L., Cohen, C., Debeir, T., Delzescaux, T., Rooney, T., & Dhenain, M. (2016). In vivo detection of amyloid plaques by gadolinium-stained mri can be used to demonstrate the efficacy of an anti-amyloid immunotherapy. *Frontiers in Aging Neuroscience*, *8*, 55.
URL https://www.frontiersin.org/article/10.3389/fnagi.2016.00055

Scheller, F., & Schubert, F. (1991). *Biosensors*. Elsevier.

Schipper, H. M., Maes, O. C., Chertkow, H. M., & Wang, E. (2007). Microrna expression in alzheimer blood mononuclear cells. *Gene regulation and systems biology*, *1*, GRSB–S361.

Scholz, F. (2015). Voltammetric techniques of analysis: the essentials. *ChemTexts*, *1*(4), 17.

Schrader, B. (2008). *Infrared and Raman spectroscopy: methods and applications*. John Wiley & Sons.

Scott, K. (2016). Electrochemical principles and characterization of bioelectrochemical systems. In *Microbial Electrochemical and Fuel Cells*, (pp. 29–66). Elsevier.

Sethi, J., Suhail, A., Safarzadeh, M., Sattar, A., Wei, Y., & Pan, G. (2021). Nh2 linker for femtomolar label-free detection with reduced graphene oxide screen-printed electrodes. *Carbon*, *179*, 514–522.

Sethi, J., Van Bulck, M., Suhail, A., Safarzadeh, M., Perez-Castillo, A., & Pan, G. (2020). A label-free biosensor based on graphene and reduced graphene oxide dual-layer for electrochemical determination of beta-amyloid biomarkers. *Microchimica Acta*, *187*, 1–10.

Shahdeo, D., Roberts, A., Abbineni, N., & Gandhi, S. (2020). Graphene based sensors. *Comprehensive Analytical Chemistry*, *91*, 175.

Shameer, P. M., & Nishath, P. M. (2019). Exploration and enhancement on fuel stability of biodiesel: A step forward in the track of global commercialization. In *Advanced Biofuels*, (pp. 181–213). Elsevier.

Shanthi, K. B., Krishnan, S., & Rani, P. (2015). A systematic review and meta-analysis of plasma amyloid 1-42 and tau as biomarkers for alzheimer's disease. *SAGE open medicine*, *3*, 2050312115598250.

Shao, Y., Wang, J., Wu, H., Liu, J., Aksay, I. A., & Lin, Y. (2010). Graphene based electrochemical sensors and biosensors: a review. *Electroanalysis: An International Journal Devoted to Fundamental and Practical Aspects of Electroanalysis*, *22*(10), 1027–1036.

Sharma, N., & Singh, A. N. (2016). Exploring biomarkers for alzheimer's disease. *Journal of clinical and diagnostic research: JCDR*, *10*(7), KE01.

Sharma, S., Byrne, H., & O'Kennedy, R. J. (2016). Antibodies and antibody-derived analytical biosensors. *Essays in biochemistry*, *60*(1), 9–18.

Shazali, S. S., Amiri, A., Zubir, M. N. M., Rozali, S., Zabri, M. Z., & Sabri, M. F. M. (2018). Facile hydrothermal method for synthesizing nitrogen-doped graphene nanoplatelets using aqueous ammonia: dispersion, stability in solvents and thermophysical performances. *Materials Research Express*, *5*(3), 035042.

Shen, W., Li, S., Park, M.-K., Zhang, Z., Cheng, Z., Petrenko, V. A., & Chin, B. A. (2012). Blocking agent optimization for nonspecific binding on phage based magnetoelastic biosensors. *Journal of The Electrochemical Society*, *159*(10), B818.

Shi, J., Li, X., Yang, T., Tian, X., Liu, Y., Lei, S., Song, Y., & Liu, Z. (2021). Co 3 o 4 porous nanorod/n-doped reduced graphene oxide composite with fast pseudocapacitive lithium storage for high-performance lithium-ion capacitors. *Journal of Materials Science*, *56*(12), 7520–7532.

Shi, Y., Yamada, K., Liddelow, S. A., Smith, S. T., Zhao, L., Luo, W., Tsai, R. M., Spina, S., Grinberg, L. T., Rojas, J. C., et al. (2017). Apoe4 markedly exacerbates tau-mediated neurodegeneration in a mouse model of tauopathy. *Nature*, *549*(7673), 523–527.

Shoji, M., Golde, T. E., Ghiso, J., Cheung, T. T., Estus, S., Shaffer, L. M., Cai, X.-D., McKay, D. M., Tintner, R., Frangione, B., et al. (1992). Production of the alzheimer amyloid beta protein by normal proteolytic processing. *Science*, *258*(5079), 126–129.

Shui, B., Tao, D., Florea, A., Cheng, J., Zhao, Q., Gu, Y., Li, W., Jaffrezic-Renault, N., Mei, Y., & Guo, Z. (2018). Biosensors for alzheimer's disease biomarker detection: A review. *Biochimie*, *147*, 13 – 24.
URL `http://www.sciencedirect.com/science/article/pii/S0300908418300014`

Simões, F., & Xavier, M. (2017). 6 - electrochemical sensors. In A. L. Da Róz, M. Ferreira, F. de Lima Leite, & O. N. Oliveira (Eds.) *Nanoscience and its Applications*, Micro and Nano Technologies, (pp. 155 – 178). William Andrew Publishing.
URL `http://www.sciencedirect.com/science/article/pii/B9780323497800000065`

Sin, M. L., Mach, K. E., Wong, P. K., & Liao, J. C. (2014). Advances and challenges in biosensor-based diagnosis of infectious diseases. *Expert review of molecular diagnostics*, *14*(2), 225–244.

Singal, S., Srivastava, A. K., Dhakate, S., Biradar, A. M., et al. (2015). Electroactive graphene-multi-walled carbon nanotube hybrid supported impedimetric immunosensor for the detection of human cardiac troponin-i. *RSC advances*, *5*(92), 74994–75003.

Sinitskii, A., Dimiev, A., Corley, D. A., Fursina, A. A., Kosynkin, D. V., & Tour, J. M. (2010). Kinetics of diazonium functionalization of chemically converted graphene nanoribbons. *Acs Nano*, *4*(4), 1949–1954.

Sjöbring, U., Björck, L., & Kastern, W. (1991). Streptococcal protein g. gene structure and protein binding properties. *Journal of biological chemistry*, *266*(1), 399–405.

Sjögren, M., Rosengren, L., Minthon, L., Davidsson, P., Blennow, K., & Wallin, A. (2000). Cytoskeleton proteins in csf distinguish frontotemporal dementia from ad. *Neurology*, *54*(10), 1960–1964.

Smith, G. S., Walter, G. L., & Walker, R. M. (2013). Clinical pathology in non-clinical toxicology testing. In *Haschek and Rousseaux's Handbook of Toxicologic Pathology*, (pp. 565–594). Elsevier.

Sobon, G., Sotor, J., Jagiello, J., Kozinski, R., Zdrojek, M., Holdynski, M., Paletko, P., Boguslawski, J., Lipinska, L., & Abramski, K. M. (2012). Graphene oxide vs. reduced graphene oxide as saturable absorbers for er-doped passively mode-locked fiber laser. *Optics express*, *20*(17), 19463–19473.

Sohn, Y.-S., & Lee, Y. K. (2014). Site-directed immobilization of antibody using edc-nhs-activated protein a on a bimetallic-based surface plasmon resonance chip. *Journal of biomedical optics*, *19*(5), 051209.

Souza, B., Moreira, A., & Teixeira, A. (2009). Tg-ftir coupling to monitor the pyrolysis products from agricultural residues. *Journal of thermal analysis and calorimetry*, *97*(2), 637–642.

Sparks, D. L., Kryscio, R. J., Sabbagh, M. N., Ziolkowski, C., Lin, Y., Sparks, L. M., Liebsack, C., & Johnson-Traver, S. (2012). Tau is reduced in ad plasma and validation of employed elisa methods. *American journal of neurodegenerative disease*, *1*(1), 99.

Sperling, R. A., Aisen, P. S., Beckett, L. A., Bennett, D. A., Craft, S., Fagan, A. M., Iwatsubo, T., Jack Jr., C. R., Kaye, J., Montine, T. J., Park, D. C., Reiman, E. M., Rowe, C. C., Siemers, E., Stern, Y., Yaffe, K., Carrillo, M. C., Thies, B., Morrison-Bogorad, M., Wagster, M. V., & Phelps, C. H. (2011). Toward defining the preclinical stages of alzheimer's disease: Recommendations from the national institute on aging-alzheimer's association workgroups on diagnostic guidelines for alzheimer's disease. *Alzheimer's & Dementia*, *7*(3), 280–292.
URL `https://alz-journals.onlinelibrary.wiley.com/doi/abs/10.1016/j.jalz.2011.03.003`

Špringer, T., Hemmerová, E., Finocchiaro, G., Krištofiková, Z., Vyhnálek, M., & Homola, J. (2020). Surface plasmon resonance biosensor for the detection of tau-amyloid β complex. *Sensors and Actuators B: Chemical*, *316*, 128146.

Stanga, S., Lanni, C., Govoni, S., Uberti, D., D'Orazi, G., & Racchi, M. (2010). Unfolded p53 in the pathogenesis of alzheimer's disease: is hipk2 the link? *Aging (Albany NY)*, *2*(9), 545.

Steinacker, P., Semler, E., Anderl-Straub, S., Diehl-Schmid, J., Schroeter, M. L., Uttner, I., Foerstl, H., Landwehrmeyer, B., von Arnim, C. A., Kassubek, J., et al. (2017). Neurofilament as a blood marker for diagnosis and monitoring of primary progressive aphasias. *Neurology*, *88*(10), 961–969.

Su, H., Li, S., & Kerman, K. (2019). Novel thiolated-peg linker molecule for biosensor development on gold surfaces. *Biosensors and Bioelectronics*, *141*, 111477.

Su, Q., Pang, S., Alijani, V., Li, C., Feng, X., & Müllen, K. (2009). Composites of graphene with large aromatic molecules. *Advanced materials*, *21*(31), 3191–3195.

Su, Z., Wang, H., Tian, K., Xu, F., Huang, W., & Tian, X. (2016). Simultaneous reduction and surface functionalization of graphene oxide with wrinkled structure by diethylenetriamine (deta) and their reinforcing effects in the flexible poly (2-ethylhexyl acrylate)(p2eha) films. *Composites Part A: Applied Science and Manufacturing*, *84*, 64–75.

Suhail, A., Pan, G., Jenkins, D., & Islam, K. (2018). Improved efficiency of graphene/si schottky junction solar cell based on back contact structure and duv treatment. *Carbon*, *129*, 520–526.

Sun, L., Hu, N., Peng, J., Chen, L., & Weng, J. (2014). Ultrasensitive detection of mitochondrial dna mutation by graphene oxide/dna hydrogel electrode. *Advanced Functional Materials*, *24*(44), 6905–6913.

Sun, L., Zhong, Y., Gui, J., Wang, X., Zhuang, X., & Weng, J. (2018). A hydrogel biosensor for high selective and sensitive detection of amyloid-beta oligomers. *International journal of nanomedicine*, *13*, 843.

Sunderland, T., Linker, G., Mirza, N., Putnam, K. T., Friedman, D. L., Kimmel, L. H., Bergeson, J., Manetti, G. J., Zimmermann, M., Tang, B., et al. (2003). Decreased β-amyloid1-42 and increased tau levels in cerebrospinal fluid of patients with alzheimer disease. *Jama*, *289*(16), 2094–2103.

Sunderland, T., Mirza, N., Putnam, K. T., Linker, G., Bhupali, D., Durham, R., Soares, H., Kimmel, L., Friedman, D., Bergeson, J., et al. (2004). Cerebrospinal fluid β-amyloid1–42 and tau in control subjects at risk for alzheimer's disease: The effect of apoe ε4 allele. *Biological psychiatry*, *56*(9), 670–676.

Suvarnaphaet, P., & Pechprasarn, S. (2017). Graphene-based materials for biosensors: a review. *Sensors*, *17*(10), 2161.

Syedmoradi, L., Daneshpour, M., Alvandipour, M., Gomez, F. A., Hajghassem, H., & Omidfar, K. (2017). Point of care testing: The impact of nanotechnology. *Biosensors and Bioelectronics*, *87*, 373–387.

Tadyszak, K., Wychowaniec, J. K., & Litowczenko, J. (2018). Biomedical applications of graphene-based structures. *Nanomaterials*, *8*(11), 944.

Taleat, Z., Khoshroo, A., & Mazloum-Ardakani, M. (2014). Screen-printed electrodes for biosensing: a review (2008–2013). *Microchimica Acta*, *181*(9-10), 865–891.

Tang, S., & Cao, Z. (2012). Adsorption and dissociation of ammonia on graphene oxides: a first-principles study. *The Journal of Physical Chemistry C*, *116*(15), 8778–8791.

Tanzi, R. E., Kovacs, D. M., Kim, T.-W., Moir, R. D., Guenette, S. Y., & Wasco, W. (1996). The gene defects responsible for familial alzheimer's disease. *Neurobiology of disease*, *3*(3), 159.

Tao, D., Shui, B., Gu, Y., Cheng, J., Zhang, W., Jaffrezic-Renault, N., Song, S., & Guo, Z. (2019). Development of a label-free electrochemical aptasensor for the detection of tau381 and its preliminary application in ad and non-ad patients' sera. *Biosensors*, *9*(3), 84.

Tehrani, Z., Abbasi, H. Y., Devadoss, A., Evans, J. E., & Guy, O. J. (2021). Assessing surface coverage of aminophenyl bonding sites on diazotised glassy carbon electrodes for optimised electrochemical biosensor performance. *Nanomaterials*, *11*(2), 416.

Tehrani, Z., Burwell, G., Azmi, M. M., Castaing, A., Rickman, R., Almarashi, J., Dunstan, P., Beigi, A. M., Doak, S., & Guy, O. (2014). Generic epitaxial graphene biosensors for ultrasensitive detection of cancer risk biomarker. *2D Materials*, *1*(2), 025004.

Teixeira, S., Burwell, G., Castaing, A., Gonzalez, D., Conlan, R., & Guy, O. (2014). Epitaxial graphene immunosensor for human chorionic gonadotropin. *Sensors and Actuators B: Chemical*, *190*, 723–729.

Thévenot, D. R., Toth, K., Durst, R. A., & Wilson, G. S. (2001). Electrochemical biosensors: recommended definitions and classification. *Biosensors and bioelectronics*, *16*(1-2), 121–131.

Titus, D., Samuel, E. J. J., & Roopan, S. M. (2019). Nanoparticle characterization techniques. In *Green Synthesis, Characterization and Applications of Nanoparticles*, (pp. 303–319). Elsevier.

Tobias, R. S. (1967). Raman spectroscopy in inorganic chemistry. *Journal of Chemical Education*, *44*(2), 70.

Toppi, A., Busk, L. L., Hu, H., Dogan, A. A., Jönsson, A., Taboryski, R. J., & Dufva, M. (2021). Photolithographic patterning of fluoracryl for biphilic microwell-based digital bioassays and selection of bacteria. *ACS Applied Materials & Interfaces*.

Tothill, I. E. (2009). Biosensors for cancer markers diagnosis. *Seminars in Cell & Developmental Biology*, *20*(1), 55 – 62. A Special Edition on Biosensors and Development of Pigment Cells and Pigment Patterns.
URL `http://www.sciencedirect.com/science/article/pii/S1084952109000196`

Toyos-Rodríguez, C., García-Alonso, F. J., & de la Escosura-Muñiz, A. (2020). Electrochemical biosensors based on nanomaterials for early detection of alzheimer's disease. *Sensors*, *20*(17), 4748.

Trevethan, R. (2017). Sensitivity, specificity, and predictive values: foundations, pliabilities, and pitfalls in research and practice. *Frontiers in public health*, *5*, 307.

Trnkova, e., Studničková, M., & Paleček, E. (1980). 360-electrochemical behaviour of guanine and its derivatives. i. fast cyclic voltammetry of guanosine and calf thymus dna. *Bioelectrochemistry and Bioenergetics*, *7*(4), 643–658.

Utermann, G., Langenbeck, U., Beisiegel, U., & Weber, W. (1980). Genetics of the apolipoprotein e-system in man. *American journal of human genetics*, *32*(3), 339.

Van Geel, W., Rosengren, L., & Verbeek, M. (2005). An enzyme immunoassay to quantify neurofilament light chain in cerebrospinal fluid. *Journal of immunological methods*, *296*(1-2), 179–185.

Veluswamy, P., Sathiyamoorthy, S., Santhoshkumar, P., Karunakaran, G., Lee, C. W., Kuznetsov, D., Kadarkaraithangam, J., & Ikeda, H. (2018). Sono-synthesis approach of reduced graphene oxide for ammonia vapour detection at room temperature. *Ultrasonics sonochemistry*, *48*, 555–566.

Verwey, N. A., Veerhuis, R., Twaalfhoven, H. A., Wouters, D., Hoozemans, J. J., Bollen, Y. J., Killestein, J., Bibl, M., Wiltfang, J., Hack, C. E., et al. (2009). Quantification of amyloid-beta 40 in cerebrospinal fluid. *Journal of immunological methods*, *348*(1-2), 57–66.

Vestergaard, M., Kerman, K., Kim, D.-K., Hiep, H. M., & Tamiya, E. (2008). Detection of alzheimer's tau protein using localised surface plasmon resonance-based immunochip. *Talanta*, *74*(4), 1038–1042.

Vikesland, P. J., & Wigginton, K. R. (2010). Nanomaterial enabled biosensors for pathogen monitoring-a review. *Environmental science & technology*, *44*(10), 3656–3669.

Walcarius, A., Minteer, S. D., Wang, J., Lin, Y., & Merkoçi, A. (2013). Nanomaterials for bio-functionalized electrodes: recent trends. *Journal of Materials Chemistry B*, *1*(38), 4878–4908.

Wang, B., Luo, B., Liang, M., Wang, A., Wang, J., Fang, Y., Chang, Y., & Zhi, L. (2011). Chemical amination of graphene oxides and their extraordinary properties in the detection of lead ions. *Nanoscale*, *3*(12), 5059–5066.

Wang, J. (2000). Survey and summary: from dna biosensors to gene chips. *Nucleic acids research*, *28*(16), 3011–3016.

Wang, J. (2006). Electrochemical biosensors: towards point-of-care cancer diagnostics. *Biosensors and Bioelectronics*, *21*(10), 1887–1892.

Wang, S. X., Acha, D., Shah, A. J., Hills, F., Roitt, I., Demosthenous, A., & Bayford, R. H. (2017). Detection of the tau protein in human serum by a sensitive four-electrode electrochemical biosensor. *Biosensors and bioelectronics*, *92*, 482–488.

Wang, S. X., Acha, D., Shah, A. J., Hills, F., Roitt, I., Demosthenous, A., & Bayford, R. H. (2017). Detection of the tau protein in human serum by a sensitive four-electrode electrochemical biosensor. *Biosensors and Bioelectronics*, *92*, 482 – 488.
URL http://www.sciencedirect.com/science/article/pii/S0956566316311095

Wang, T., Xiao, S., Liu, Y., Lin, Z., Su, N., Li, X., Li, G., Zhang, M., & Fang, Y. (2014). The efficacy of plasma biomarkers in early diagnosis of alzheimer's disease. *International journal of geriatric psychiatry*, *29*(7), 713–719.

Wang, T., Zhang, M., Dreher, D. D., & Zeng, Y. (2013). Ultrasensitive microfluidic solid-phase elisa using an actuatable microwell-patterned pdms chip. *Lab on a Chip*, *13*(21), 4190–4197.

Wang, X., Li, X., Zhang, L., Yoon, Y., Weber, P. K., Wang, H., Guo, J., & Dai, H. (2009a). N-doping of graphene through electrothermal reactions with ammonia. *science*, *324*(5928), 768–771.

Wang, Y., Fan, D., Zhao, G., Feng, J., Wei, D., Zhang, N., Cao, W., Du, B., & Wei, Q. (2018a). Ultrasensitive photoelectrochemical immunosensor for the detection of amyloid β-protein based on sno2/sns2/ag2s nanocomposites. *Biosensors and Bioelectronics*, *120*, 1–7.

Wang, Y.-S., Yau, S., Chau, L.-K., Mohamed, A., & Huang, C.-J. (2018b). Functional biointerfaces based on mixed zwitterionic self-assembled monolayers for biosensing applications. *Langmuir*, *35*(5), 1652–1661.

Wang, Z., Liu, T., Asif, M., Yu, Y., Wang, W., Wang, H., Xiao, F., & Liu, H. (2018c). Rimelike structure-inspired approach toward in situ-oriented self-assembly of hierarchical porous mof films as a sweat biosensor. *ACS applied materials & interfaces*, *10*(33), 27936–27946.

Wang, Z., Xu, Q., Wang, H.-Q., Yang, Q., Yu, J.-H., & Zhao, Y.-D. (2009b). Hydrogen peroxide biosensor based on direct electron transfer of horseradish peroxidase with vapor deposited quantum dots. *Sensors and Actuators B: Chemical*, *138*(1), 278–282.

Weiss, N. O., Zhou, H., Liao, L., Liu, Y., Jiang, S., Huang, Y., & Duan, X. (2012). Graphene: an emerging electronic material. *Advanced materials*, *24*(43), 5782–5825.

Welch, N. G., Scoble, J. A., Muir, B. W., & Pigram, P. J. (2017). Orientation and characterization of immobilized antibodies for improved immunoassays. *Biointerphases*, *12*(2), 02D301.

West, T., Kirmess, K. M., Meyer, M. R., Holubasch, M. S., Knapik, S. S., Hu, Y., Contois, J. H., Jackson, E. N., Harpstrite, S. E., Bateman, R. J., et al. (2021). A blood-based diagnostic test incorporating plasma aβ42/40 ratio, apoe proteotype, and age accurately identifies brain amyloid status: findings from a multi cohort validity analysis. *Molecular neurodegeneration*, *16*(1), 1–12.

Wiencek, J. R., Duh, S.-H., & Christenson, R. H. (2020). Proteins: analysis and interpretation in serum, urine, and cerebrospinal fluid. In *Contemporary Practice in Clinical Chemistry*, (pp. 365–390). Elsevier.

Wu, C., Garden, P. M., & Walt, D. R. (2020). Ultrasensitive detection of attomolar protein concentrations by dropcast single molecule assays. *Journal of the American Chemical Society*, *142*(28), 12314–12323.

Wu, C.-C., Ku, B.-C., Ko, C.-H., Chiu, C.-C., Wang, G.-J., Yang, Y.-H., & Wu, S.-J. (2014). Electrochemical impedance spectroscopy analysis of a-beta (1-42) peptide using a nanostructured biochip. *Electrochimica Acta*, *134*, 249–257.

Wu, D., Zhang, F., Liu, P., & Feng, X. (2011). Two-dimensional nanocomposites based on chemically modified graphene. *Chemistry–A European Journal*, *17*(39), 10804–10812.

Wu, L., Ji, H., Sun, H., Ding, C., Ren, J., & Qu, X. (2016). Label-free ratiometric electrochemical detection of the mutated apolipoprotein e gene associated with alzheimer's disease. *Chemical Communications*, *52*(81), 12080–12083.

Wustoni, S., Wang, S., Alvarez, J. R., Hidalgo, T. C., Nunes, S. P., & Inal, S. (2019). An organic electrochemical transistor integrated with a molecularly selective isoporous membrane for amyloid-β detection. *Biosensors and Bioelectronics*, *143*, 111561.

Xia, N., Wang, X., Yu, J., Wu, Y., Cheng, S., Xing, Y., & Liu, L. (2017). Design of electrochemical biosensors with peptide probes as the receptors of targets and the inducers of gold nanoparticles assembly on electrode surface. *Sensors and Actuators B: Chemical*, *239*, 834–840.

Xia, N., Wang, X., Zhou, B., Wu, Y., Mao, W., & Liu, L. (2016). Electrochemical detection of amyloid-β oligomers based on the signal amplification of a network of silver nanoparticles. *ACS applied materials & interfaces*, *8*(30), 19303–19311.

Xing, Z., Ju, Z., Zhao, Y., Wan, J., Zhu, Y., Qiang, Y., & Qian, Y. (2016). One-pot hydrothermal synthesis of nitrogen-doped graphene as high-performance anode materials for lithium ion batteries. *Scientific reports*, *6*(1), 1–10.

Xu, J., Wang, Y., & Hu, S. (2017a). Nanocomposites of graphene and graphene oxides: synthesis, molecular functionalization and application in electrochemical sensors and biosensors. a review. *Microchimica Acta*, *184*(1), 1–44.

Xu, S., Zhan, J., Man, B., Jiang, S., Yue, W., Gao, S., Guo, C., Liu, H., Li, Z., Wang, J., et al. (2017b). Real-time reliable determination of binding kinetics of dna hybridization using a multi-channel graphene biosensor. *Nature communications*, *8*, 14902.

Yamanaka, Y., Matsugano, S., Yoshikawa, Y., & Orino, K. (2016). Binding analysis of human immunoglobulin g as a zinc-binding protein. *Antibodies*, *5*(2), 13.

Yang, M., Kim, T.-Y., Hwang, H.-C., Yi, S.-K., & Kim, D.-H. (2008). Development of a palm portable mass spectrometer. *Journal of the American Society for Mass Spectrometry*, *19*(10), 1442–1448.

Yang, W., Ratinac, K., Ringer, S., Thordarson, P., Gooding, J., & Braet, F. (2010a). Carbon nanomaterials in biosensors: Should you use nanotubes or graphene? *Angewandte Chemie International Edition*, *49*(12), 2114–2138.
URL `https://onlinelibrary.wiley.com/doi/abs/10.1002/anie.200903463`

Yang, W., Ratinac, K. R., Ringer, S. P., Thordarson, P., Gooding, J. J., & Braet, F. (2010b). Carbon nanomaterials in biosensors: should you use nanotubes or graphene? *Angewandte Chemie International Edition*, *49*(12), 2114–2138.

Yang, Y., Asiri, A. M., Tang, Z., Du, D., & Lin, Y. (2013). Graphene based materials for biomedical applications. *Materials Today*, *16*(10), 365 – 373.
URL `http://www.sciencedirect.com/science/article/pii/S1369702113003015`

Yang, Y., Huang, Y., & Li, C. (2019). A reusable electrochemical sensor for one-step biosensing in complex media using triplex-forming oligonucleotide coupled dna nanostructure. *Analytica chimica acta*, *1055*, 90–97.

Ye, M., Jiang, M., Cheng, J., Li, X., Liu, Z., Zhang, W., Mugo, S. M., Jaffrezic-Renault, N., & Guo, Z. (2020). Single-layer exfoliated reduced graphene oxide-antibody tau sensor for detection in human serum. *Sensors and Actuators B: Chemical*, *308*, 127692.

Yogeswaran, U., & Chen, S.-M. (2008). A review on the electrochemical sensors and biosensors composed of nanowires as sensing material. *Sensors*, *8*(1), 290–313. URL http://dx.doi.org/10.3390/s8010290

Yoo, Y. K., Kim, G., Park, D., Kim, J., Kim, Y., Yun Kim, H., Yang, S. H., Lee, J. H., & Hwang, K. S. (2020). Gold nanoparticles assisted sensitivity improvement of interdigitated microelectrodes biosensor for amyloid-β detection in plasma sample. *Sensors and Actuators B: Chemical*, *308*, 127710. URL http://www.sciencedirect.com/science/article/pii/S0925400520300575

Yoo, Y. K., Kim, J., Kim, G., Kim, Y. S., Kim, H. Y., Lee, S., Cho, W. W., Kim, S., Lee, S.-M., Lee, B. C., Lee, J. H., & Hwang, K. S. (2017a). A highly sensitive plasma-based amyloid-β detection system through medium-changing and noise cancellation system for early diagnosis of the alzheimer's disease. *Scientific Reports*, *7*(1), 8882. URL https://doi.org/10.1038/s41598-017-09370-3

Yoo, Y. K., Kim, J., Kim, G., Kim, Y. S., Kim, H. Y., Lee, S., Cho, W. W., Kim, S., Lee, S.-M., Lee, B. C., et al. (2017b). A highly sensitive plasma-based amyloid-β detection system through medium-changing and noise cancellation system for early diagnosis of the alzheimer's disease. *Scientific reports*, *7*(1), 1–10.

Yoshida, K., Kuroda, D., Kiyoshi, M., Nakakido, M., Nagatoishi, S., Soga, S., Shirai, H., & Tsumoto, K. (2019). Exploring designability of electrostatic complementarity at an antigen-antibody interface directed by mutagenesis, biophysical analysis, and molecular dynamics simulations. *Scientific reports*, *9*(1), 1–11.

You, M., Yang, S., An, Y., Zhang, F., & He, P. (2020). A novel electrochemical biosensor with molecularly imprinted polymers and aptamer-based sandwich assay for determining amyloid-β oligomer. *Journal of Electroanalytical Chemistry*, *862*, 114017. URL http://www.sciencedirect.com/science/article/pii/S1572665720302009

Youmans, K. L., Tai, L. M., Kanekiyo, T., Stine Jr, W. B., Michon, S.-C., Nwabuisi-Heath, E., Manelli, A. M., Fu, Y., Riordan, S., Eimer, W. A., et al. (2012). Intraneuronal aβ detection in 5xfad mice by a new aβ-specific antibody. *Molecular neurodegeneration*, *7*(1), 1–14.

Yu, Y., Sun, X., Tang, D., Li, C., Zhang, L., Nie, D., Yin, X., & Shi, G. (2015). Gelsolin bound β-amyloid peptides (1–40/1–42): electrochemical evaluation of levels of soluble peptide associated with alzheimer's disease. *Biosensors and bioelectronics*, *68*, 115–121.

Yuan, Q., Liu, Y., Ye, C., Sun, H., Dai, D., Wei, Q., Lai, G., Wu, T., Yu, A., Fu, L., et al. (2018). Highly stable and regenerative graphene–diamond hybrid electrochemical biosensor for fouling target dopamine detection. *Biosensors and Bioelectronics*, *111*, 117–123.

Zakaria, N., Ramli, M. Z., Ramasamy, K., Meng, L. S., Yean, C. Y., Singh, K. K. B., Zain, Z. M., & Low, K.-F. (2018). An impedimetric micro-immunosensing assay to detect alzheimer's disease biomarker: Aβ40. *Analytical biochemistry*, *555*, 12–21.

Zetterberg, H. (2017a). Applying fluid biomarkers to alzheimer's disease. *American Journal of Physiology-Cell Physiology*, *313*(1), C3–C10.

Zetterberg, H. (2017b). Tau in biofluids–relation to pathology, imaging and clinical features. *Neuropathology and applied neurobiology*, *43*(3), 194–199.

Zetterberg, H. (2019). Blood-based biomarkers for alzheimer's disease—an update. *Journal of Neuroscience Methods*, *319*, 2 – 6. Methods and Models in Alzheimer's Disease Research. URL http://www.sciencedirect.com/science/article/pii/S016502701830339X

Zetterberg, H., Mörtberg, E., Song, L., Chang, L., Provuncher, G. K., Patel, P. P., Ferrell, E., Fournier, D. R., Kan, C. W., Campbell, T. G., et al. (2011). Hypoxia due to cardiac arrest induces a time-dependent increase in serum amyloid β levels in humans. *PloS one*, *6*(12), e28263.

Zetterberg, H., Wilson, D., Andreasson, U., Minthon, L., Blennow, K., Randall, J., & Hansson, O. (2013). Plasma tau levels in alzheimer's disease. *Alzheimer's research & therapy*, *5*(2), 1–3.

Zhang, J., Gao, J., Song, Q., Guo, Z., Chen, A., Chen, G., & Zhou, S. (2016). N-substituted carboxyl polyaniline covalent grafting reduced graphene oxide nanocomposites and its application in supercapacitor. *Electrochimica Acta*, *199*, 70–79.

Zhao, S., Zhou, Y., Wei, L., & Chen, L. (2020). Low fouling strategy of electrochemical biosensor based on chondroitin sulfate functionalized gold magnetic particle for voltammetric determination of mycoplasma ovipneumonia in whole serum. *Analytica Chimica Acta*, *1126*, 91–99.

Zhao, Z., Zhu, L., Bu, X., Ma, H., Yang, S., Yang, Y., & Hu, Z. (2015). Label-free detection of alzheimer's disease through the adp3 peptoid recognizing the serum amyloid-beta42 peptide. *Chemical Communications*, *51*(4), 718–721.

Zhong, Z., Gao, X., Gao, R., & Jia, L. (2018). Selective capture and sensitive fluorometric determination of pseudomonas aeruginosa by using aptamer modified magnetic nanoparticles. *Microchimica Acta*, *185*(8), 377.

Zhou, W., Zhang, J., Ye, F., Xu, G., Su, H., Su, Y., & Zhang, X. (2017). Plasma neurofilament light chain levels in alzheimer's disease. *Neuroscience Letters*, *650*, 60 – 64.
URL `http://www.sciencedirect.com/science/article/pii/S0304394017303282`

Zhou, X., & Ashford, J. W. (2019). Advances in screening instruments for alzheimer's disease. *AGING MEDICINE*, *2*(2), 88–93.
URL `https://onlinelibrary.wiley.com/doi/abs/10.1002/agm2.12069`

Zhou, Y., Li, C., Li, X., Zhu, X., Ye, B., & Xu, M. (2018). A sensitive aptasensor for the detection of β-amyloid oligomers based on metal–organic frameworks as electrochemical signal probes. *Analytical Methods*, *10*(36), 4430–4437.

Zhou, Y., Zhang, H., Liu, L., Li, C., Chang, Z., Zhu, X., Ye, B., & Xu, M. (2016). Fabrication of an antibody-aptamer sandwich assay for electrochemical evaluation of levels of β-amyloid oligomers. *Scientific reports*, *6*(1), 1–8.

Zhu, Y., Murali, S., Cai, W., Li, X., Suk, J. W., Potts, J. R., & Ruoff, R. S. (2010). Graphene and graphene oxide: synthesis, properties, and applications. *Advanced materials*, *22*(35), 3906–3924.

Ziegler, C., & Göpel, W. (1998). Biosensor development. *Current opinion in chemical biology*, *2*(5), 585–591.

Zupančič, U., Jolly, P., Estrela, P., Moschou, D., & Ingber, D. E. (2021). Graphene enabled low-noise surface chemistry for multiplexed sepsis biomarker detection in whole blood. *Advanced Functional Materials*, *31*(16), 2010638.